NTNU

Norwegian University of
Science and Technology

Mooring System Design for a Large Floating Wind Turbine in Shallow Water

Tiril Stenlund

Marine Technology
Submission date: June 2018
Supervisor: Erin Bachynski, IMT
Co-supervisor: Kjell Larsen, IMT

Norwegian University of Science and Technology
Department of Marine Technology

NTNU Trondheim
Norwegian University of Science and Technology
Department of Marine Technology – Group of Marine Structures

PROJECT THESIS IN MARINE TECHNOLOGY

SPRING 2018

FOR

STUD.TECHN. Tiril Stenlund

Mooring system design for a large floating wind turbine in shallow water

Forankringssystemdesign for en stor flytende vindturbin på grunt vann

Background:
In the development of floating wind turbines (FWTs) for harnessing the wind resource in deep water, various technologies from the offshore oil and gas (O&G) industry have been adopted, including mooring system solutions. Compared to O&G installations, FWTs tend to be significantly smaller, with large mean loads (due to the rotor thrust) in moderate wave conditions, and tend to have less strict stationkeeping requirements.

In order to bring FWTs closer to commercial feasibility, cost reductions are needed. Novel mooring system designs – using less or different materials, novel anchors, or new installation methods – offer one possible area for cost reduction. Novel mooring systems may also allow FWTs to be applied in shallower water, such that they may become competitive in a wider range of locations.

The aim of the thesis work is to examine design requirements for the mooring system of the CSC 10MW floating wind turbine in 70 m water depth, and to establish feasible mooring systems. High-fidelity global analysis of the structure will be used to investigate the performance of the proposed mooring systems, with a particular focus on ULS and ALS.

Assignment:
The following tasks should be addressed in the project work:

1. Literature study regarding stationkeeping requirements for offshore wind turbines as well as mooring system design and analysis. Consideration shall be given to mooring line failure modes (ultimate and fatigue limit states) for chain, wire, and fiber rope.

2. Literature study regarding environmental characteristics (wind speed, significant wave height, peak period, and soil conditions) of a representative location.

3. Design chain and fiber rope mooring systems for the selected locations assuming 70 m water depth. Carry out global numerical analysis of selected systems. Evaluate the designs with respect to ULS and ALS.

4. Compare global simulation results for a selected design against simpler models established by other students.

5. Report and conclude on the investigation.

The work scope could be larger than anticipated. Subject to approval from the supervisors, topics may be deleted from the list above or reduced in extent.

In the project, the candidate shall present his personal contribution to the resolution of problem within the scope of the project work.

Theories and conclusions should be based on mathematical derivations and/or logic reasoning identifying the various steps in the deduction.

The candidate should utilize the existing possibilities for obtaining relevant literature.

The project report should be organized in a rational manner to give a clear exposition of results, assessments, and conclusions. The text should be brief and to the point, with a clear language. Telegraphic language should be avoided.

The project report shall contain the following elements: A text defining the scope, preface, list of contents, main body of the project report, conclusions with recommendations for further work, list of symbols and acronyms, reference and (optional) appendices. All figures, tables and equations shall be numerated.

The supervisor may require that the candidate, in an early stage of the work, present a written plan for the completion of the work. The plan should include a budget for the use of computer and laboratory resources that will be charged to the department. Overruns shall be reported to the supervisor.

The original contribution of the candidate and material taken from other sources shall be clearly defined. Work from other sources shall be properly referenced using an acknowledged referencing system.

The project report shall be submitted in two copies:

- Signed by the candidate
- The text defining the scope included
- In bound volume(s)
- Drawings and/or computer prints which cannot be bound should be organized in a separate folder.

Erin Bachynski
Kjell Larsen
Supervisors

Deadline: 11.06.2018

Preface

This Master thesis is written in the hydrodynamics specialization at the Department of Marine Technology at the Norwegian University of Science and Technology (NTNU). The thesis was conducted during spring 2018. The problem statement was originally purposed by Equinor, and has been revised throughout the year.

In the project, an offshore semi-submersible 10MW wind turbine at 200 m water depth has been implemented to a 70 m water depth with several different mooring system designs. The thesis is a continuation of a project thesis written spring 2017. Most of the time has been spent at and working with the model in SIMA, solving different problems showing up when implementing different mooring systems. Some time has also been spent to literature research about wind turbines, mooring and stationkeeping requirements.

I want to thank my supervisor, dr. Erin Bachynski, for good advises and guidance. I also want to thank her for for helping me out in SIMA and for her quick responses of my e-mails. I would also like to thank my co-supervisor prof. Kjell Larsen for teaching me about mooring, for discussion of my results and for bringing up new mooring ideas from Equinor. Furthermore, I want to thank my fellow student, Kjetil Blindheim Hole, for good discussions about the comparison of our SIMA models. I also want to thank PhD candidate, Kun Xu, for his presentation about his work regarding mooring systems. Finally, I want to thank my friends and family of their support and help throughout my degree.

Trondheim, 11/06/2018

Tiril Stenlund

Summary

Offshore wind turbines having a semi-submersible sub-structure have been suggested as a good solution at shallow water depths due to its small draft. One of the challenges of having a semi-submersible wind turbine in shallow waters is the mooring system design. The mooring lines should provide enough stiffness to limit the horizontal offset of the structure. However, the stiffness should also be limited to avoid too large forces in the fairleads due to the excitation forces. For chain catenary mooring systems, a large part of the mooring line should be resting on the sea bed to avoid vertical forces at the anchor point. Furthermore, the mooring lines need to have a sufficient Fatigue Limit State (FLS), Ultimate Limit State (ULS) and Accidental Limit State (ALS) when subjected to the environmental forces.

In this Master thesis, an already existing floating semi-submersible wind turbine model in SIMA is implemented from a water depth of 200 m to a water depth of 70 m. The floating wind turbine has a DTU 10MW reference wind turbine [9], and a semi-submersible sub-structure developed in Qiang Wang's Master thesis [37]. Three different mooring systems have been investigated: The initial mooring system already being in the model, a catenary chain mooring system based on Hywind Scotland mooring system used for the spar buoys in Equinor's pilot park, and a taut polyester system. In addition, the Hywind Scotland model has been compared to a simplified Hywind Scotland model, developed by fellow student Kjetil Blindheim Hole in his Master thesis. The simplified model is modelled without the wind turbine and tower. SIMA has been used to do the model analysis, and MATLAB has been used for validation of static results and for pre-processing.

Static analyses were conducted to find the anchor positions, to find the line characteristics and to find the mooring line shape of the three mooring systems. The natural periods and damping of the models were found in a decay test. The change of mooring system affected the surge and yaw natural period the most, showing that the mooring systems had a minor effect on heave and pitch. Most of the natural periods in surge were too small when comparing to the typical surge periods of a mooring system of a semi-submersible wind turbine. Wave-only response analyses were conducted to find the response amplitude operators (RAOs). The results showed again that the change of mooring system affected heave and pitch motion the least. In addition, resonance peaks were seen for the heave and pitch RAOs.

Constant wind tests were executed for an under rated, and over rated, the rated and a 50 year return period extreme wind condition. The results showed that the rated and the extreme conditions gave the largest mooring line tensions and offsets. Comparing the three mooring line models, the Hywind model gave the largest mean offsets in surge, heave and pitch, while the initial model gave the largest mean line tension.

Extreme conditions were then conducted for all the models. The conditions having extreme turbulent wind was using either NPD turbulent wind or TurbSim turbulent wind. The results showed that the extreme wind affected the mean line tension and the mean offsets in surge and pitch the most. The conditions using the TurbSim model gave a slightly higher wind speed and a lower standard deviation of the wind speed than when using the NPD turbulent model. This could also be seen in the mean line tensions and the mean offsets in surge, heave and pitch. The condition having only extreme waves showed that the extreme waves did not affect the mean line tension, and the mean offsets. However, the extreme waves gave large maximum peaks of the results. Extreme current had a minor effect on the line tension and the offsets.

The ULS mooring line calculations showed that only the polyester system was within the ULS criteria. However, the lee lines of the polyester went into slack. All the systems passed the ALS mooring line criteria, being the extreme ULS condition with one mooring line missing. FLS calculations were not conducted.

When comparing the original Hywind system to the simplified Hywind system, it was found that the results of the simplified model were acceptable. Using the simplified model in an ULS calculation gave a 35 % shorter calculation time in SIMA.

Sammendrag

Offshore vindturbiner som har halvt nedsenkbare understrukturer har blitt foreslått som gode alternativer på grunt vann på grunn av deres lave dypgang. En av utfordringene med å ha halvt nedsenkbare vindturbiner på grunt vann er forankringssystemdesignet. Forankringslinene må gi nok stivhet til å begrense de horisontale forflytningene av strukturen. Stivheten må heller ikke være for høy slik at det ikke oppstår for store krefter i toppen av lina. For kjettingsystemer, bør en stor del av forankringslina ligge langs havbunnen for å unngå vertikale krefter ved ankeret. I tillegg må forankringslinene være innenfor for kriteriene for bruddgrensetilstand (ULS), ulykkesgrensetilstand (ALS), og utmattingsgrensetilstand (FLS) ved vind, bølger og strøm

I denne masteroppgaven skal en eksisterende SIMA-modell av en flytende halvt nedsenkbar vindturbin bli implementert fra 200 m vanndyp til 70 m vanndyp. Den flytende vindturbinen har en DTU 10MW referansevindturbin [9], og en halvt nedsenkbar understruktur som har blitt designet i Qiang Wangs masteroppgave [37]. Tre forskjellige forankringssystemer har blitt undersøkt: Det opprinnelige systemet som var i modellen fra før, et kjettingsystem basert på Hywinds forankringssystem som er brukt på sparbøyene i Equinors pilotpark ved Skottland, og et stramt polyestersystem. I tillegg har den Hywind-baserte modellen blitt sammenlignet med en forenklet modell utviklet av medstudent Kjetil Blindheim Hole i hans masteroppgave. Den forenklede modellen er modellert uten tårn og vindturbin. SIMA har blitt brukt til analysene av modellen, og MATLAB har blitt brukt til validering av de statiske resultatene, og for postprosessering.

Statiske analyser ble gjennomført for å finne ankerposisjonene, for å se på linekarakteristikker, og for å se på ankerlineformen av de tre forankringssystemene. De naturlige periodene og dempingskoeffisientene til modellene ble funnet i en reduksjonstest (decay test). Endringen av forankringssystemet påvirket de naturlige periodene i jag og gir mest. Dette viste at forankringssystemet hadde en liten effekt på de naturlige periodene i hiv og stamp. De fleste av de naturlige periodene i jag var for små sammenlignet med typiske jagperioder for et forankringssystem på en halvt nedsenkbar vindturbin. Responsamplitudeoperatorer (RAOer) ble funnet ved å utsette strukturen for kun regulære bølger. Resultatene viste igjen at endring av ankersystemet påvirker hiv- og stampbevegelse minst. I tillegg ble det funnet resonanstopper i hiv- og stamp-RAOene.

Konstant vind-tester ble utført for en underratet vindkondisjon, en overratet vindkondisjon, en ratet vindkondisjon og en vindkondisjon med 50 års returperiode. Resultatene fra testene viste at den overratede vindkondisjonen og den ekstreme vindkondisjonen ga høyest linestrekk, og forflytninger av strukturen. Ved sammenligning av de tre forankringssystemene, ble det funnet at Hywind-modellen ga høyest gjennomsnittsforskyvning i jag, hiv, og stamp, mens den opprinnglige modellen ga høyest gjennomsnittlig linestrekk.

De tre modellene ble deretter utsatt for ekstremkondisjoner. Kondisjonene som hadde ekstrem turbulent vind brukte enten NPD turbulent vind eller TurbSim turbulent vind. Resultatene viste at den ekstreme vinden påvirket det gjennomsnittlige linestrekket og gjennomsnittsforskyvningene i jag og stamp mest. Kondisjonene som brukte TurbSim turbulent vindmodell ga en litt høyere vindhastighet og et lavere standardavvik av vindhastigheten enn ved bruk av NPD turbulent vindmodell. Dette kunne dermed også bli sett for det gjennomsnittlige linestrekket og den gjennomsnittlige forskyvningen i jag, hiv og stamp. Resultatene fra kondisjonen som kun hadde ekstreme bølger viste at de ekstreme bølgene ikke påvirket det gjennomsnittlige linestrekket, og de gjennomsnittlige forskyvningene. De ekstreme bølgene ga derimot svært store maksimumtopper i resultatene. Ekstrem strøm hadde liten effekt på linestrekket og forskyvningene.

Utregningene av bruddgrensetilstanden (ULS) viste at kun polyestersystemet var innenfor kriteriene. Derimot gikk le-linene i slakk for dette systemet. Alle systemene var innenfor kriteriene for ulykkesgrensetilstanden (ALS) ved ekstremkjøringer med en manglende line. Utmattingsgrensetilstanden (FLS) ble ikke sjekket.

Ved sammenligning av det originale Hywind-systemet og det forenklede Hywind-systemet ble det funnet at resultatene for det forenklede systemet var akseptable. Ved å gå fra den originale modellen til den forenklede modellen, ble 35 % av utregningestiden i SIMA spart ved kjøring av en 3 timers ekstremkondisjon.

Contents

List of Figures

List of Tables

Chapter 1

Introduction

1.1 Background

In the recent years, the offshore wind turbine market has increased significantly. Due to the large available areas, the high wind velocity, and the low noise and visual impact issues offshore, this has been a good alternative to onshore wind turbines. Floating offshore wind turbines make it possible to locate wind turbines in deep water. Furthermore, the low draft of the floating wind turbines make it possible to locate them in shallow water. In order to make the offshore wind turbines commercial feasible, it is important to have a novel mooring system. To do this, several different mooring line materials, different anchor types, installation methods and mooring line lengths can be checked in order to find the best solution having a low cost.

1.2 Offshore Wind Turbines

The first prototypes of wind turbines were developed during the 1990s. Since then, the wind turbine market has been growing fast, especially in Europe. The reason for most offshore wind turbines being located in Europe is the low water depth, the good wind resources and because of the pressure on the areas and resources on land. The first offshore wind farm made, was the 5 MW wind farm in Vindeby in Denmark in 1991 [7]. Since then, a number of commercial wind farms have been created. Today, wind power is covering 10.4 % of Europe's total electricity consumption, where 141.1 GW is onshore and 12.6 GW is offshore [39]. As of 2016, there are 3589 grid-connected offshore wind turbines in Europe [38]. Figure 1.1 shows how wind power (onshore and offshore) has been growing to become the second largest form of power generation capacity in Europe.

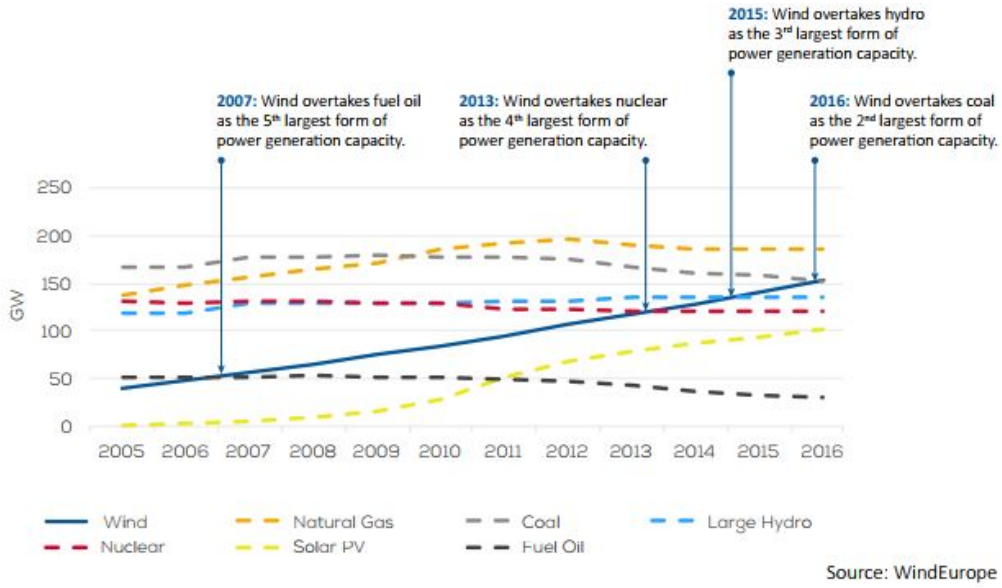

Figure 1.1: Development of wind power energy in the European Union compared to other power resources [39]

Figure 1.2 shows the cumulative and annual offshore wind turbine installations. The capacity has been growing fast the last decade. Figure 1.3 shows how the average rated capacity has grown to 4.8 MW in 2016, which is an increase of 62 % over the last ten years. The largest turbine installed and operating within 2016 is the V-164 8 MW wind turbine [38]. Figure 1.4 shows the average total site capacity of wind turbine farms. It can be seen that it has increased a lot the last decade, from 46.3 MW in 2006 to 379.5 MW in 2016, and that it is expected to grow even more in the next few years.

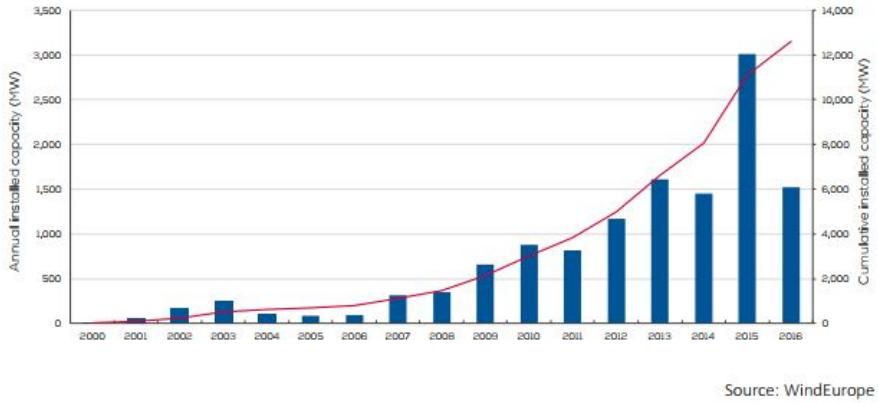

Figure 1.2: Cumulative and annual offshore wind installations [38]

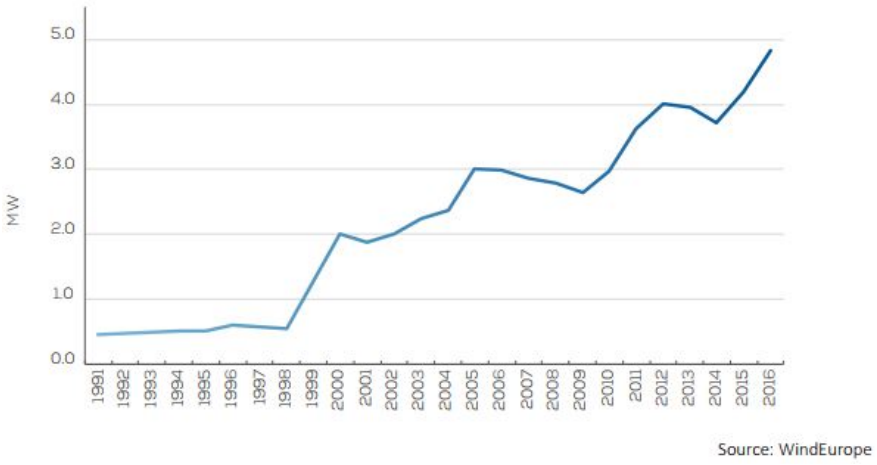

Figure 1.3: Average rated capacity of offshore wind turbines [38]

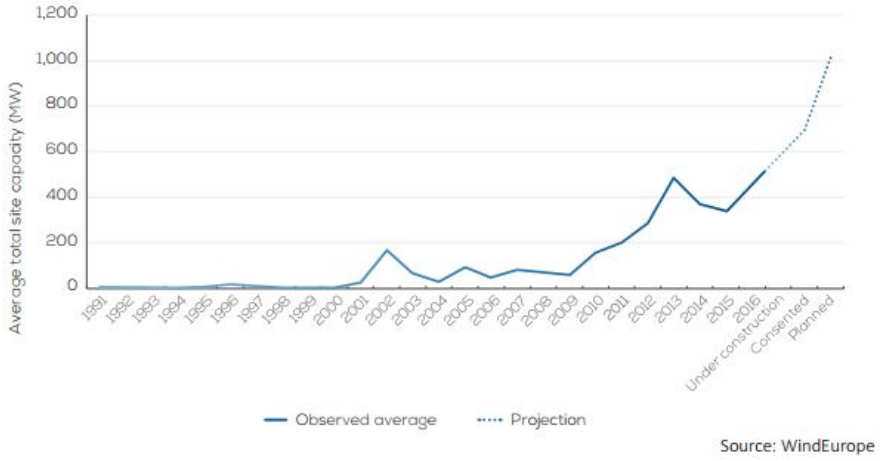

Figure 1.4: Average size of wind turbine farm projects [38]

One of the advantages of having offshore wind turbines is that there are large areas available offshore at a low price. This means that there is a potential to build larger turbines and larger wind farms. In contrast to the land-based wind turbines, there are no noise and visual impacts for humans since the wind turbines are offshore. In addition, there are no conflicts with conservation, contrary to the land-based wind turbines where the the wind turbines and the infrastructure may harm the bird and animal life. Furthermore, there are no restrictions with the infrastructure for transportation and installation. In addition, the offshore wind is generally higher and less turbulent than on land [7].

One of the challenges of having offshore wind turbines compared to land-based wind turbines is that offshore wind turbines are located in a wet environment, and hence they might have corrosion issues. Furthermore, it can be hard to access the wind turbines, especially in bad

weather. Therefore, the installation and maintenance is often challenging and expensive. The bad weather might also lead to down time, so the wind turbines have to be designed to withstand extreme weather conditions. For bottom-fixed wind turbines, a seabed preparation is needed, which is expensive [7].

There are several possible substructures being suitable for offshore wind turbines. Some of the types are listed below

- Monopile
- Jacket
- Gravity-based
- Tripod
- Floating
  - Tension-leg platform (figure 1.5a): Use mooring lines (tendons) to obtain stability. Typically located in intermediate water depths of 50-80 m.
  - Spar buoy (figure 1.5b): Use ballast to obtain stability. Typically located in deep waters, beyond 120 m, due to the large draft.
  - Semi-submersible (figure 1.5c): Use buoyancy to obtain stability. Typically located in intermediate water depths of 50-80 m, due to the low draft, but it also has a potential of being located in deep waters.

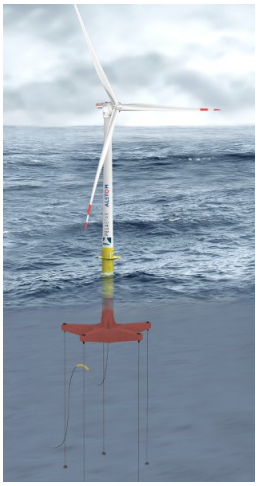

(a) TLP, Pelastar [27]

(b) Spar buoy, Hywind Scotland [31]

(c) Semi-submersible, FORWARD [18]

Figure 1.5: Examples of floating wind turbines

The number of different substructures for grid-connected wind turbines installed in Europe is shown in Figure 1.6. The most common substructure is monopiles, with 80.8 % of the installations.

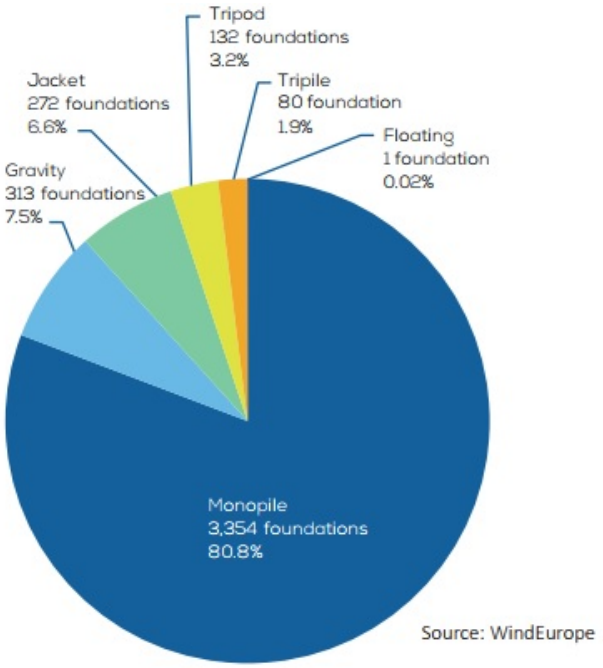

Figure 1.6: Types of substructures for grid-connected offshore wind turbines in Europe [38]

Figure 1.7: Illustration by Joshua Bauer, NREL

1.2.1 Floating wind turbines

In 2009, the first floating prototype wind turbine, a 2.3 MW Siemens wind turbine called Hywind Demo, was made by Equinor. The floating wind turbine was tested outside Karmøy in Norway until 2017. In October 2017, the first floating full-scale commercial wind farm, Hywind Scotland, was built by Equinor [12]. In 2011, Principle Power made a full-scale prototype of a 2 MW WindFloat, which was located outside Portugal [29]. Other floating wind turbine projects are the Fukushima Floating Offshore Wind Farm Demonstration Project (Fukushima FORWARD), where one 2 MW floating wind turbine and other designs were made in 2013, [18], and DeepCwind Consortium, where two floating wind turbines were developed for intermediate and deep water depths respectively [36].

Since semi-submersibles are not bottom-fixed, there are less depth restrictions for the semi-submersibles, and hence they can be located in deep water. This is good for areas that do not have much shallow water (depth less than 45 m), like Norway, the US and Japan. Since semi-submersibles have a small draft, they are also suitable for shallow water. The main challenge about having a semi-submersible in shallow water is the mooring line design. This is because the mooring system in shallow water is much more stiff than a mooring system in deep water, having the same mooring line type, because the part of the mooring line being in the vertical water span is so small.

1.3 Programs used in the analysis

For a floating wind turbine, consisting of rotor, nacelle, tower, a floating sub-structure and a mooring system, coupled analysis is important to see the whole picture when exposed to wind, waves and current. It is important to find the coupling between the responses of the wind turbine, the sub-structure and mooring system when exposed to dynamic and non-linear loads. For the analysis of the FWT, SIMA will be used. A model of the floating wind turbine in SIMA is provided. The model is a DTU 10MW RWT having a semi-submersible substructure. For the extreme wind-cases, TurbSim will be used to generate turbulent wind fields. The post-processing will be conducted in MATLAB and SIMA. MATLAB will also be used to validate the results from the static analysis, and to help implementing the model from 200 m water depth to 70 m water depth. The results of the analysis are presented in tables or figures.

1.3.1 SIMA

The software SIMA (Simulation Workbench for Marine Applications) was used to do the model identification by static and dynamic analysis. SIMA is a tool used for modelling and analysis of marine technology problems. It was made by SINTEF Ocean and Equinor as a Joint Industry Project. SIMA is a workbench combining several other software programs, such as SIMO (Simultion of Marine Operations), RIXLEX (Flexible Riser System Analysis Program) and RIFLEX -SIMO Coupled. SIMO is a software developed by SINTEF Ocean, used to model marine operatins by time domain simulation. It can be used for multi-body hydrodynamic systems like complex station-keeping problems consisting of floating structures and suspended loads [33]. RIFLEX is used to model slender element systems, like mooring systems, using non-linear FEM analysis of slender structures. It was developed by SINTEF Ocean to analyze flexible marine riser systems, and can be used for any slender element system. [34]. RIFLEX-SIMO Coupled is a program coupling SIMO and RIFLEX. Hence, SIMA can be used to model slender, flexible structures in marine operations, e.g moored floating structures. It is also possible to make 3D-figures of the models as they are being modelled, instead of modelling in SIMO and RIFLEX by text-editing. Since SIMA makes it possible to work with both SIMO and RIFLEX coupled, or the programs separated, it shortens the time.

In the SIMA model used in this thesis, the tower and wind turbine blades are modelled as beam elements, and the mooring system is modelled as bar elements. The nacelle, hub and semi-submersible are modelled in SIMO as rigid bodies. The blades experience turbulent wind by the BEM (blade element momentum) or GDW (generalized dynamic wake) model. The nacelle and hub experience loads from the turbulent wind. The tower experience drag forces from the turbulent wind. The semi-submersible and mooring system experience hydrodynamic forces.

1.3.2 TurbSim

The turbulent wind simulated in SIMA can be modelled by two programss: IEC Turbulence Simulator or TurbSim. Turbulent wind from TurbSim will be used in this thesis. TurbSim is a turbulence simulator developed by the National Renewable Energy Laboratory (NREL) and Sandia National Laboratories (SNL) [20]. The tool gives numerical simulations of stochastic, full-field turbulent wind. The wind files contain coherent turbulence that are in consistency with the wind spectrum [26]. The wind files contain time series of wind speed vectors of three components at points in a 2D rectangular grid [20]. The turbulent wind files are going through the wind turbine domain as illustrated in Figure 1.8 at the chosen mean wind speed.

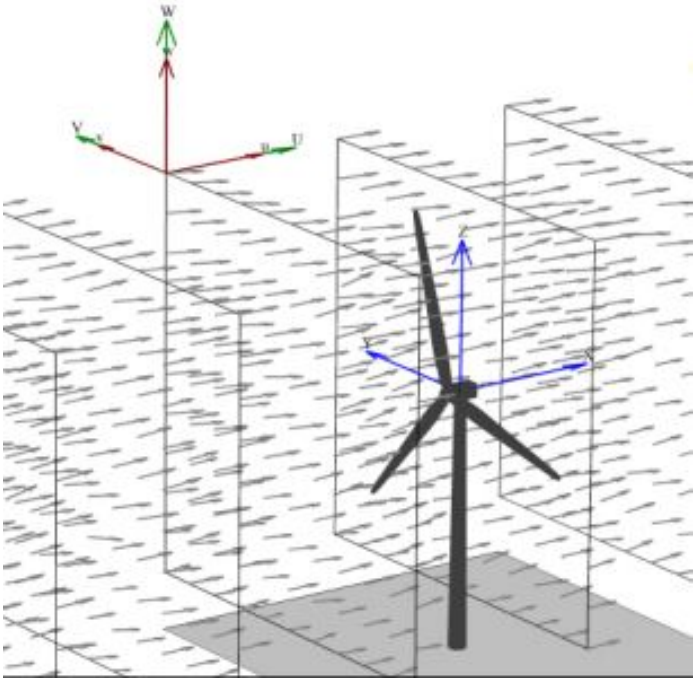

Figure 1.8: TurbSim wind files going through the wind turbine [20]

1.4 Scope and objectives

The aim of this Master thesis is to look at different mooring system designs of a floating 10 MW offshore wind turbine. Stationkeeping requirements for offshore wind turbines, design and analysis of mooring systems, mooring line failure modes and different mooring line materials will be investigated. Different mooring system designs of an already existing SIMA model of the DTU 10 MW reference wind turbine [9], being supported by a semi-submersible sub-structure developed in Qiang Wang's Master thesis [37], is going to be examined. The main objectives of the Master's thesis are:

1. The floating wind turbine SIMA model is presented, and implemented from 200 m water depth to 70 m water depth. Mass and hydrostatic stiffness calculations are conducted. Static calculations of the chain catenary anchor system are conducted in MATLAB and SIMA for comparison.

2. A new anchor system, being the chain catenary anchor system used on the spar buoys in Equinor's Scotland Hywind pilot park at Buchan Deep, is presented. The initial and the Hywind mooring systems are compared regarding natural periods, damping, wave-only and constant wind response, ULS (ultimate limite state) and ALS (accidental limit state) conditions.

3. The Hywind model is compared to a simplified Hywind model developed by Master student Kjetil Blindheim Hole. Natural periods, wave-only and constant wind response, extreme wind and wave conditions, and SIMA calculation time are investigated.

4. A taut polyester system is introduced to the floating wind turbine. Comparisons between the chain mooring systems and the polyester mooring system are conducted regarding natural periods, damping, wave-only and constant wind response, ULS and ALS conditions.

1.5 Limitations

One of the main challenges about mooring of a floating wind turbine is the stiffness created by the mooring lines. It is important to have enough stiffness to limit the horizontal offset of the floating wind turbine. At the same time, the stiffness should be limited to keep the tension in the lines low so that too large forces on the mooring lines are avoided. In the thesis, static analysis, simple identification tests like decay test, constant wind test and wave-only response tests, and ULS and ALS conditions of the mooring lines are going to be carried out. Installation methods, maintenance, fatigue analyses, fault analyses and costs will not be considered.

Chapter 2

Mooring

The mooring system is mainly limiting the horizontal offset of the floating wind turbine. The mooring lines are absorbing wave frequency (WF) motions, and limiting the mean and low frequency (LF) horizontal motions. This is in order to keep a safe distance to other structures and to keep the power cable intact. The stationkeeping requirements for a floating structure can be satisfied by either mooring lines, thruster assisted mooring lines, or a dynamic positioning system. For floating wind turbines, only the first type is used. The mooring lines can be made of either chain, steel rope, synthetic fiber rope, or a combination of these. The lines are often made up of different components held together by connecting links. The top end of a mooring line, called a fairlead, is connected to the floating construction, and is anchored to the sea bottom in the other end.

2.1 Mooring system types

There are mainly three different mooring system types: taut mooring, catenary mooring, and tension leg mooring. The different types are presented below.

2.1.1 Taut mooring

A taut mooring system has light-weight mooring lines that are tight, radiating outwards from the floating structure (Figure 2.1). The taut mooring system obtains its restoring force by stretching of the lines. The mooring lines are usually made of light weight synthetic fiber ropes [10].

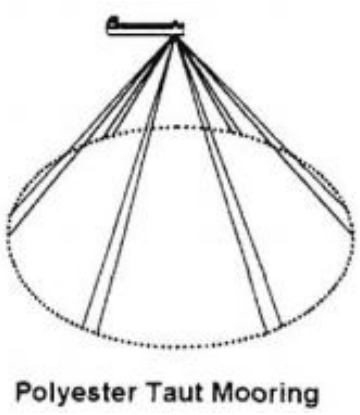

Figure 2.1: Taut mooring [10]

2.1.2 Catenary mooring

A catenary mooring system (Figure 2.2) is usually made of chain and steel wire ropes. The system obtains its restoring force by changing the weight of the mooring line being in the vertical water span by lifting and lowering of the line from the ground. It is common that these systems have anchors that can not experience any vertical forces, leading to very long mooring lines since most of the line has to lay on the ground to keep the anchor in place. The catenary system can also have clump buoyancy elements with clump weights of buoys attached to the lines [10]. Most semi-submersibles today use a catenary mooring system. For offshore wind turbines having a semi-submersible sub-structure, only catenary mooring systems have been used so far.

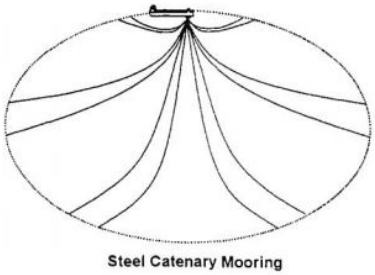

Figure 2.2: Catenary mooring [10]

2.1.3 Tension Leg Mooring

The tension leg mooring system is mainly for tension leg platforms (TLPs). For this system, the buoyancy is greater than the weight, so that the tension leg mooring system contributes with an extra vertical force pointing downwards. The tension leg mooring system is fastened to the seabed by anchor piles.

2.2 Mooring line materials

There are mainly three different mooring line materials: chain, steel wire rope, and synthetic fiber robes.

2.2.1 Chain

Steel chain has large weight, high stiffness, and good abrasion characteristics. The chain links are either studless or studded, as shown in Figure 2.3. The stud-link chains have mostly been used for mooring in shallow water and are easier to handle, while the studless chain is mostly used for permanent mooring. Since the studded chains have a higher weight than the stud-less chain, the stud-less chain will have a lower weight per unit of strength, and thus a longer fatigue life. Chain mooring might not be the best mooring line material when increasing the water depth because of the large weight and the expensive cost due to the increased length. Today, chain is the most used mooring line type for catenary mooring. In shallow water, most structures have chain mooring lines, while in deeper water, it is more popular to have a combination of chain and steel wire ropes.

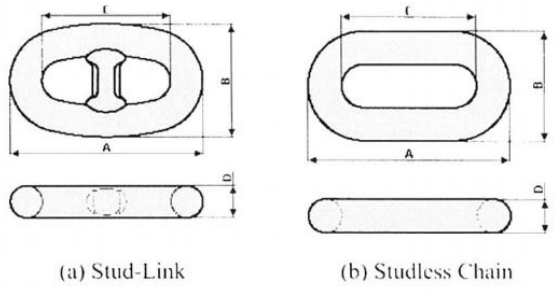

Figure 2.3: Studded and studless chain [10].

2.2.2 Steel Wire Ropes

Steel wire ropes are lighter than chain, and therefore often used in the water span part of the mooring. The two main types of steel wire ropes are single-strand or spiral strand, and six strand or multi-strand. A strand consists of individual wires wound in a helical pattern. The flexibility and axial stiffness of the wire rope are depending on the strand.

Single-strand ropes have wires wounded in a helical pattern, where each layer in the helix has a different direction. This prevents the rope from twisting when subjected to a load. Compared to the multi-strand rope, the single-strand rope has a longer fatigue life. To prevent the rope

from corroding, it is often covered by polyurethane or galvanised by adding zink filler wires. The plastic covering gives a better performance than galvanising the rope. However, if the rope is covered in plastic sheat, it is important that the sheat does not get damaged. The single-strand is mostly used for permanent mooring of large structures.

Multi-stand ropes have cores which support the outer wires and absorb shock loading. The cores consist of either a fibre core or a metallic core. The fibre core is used only for light structures, while the metallic core is used for heavy structures. The most common steel rope type used offshore today is the six-strand muliti-strand. Examples of common multi-stand rope classes are 6x7 Class, having seven wires per strand and a minimum drum diameter, D/d of 42. This rope has good abrasion resistance, but poor flexibility and fatigue life. 6x19 Class, has 16-27 wires per strand and a minimum drum diameter of 26-33. This rope has a very good abrasion, flexibility and fatigue life. The 6x19 Class is mostly used for lifting and dredging. 6x37 Class, has 27-49 wired per strand and a minimum drum diameter of 16-26. This rope has a very good flexibility and fatigue life, but poor abrasion resistance [10].

2.2.3 Fiber ropes

Synthetic fiber ropes are made of polyester or other high-tech fibres. Since synthetic fiber ropes are elastic, they will be stretched to compensate for the increasing tension. This is different than for chain, where the tension is compensated for by changing catenary shape of the line instead of stretching. Fiber ropes can stretch 1.2-20 times more than chain. This leads to decreased wave- and drift frequency response. The use of synthetic fiber ropes with taut mooring requires anchors that allow uplift of the mooring line from the seabed, like suction anchors.

Fiber ropes have a light weight and a high elasticity. Because of this, fiber ropes might be a good alternative to chain for the deep water mooring because of the decreased length needed, the smaller footprint on the seabed, the light weight, flexibility, and ability to extend without causing too much tension when imposed to a dynamic load. In addition, the mean- and low frequency offsets are smaller than for chain- and steel rope mooring, and the vertical load is smaller leading to a greater payload. Because of the reduced length of needed fiber rope compared to chain and steel rope, synthetic fiber rope is a less expensive alternative than chain catenary mooring. It also has a cheaper and easier installment.

However, since fiber ropes is a recently new developed mooring line type, there is not much experience and analysis in using this mooring line type. The properties of synthetic fiber ropes are also complex, leading to an overestimation of the calculations, using large safety factors. This makes the fiber ropes less optimized, and its properties do not get to be fully exploited. In addition, the stiffness properties of fiber ropes change with age, leading to a more complex

calculation. Furthermore, cyclic loading of the fiber ropes can lead to heat generation due to the rubbing of rope components against each other. This may lead to melting of fibers. This is only a problem for ropes with large diameters, or ropes with certain lay types. In addition, some parts of the rope in tension might go into compression (called slack), leading to buckling and damage of the fibers. In addition, the strength of fiber ropes is approximately half of the strength of a steel wire rope having the same diameter. Also, the synthetic fiber ropes are sensitive to cutting by sharp objects, like fish bites.

2.3 Anchors

Anchors can be divided into two types: self-weight anchors or suction forces anchors. Most anchors are not made for resisting vertical forces. How good an anchor is depends on anchor weight and seabed type. The most widely used anchor type for floating wind turbines today is suction anchors. Suction anchors allow vertical forces, and thus can be used in taut mooring systems. However, suction anchors are expensive. Some anchor types are listed below.

- Suction anchor
- Plate anchor
- Fluke anchor
- Deep penetrating anchor/torpedo piles

Chapter 3

Theory

3.1 Degrees of freedom

For a floating structure, there are six degrees of freedom, as listed below [3] and illustrated in Figure 3.1.

- Surge: Translation along longitudinal axis, being the main wind direction
- Sway: Translation along lateral axis, being transverse to main wind direction
- Heave: Translation along the vertical axis
- Roll: Rotation about the longitudinal axis
- Pitch: Rotation about the transverse axis
- Yaw: Rotation about the vertical axis

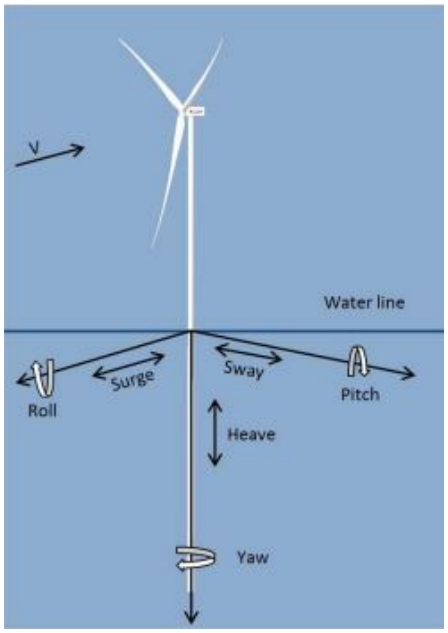

Figure 3.1: Heeling semi submersible

3.2 Stability

Stability of a floating structure is defined as the ability to go back to upright position after heeling to one side [15]. When a structure heels, it is exposed to moments, leading to a deviation from the equilibrium position. The stability of a structure having a heeling angle up to $\pm 10°$ is called initial stability, meaning that the stability is approximately similar to the stability when the structure is in the equilibrium position, $\phi = 0°$. The initial stability can tell if a floating structure will go back to equilibrium position, or capsize, when exposed to environmental forces.

A heeling semi submersible is shown in Figure 3.2. The semi submersible is first floating freely on water line 1 ($WL1$). Here, the center of gravity, CG, is marked as G, the center of buoyancy, CB, is marked as B and the keel is marked as K. Heeling the semi submersible an angle ϕ about the vertical center line, gives a new water line, $WL2$. Due to the change of submersed volume, the center of buoyancy will move from B to B' as shown in the figure. The point where the new vertical center line crosses the old vertical center line is called the meta center, M. When the floating structure heels, it can be assumed that it will rotate around the meta center for small heel angels ($\phi = \pm 10°$).

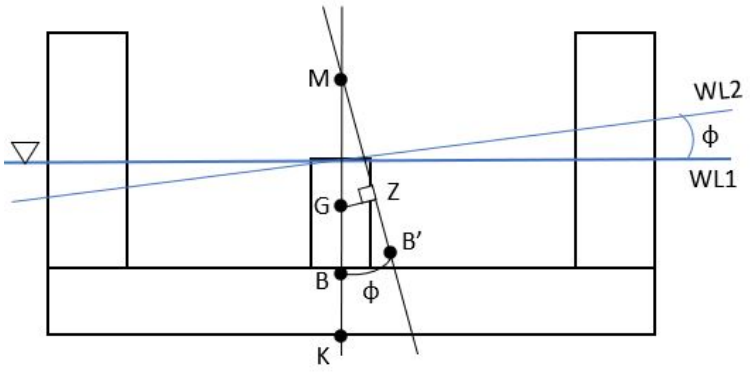

Figure 3.2: Heeling semi submersible

The initial meta center height, GM, is given by Equation 3.1 [15], as shown in Figure 3.2. The vertical position of the center of buoyancy and the center of gravity above the keel, KB and KG are already known parameters for a semi submersible when CG and CB are known. The initial meta center radius, BM, depends on the displacement of the structure, ∇, and the second moment of inertia about water line $WL1$, I_{wl}. BM is given in Equation 3.2.

$$GM = KB + BM - KG \tag{3.1}$$

$$BM = \frac{I_{wp}}{\nabla} \tag{3.2}$$

where I_{wl} is calculated as in Equation 3.3 or Equation 3.4 depending on if the transverse (I_x calculated) or longitudinal (I_y calculated) metacentric height is wanted [15].

$$I_{wp} = I_x = \int_{A_{wp}} y^2 dA_{wp} \tag{3.3}$$

$$I_{wp} = I_y = \int_{A_{wp}} x^2 dA_{wp} \tag{3.4}$$

where A_{wp} is the water plane area and y and x are the distance from the center of the water line area, C, to the area element dA_{wl}. The second moment of interia for a circular cylinder, i.e a column of a semi submersible, can be calculated as $I_{cyl} = \frac{\pi D}{64}$ [28]. If a structure consists of several geometrical elements, Steiners' theorem and the superposition principle have to be used. The restoring forces and moments of a freely floating body can be written as in Equation 3.5 [16].

$$F_k = -C_{kj}\eta_j \tag{3.5}$$

where C_{kj} are the restoring coefficients. The only parts of the stiffness matrix of a body with xz-symmetry plane that are not zero are C_{33}, C_{44} and C_{55} given in Equation 3.6, 3.7 and 3.8 respectively. C_{35} and C_{53} will be zero due to the vertical walls of the semi-submersible columns being in the water plane.

$$C_{33} = \rho g A_{wp} \tag{3.6}$$

$$C_{44} = \rho g \nabla (z_B - z_G) + \rho g \iint_{Awp} y^2 ds = \rho g \overline{GM}_T \tag{3.7}$$

$$C_{55} = \rho g \nabla (z_B - z_G) + \rho g \iint_{Awp} x^2 ds = \rho g \overline{GM}_L \tag{3.8}$$

where ρ is the water density, A_{wp} is the waterplane area, ∇ is the displaced volume of water, z_B is the z-coordinate of the center of buoyancy, z_G is the z-coordinate of the center of gravity, and $\overline{GM}_T$ and $\overline{GM}_L$ are the transverse and longitudinal metacentric height respectively.

3.3 Wave loads

The excitation forces working on the structure are wind, waves and current. Wave loads can be divided into the following regimes:

- Mean wave drift force
- Low-frequency (LF) 2nd order difference frequency (typically 30-500 s)
- Wave-frequency (WF) 1st order forces (typically 5-30 s)

The mooring system should control the mean offset and low-frequency (LF) motions, and absorb the wave-frequency (WF) motions. For floating sub-structures, the second order wave loads are of importance, and should be taken into account. They can cause resonant behaviour in surge, sway and yaw. Methods for calculating second order wave loads are direct pressure integration and conservation of fluid momentum.

3.4 Aerodynamics

A propeller blade has a length, s, called the span. The cross-section of the blade is called an airfoil. An airfoil can be presented as in Figure 3.3. The airfoil is experiencing a drag force, a lift force, and a pitching moment. The drag force, D, is parallel to the incoming flow, called the relative velocity. The lift force, L, is normal to the relative velocity. The lift force is created by the pressure differential between the upper and lower side of the airfoil due to different velocities over and under the airfoil. The drag force is created due to a pressure differential and viscous forces in the boundary layer. The airfoil also experiences a pitching moment, M. Some basic airfoil terminologies are:

- The leading edge of the foil is the forward end point of the foil crossing the mean camber line
- The trailing edge of the foil is the rear end point of the airfoil crossing the mean camber line.
- The mean camber line, seen as the dotted line in Figure 3.3, is the line going from the leading edge to the trailing edge, between the upper and lower edge of the airfoil.
- The chord line is the chord between the leading and trailing edge.
- The camber is the distance between the mean camber line and the chord line.
- The thickness of the foil is the distance between the upper edge and the chord line
- The angle of attack α is the angle between the relative wind and the chord line.

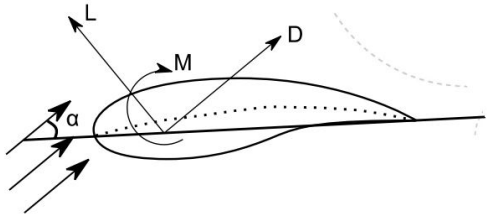

Figure 3.3: Airfoil [6]

The lift coefficient C_L, and the drag coefficient, C_D, can be written as in Equation 3.9.

$$C_L = \frac{L}{\frac{1}{2}\rho U^2 cl} \quad \text{and} \quad C_D = \frac{D}{\frac{1}{2}\rho U^2 cl} \tag{3.9}$$

3.4.1 1D momentum theory

One of the simplest ways to look at an airfoil is the 1D momentum theory. Here, the turbine disk is simplified to the illustration in Figure 3.4

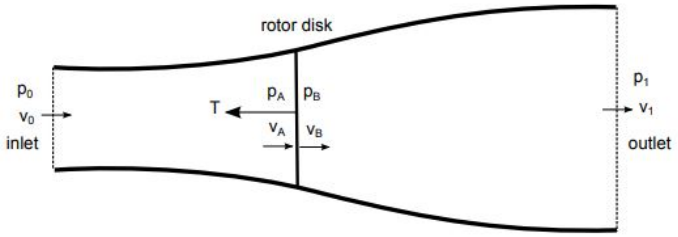

Figure 3.4: 1D momentum theory [6]

In this approach, the conservation of mass, the conservation of momentum and the Bernoulli equation are used to find an equation for the speed at the propeller disk, found to be as in Equation 3.10.

$$v_a = \frac{1}{2}(v_0 + v_1) \tag{3.10}$$

where v_1 and v_0 are the outgoing and incoming velocities of the turbine respectively, as seen in Figure 3.4. This expression is used to find the power, given by Equation 3.11, by using the axial induction factor, a given by Equation 7.1.

$$P = \frac{1}{2}\rho A v_0^3 4a(1-a)^2 \tag{3.11}$$

$$a = \frac{v_0 - v_A}{v_0} \tag{3.12}$$

The maximum power coefficient, C_p, given by Equation 3.13, can be found to be 16/27=59%, which is called the Betz limit. The Betz limit is illustrated in Figure 3.5

$$C_p = \frac{P}{\frac{1}{2}\rho v_0^3 A} = 4a(1-a)^2 \tag{3.13}$$

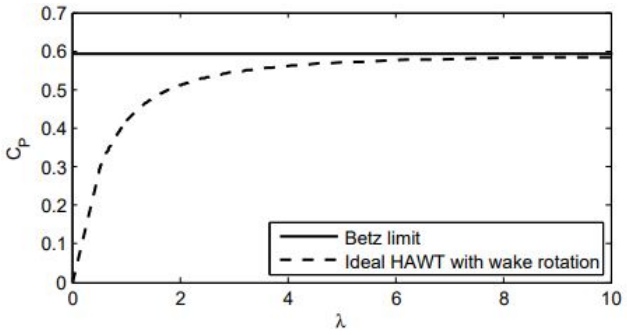

Figure 3.5: Betz limit for the power coefficient [6]

Taking the wake rotation into account, the angular induction factor a', and the tip speed ratio, λ, can be obtained by Equation 3.14 and 3.15 respectively.

$$a' = \frac{\omega}{2\Omega} = \frac{1-3a}{4a-1} \tag{3.14}$$

$$\lambda = \frac{\Omega R}{v_0} \tag{3.15}$$

Looking at the power coefficient, it can be seen that the coefficient is approaching the Betz limit for increasing tip speed ratio.

3.4.2 Blade Element/Momentum (BEM) theory

In SIMA, the Blade Element/ Momentum theory (BEM) is used. This is a theory that combines rotational wake theory with airfoil theory. Figure 3.6 illustrates an airflow with wind velocity, V_0, relative wind velocity, V_{rel}, local twist angle, θ, flow angle, ϕ, angle of attack, α, distance to the center of rotation, r and rotation angular velocity, ω.

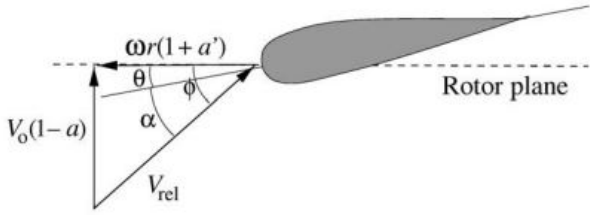

Figure 3.6: Airfoil in the BEM theory [17]

In the BEM method, some new expressions for the axial and angular induction factor are found as in Equation 3.16 [6].

$$a = \frac{1}{\frac{4\sin^2\phi}{\sigma C_n} + 1}, \quad a' = \frac{1}{\frac{4\sin\phi\cos\phi}{\sigma C_t} + 1} \tag{3.16}$$

where $C_n = C_l\cos\phi + C_d\sin\phi$ is the normal force coefficient, σ is the solidity ratio, and $C_t = C_l\sin\phi - C_d\cos\phi$ is the tangential force coefficient. The BEM method is an iteration method where values of a and a' are guessed, and then the flow angle, ϕ is calculated by Equation 3.17

$$\tan\phi = \frac{V_0}{\omega r}\frac{1-a}{1+a'} \tag{3.17}$$

then the angle of attack, $\alpha = \phi - \theta$, C_L and C_D can be found from tables. Updated values of a and a' are now found. This procedure is repeated until convergence.

Several corrections can be applied to this method. The Prandtl's tip loss correction factor corrects for tip loss due to finite number of blades. The Glauert correction corrects for high induction factors. The Øye correction corrects for dynamic wake. Another way to look at the wind turbine is the Generalized Dynamic Wake (GDW), where iteration is not needed.

3.5 Wind

Wind consists of a mean component and a fluctuating gust component, as given in Equation 3.18. The mean component, $U(z)$ is only dependent of height above the SWL, z. The gust component, $u(z,t)$ is depending on both z and time, t.

$$U(z,t) = U(z) + u(z,t) \tag{3.18}$$

3.5.1 Tower drag

A cylinder in an incoming stationary flow having a velocity, U, will experience a lift force, F_L normal to the incoming velocity, and a drag force, F_D parallel to the incoming velocity (see Figure 3.7). For a wind turbine, the incoming wind creates a tower drag on the circular tower. The drag force on the cylinder can be expressed by Equation 3.19 [28].

$$F_D = \frac{1}{2}\rho C_D A U^2 \tag{3.19}$$

where C_D is the drag coefficient, and A is the area met by the incoming flow having a velocity U.

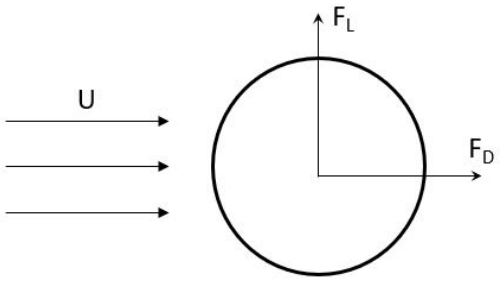

Figure 3.7: Flow around a cylinder

The tower drag coefficient can be found from Figure 3.8 [4]. In the figure, $\Delta = k/D$ is the roughness of the cylinder, and Re is the Reynolds number, defined as in Equation 3.20 [4]

$$Re = \frac{UD}{\nu} \tag{3.20}$$

where ν is the kinematic viscosity of the wind.

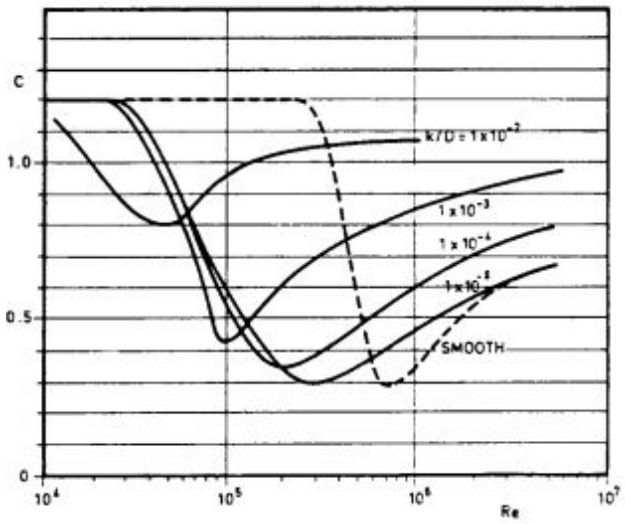

Figure 3.8: Drag coefficients for a fixed circular cross-section for steady flow with varying roughness [4]

3.5.2 Kaimal wind model

Two turbulent wind models are used in this thesis: TurbSim and NPD wind. The turbulent wind model used in TurbSim is the Kaimal model. This model is given by Equation 3.21 [1].

$$S_k(f) = 4\sigma_k^2 \frac{\frac{L_k}{V_{hub}}}{\left(1 + 6f\frac{L_k}{V_{hub}}\right)^{\frac{5}{3}}} \tag{3.21}$$

where

- V_{hub} is the mean speed at hub height
- σ_k is the standard deviation of the wind speed in direction k
- f is the frequency
- L_k is a integral scale parameter

3.5.3 NPD wind

NPD (Norwegian Petroleum Directorate) wave spectrum, also called ISO 19901-1 wave spectrum, is describing the varying gust part of the wind. The wind velocity at height z is described by Equation 3.22 for normal wind velocities, found in DNV-RP-C205 (April 2014) [4].

$$U(z) = U(H)\left(\frac{z}{H}\right)^{\alpha} \tag{3.22}$$

Where $U(z)$ is the wind speed at height z, $U(H)$ is the wind speed at reference height H, and α is a parameter depending on roughness of the sea. α is found to be 0.12 [4]. For high wind velocities, the mean wind speed is found by Equation 3.23 [32].

$$u(z,t) = U(z)\left[1 - 0.41 I_u(z)\ln\left(\frac{t}{t_0}\right)\right] \tag{3.23}$$

where t and t_0 are defined by the averaging time period, $t \leq t_0 = 3600s$, and $U(z)$ is the 1 hour mean wind speed, given by

$$U(z) = U_0\left[1 + C\ln\left(\frac{z}{10}\right)\right] \tag{3.24}$$

where

$$C = 5.73\dot{1}0^{-2}\,(1 + 0.15U_0)^{-0.5} \tag{3.25}$$

where U_0 is the 1 hour mean wind speed at reference height 10 m, and I_u is the turbulence intensity factor given by

$$I_u(z) = 0.061 + 0.043U_0\left(\frac{z}{10}\right)^{-0.22} \tag{3.26}$$

The NPD wind spectrum, $F(f)$ is given by Equation 3.27 [32].

$$S(f) = \frac{320\left(\frac{U_0}{10}\right)^2\left(\frac{z}{10}\right)^{0.45}}{\left(1 + f_m^n\right)^{\frac{5}{3n}}} \tag{3.27}$$

where

$$f_m = 172f\left(\frac{z}{10}\right)^{\frac{2}{3}}\left(\frac{U_0}{10}\right)^{-0.75} \tag{3.28}$$

where $n = 0.468$ and f is the frequency in the range $1/600Hz \leq f \leq 0.5Hz$.

3.6 Static analysis of a mooring line

Mooring of floating wind turbines is less restrictive than permanent moored structures. The lines are giving a restoring force caused by the increased tension in the lines as the horizontal offset increases. The restoring force balances the excitation forces on the floating wind turbine caused by the environment (waves, wind, and current).

As the horizontal offset increases, the mooring line is lifted off the seabed. Looking at the catenary line statically, the increased weight of line in the vertical water span leads to an increased tension and hence increased stiffness. The horizontal restoring force on the moored structure will then increase with the horizontal offset in a non-linear way [10]. Figure 3.9 shows a 2D sketch of a mooring line element. When the element is in static equilibrium, Equation 3.29 and 3.30 can be obtained. T is the tension in the mooring line, D and F are external forces in the tangential and normal direction of the line, respectively, EA is the axial stiffness, and w is the unit weight of chain in water.

$$dT = \left(w \sin\phi - F\left(1 + \frac{T}{EA}\right)\right) ds \tag{3.29}$$

$$T d\phi = \left(w \cos\phi + D\left(a + \frac{T}{EA}\right)\right) ds \tag{3.30}$$

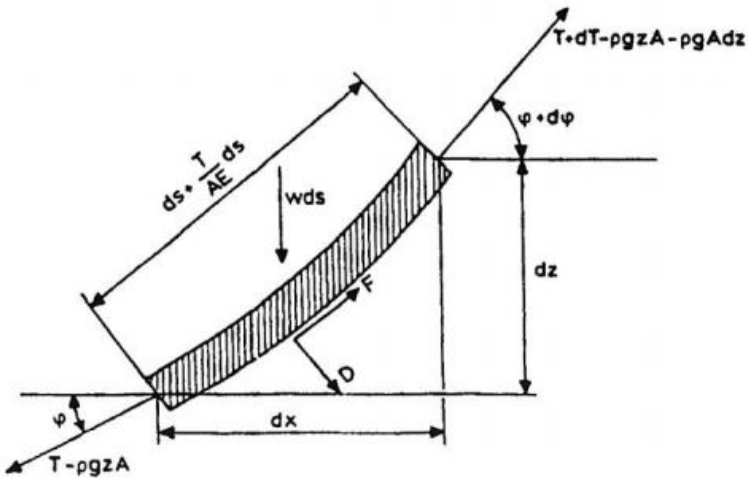

Figure 3.9: Catenary element [10]

The two equations (Equation 3.29 and 3.30) can not be solved explicitly because they are non-linear. Below, the two equations will be solved for an inelastic catenary mooring line, and an elastic catenary mooring line. In addition, the static analysis for a taut polyester rope will be presented.

3.6.1 Inelastic catenary mooring lines

Figure 3.10 shows a mooring line connected to a structure floating on the water, anchored a horizontal distance, X away from the fairlead.

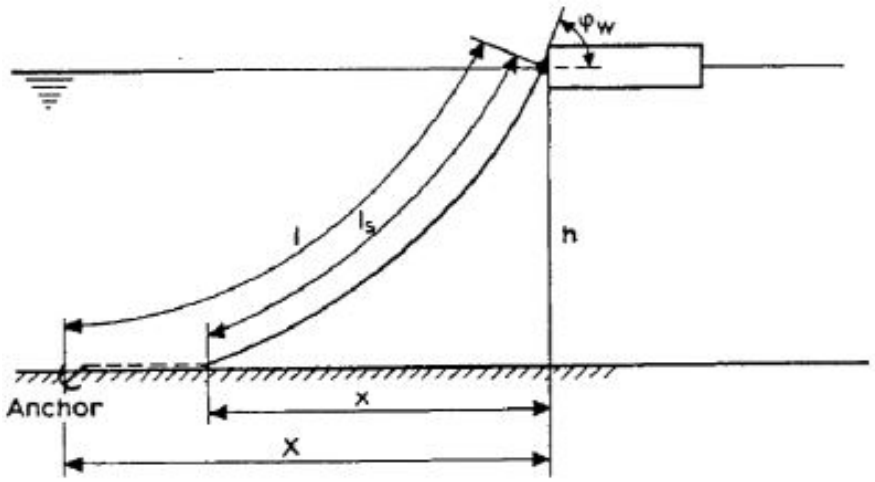

Figure 3.10: Catenary lines [16]

Since the ratio between the tension and the axial stiffness is small for a catenary chain mooring line, it can be neglected. Hence an inelastic mooring line will have the following catenary equations in static equilibrium, assuming a horizontal seabed, neglecting line dynamics and bending stiffness effects. The vertical component of the line tension at the top end, T_z, is given by Equation 3.31

$$T_z = w l_S \tag{3.31}$$

where the unit weight of the submerged line, w, is an already known parameter, and the length of the line in the vertical water span, l_S, is given by Equation 3.32.

$$l_S = \left(\frac{T_H}{w}\right) \sinh\left(\frac{wx}{T_H}\right) \tag{3.32}$$

The horizontal length of the mooring line in the vertical water span, x, can be found by Equation 3.33 by setting the vertical dimension h equal to the vertical distance from the top of the line to the sea bottom. h is an already known parameter.

$$h = \left(\frac{T_H}{w}\right)\left[\cosh\left(\frac{wx}{T_H}\right) - 1\right] \tag{3.33}$$

Solving Equation 3.33 for x gives Equation 3.34

$$x = \left(\frac{T_H}{w}\right)\cosh^{-1}\left(1 + \frac{hw}{T_H}\right) \tag{3.34}$$

Having found x, the corresponding vertical position, y, of the mooring line can be found as in Equation 3.35.

$$y = \frac{T_H}{w}\left(\cosh\left(\frac{hw}{T_H}\right) - 1\right) \tag{3.35}$$

Combining Equation 3.32 and 3.33 leads to the relationship given in Equation 3.36

$$l_S^2 = h^2 + \frac{2hT_H}{w} \tag{3.36}$$

To find the horizontal tension in the fairlead, T_H, as a function of the horizontal distance between the structure and the anchor, X, Equation 3.37 has to be used.

$$X_l = l - l_S + x \tag{3.37}$$

where the total length of the line, l, is a known parameter. Inserting Equation 3.36 and 3.34 in Equation 3.37 leads to the relationship given in Equation 3.38

$$X_l = l - h\sqrt{1 + \frac{2T_H}{hw}} + \left(\frac{T_H}{w}\right)\cosh^{-1}\left(1 + \frac{hw}{T_H}\right) \tag{3.38}$$

3.6.2 Elastic catenary mooring lines

For elastic mooring lines, the elasticity of the line, EA has to be taken into consideration. This is especially important for long mooring lines, mooring lines having high tension and mooring line parts of an elastic material [22]. The known parameters are the water depth, h, being the vertical distance from fairlead to the sea bottom, the unit weight of the mooring line in water, w,

the un-stretched length of the mooring line, l_0, and the elastic stiffness, EA. The vertical tension in fairlead, T_z is given by Equation 3.39

$$T_z = ws \tag{3.39}$$

It can be shown that the horizontal mooring line tension at fairlead, T_H, is given by Equation 3.40 or 3.41 [22]

$$T_H = \frac{T_z^2 - \left(wh - \frac{T_z^2}{2EA}\right)^2}{2\left(wh - \frac{T_z^2}{2EA}\right)} \tag{3.40}$$

$$T_H = EA\left(\sqrt{\left(\frac{T}{EA} + 1\right)^2 - \frac{2wh}{EA}} - 1\right) \tag{3.41}$$

The horizontal length of the mooring line being in the vertical water span, x, is given by Equation 3.42

$$x = \frac{T_H}{w}\sinh^{-1}\left(\frac{T_z}{T_H}\right) + \frac{T_H T_z}{wEA} \tag{3.42}$$

Then, the horizontal distance from the anchor to the fairlead, X can be found by Equation 3.43

$$X = \left(l_0 - \frac{T_z}{w}\right)\left(1 + \frac{T_H}{EA}\right) \tag{3.43}$$

The static analysis of a mooring system is often carried out at an early design stage, before starting the dynamic analysis. The analysis is carried out by using the catenary equations as described above. Figure 3.11 shows the typical line characteristics and restoring forces for a catenary mooring system. The line tension starting at the y-axis is the pre-tension of the mooring line. Moving to the right in the figure gives the horizontal offset when moving in the direction away from the anchor point. The restoring force is starting at a zero force value when the structure is in its mean position. Then the restoring force is increasing for increasing offset as shown in the figure. The force can be described as in Equation 3.44.

$$F_x(t) = C_t x \tag{3.44}$$

where C_t is the equivalent linear stiffness, equal to the slope of the force curve, and x is the horizontal offset. If the maximum line tension is known, the maximum dynamic offset can be found. Having a stiffer system, the slope of the force curve will be steeper, leading to a faster increasing restoring force and line tension for increasing offset. After finding the maximum tension of the mooring line, it should be compared to the breaking strength of the mooring material.

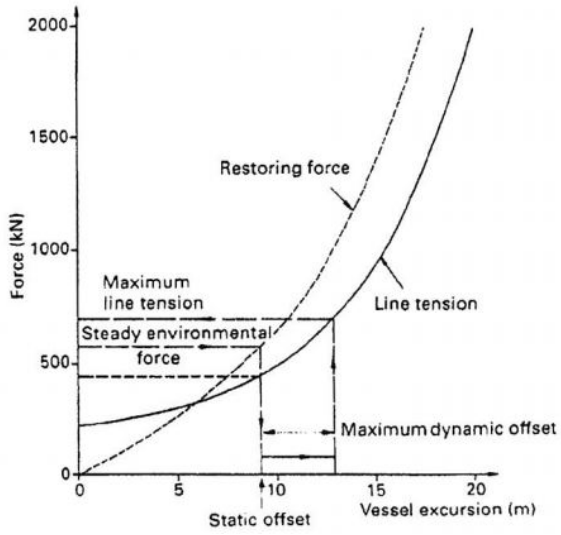

Figure 3.11: The relation between line tension and restoring force for a system with different offsets in static equilibrium [10]

3.6.3 Taut polyester rope mooring lines

Since taut mooring systems obtain stiffness by elasticity, and not by its weight like for catenary mooring systems, the tension has to be found in another way than what is written previously. It is assumed that the mooring line has no weight in water. Figure 3.12 shows a sketch of a taut polyester mooring line. The line is simplified to a spring having stiffness $k = \frac{EA}{l_0}$.

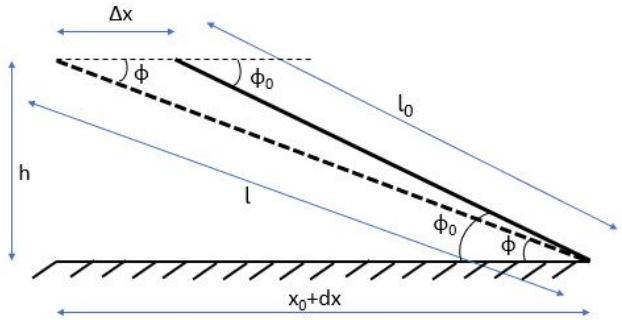

Figure 3.12: Sketch of stretching of a mooring line

The known parameters are the vertical distance from the fairlead to the sea bottom, h, the unstretched length of the mooring line, l_0, and the elastic stiffness, EA. The initial top angle, ϕ_0, and the initial horizontal distance from the anchor to the fairlead, x_0, are given by $\phi_0 = \sin^{-1}\left(\frac{h}{l_0}\right)$ and $x_0 = l_0 \cos\phi_0$ by geometry.

The unstretched line is then stretched a horizontal distance Δx, giving it a total horizontal stretched length of $dx = dx + \Delta x$, where dx is the total horizontal stretched distance. Hence, in the first stretching of the line, $dx = 0$. The total horizontal distance, x, will then be $x = x_0 + dx$. The new top angle is now given by Equation 3.45

$$\phi = \tan^{-1}\left(\frac{h}{x_0 + dx}\right) \tag{3.45}$$

By geometry, the line have now been stretched a distance $dl = dl + \Delta l$, where $\Delta l = \Delta x \cos\phi$. The tension, T, and the horizontal tension , T_H at fairlead are then given by Equation 3.46 and 3.47 respectively.

$$T = \frac{EA}{l_0} dl \tag{3.46}$$

$$T_H = T\cos\phi \tag{3.47}$$

3.7 Analysis of fiber rope mooring systems

The original length of a fiber rope, l_0, is the length of the rope after production. The original length is measured after holding the rope at a reference-tension for a given time. The reference tension can be found in DNV-OS-E303 (October 2010) [11] to be 5 N/ktex held in 17 minutes. The strain, ϵ, of a fiber rope is given by the ratio of the change in length (stretch) to the original length of the fiber rope, where the stretch is given by $dl = l - l_0$.

The spring-dashpot model in Figure 3.13 can be used as a simplied model of how a fiber rope behaves. It consists of a permanent strain part and an elastic strain part. The effects of having chain at the beginning and end of the rope, and the effect of buoys are not included in the model. This leads to a missing geometric stiffness from the chain, and some drag effects [11].

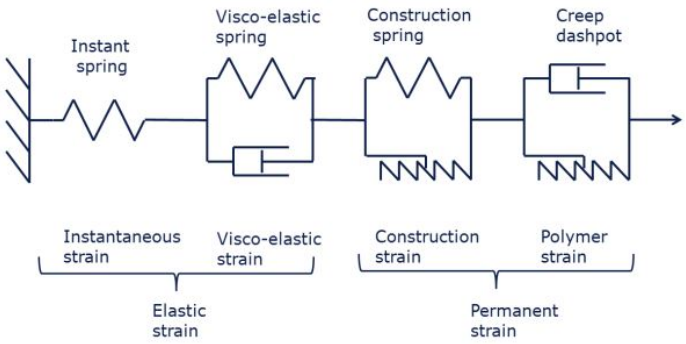

Figure 3.13: Spring-dash model of a fiber rope [11]

The typical behavior of a fiber rope is given in Figure 3.14. The four expressions representing the arrows in the figures are explained below

- Extension: When the fiber rope length increases because of increasing tension
- Elongation: When the fiber rope length increases at a constant tension
- Retraction: When the fiber rope length decreases because of decreased tension
- Contraction: When the fiber rope length decreases at a constant tension

It can be seen that the rope is elongated after reaching a wanted value of the tension. When the tension then decreases, the rope is more elongated than before the extension. When reaching the lower value of the tension, the rope will then start contracting.

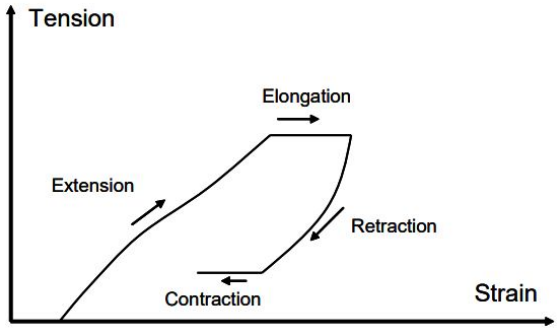

Figure 3.14: Typical behaviour of a fiber rope [11]

When increasing the axial tension in the rope fast for the first time, the tension-strain curve that is obtained is called the original curve, as shown by the red curve in Figure 3.15. The maximum curve, shown as the green curve, is the original curve added with visco-elastic strain and polymer strain. This curve is also called the original working curve [5], and represents the working points when the fiber rope is at is previous highest mean tension. To obtain the green curve, the

tension has to either be increased very slowly, or it has to be increased fast in steps holding the tension between each loading until the polymer strain and working strain has been taken out [5]. After stabilizing the visco-elastic strain at a tension lower than the maximum mean tension, the stress-strain curve will be as a blue curve given in the figure. The curve is called a working curve. The stationary sea-state decides which highest mean tension, called a working point, the rope will have, and hence which of the working curves it will follow. The stress-strain relationship will move up and down along a working curve during a stationary sea-state. Each stationary sea state is assumed to last 3 hours. The mean working length of the rope will then be decided by the working curve and mean tension. When doing fiber rope calculations, the working curve is used to calculate the offset statically, and the dynamic stiffness curve is used to calculate the strain. The dynamic stiffness can be seen as the purple lines in the figure. Increasing the mean tension will increase the dynamic stiffness. Testings of fiber ropes have shown that the dynamic stiffness increases with time for a rope being in use. Hence, for extreme value calculations, the upper limit of the dynamic stiffness should be used. Experiments have shown that the dynamic follows a linear model given by Equation 3.48 [11].

$$K_d = a + bT_{mean} \tag{3.48}$$

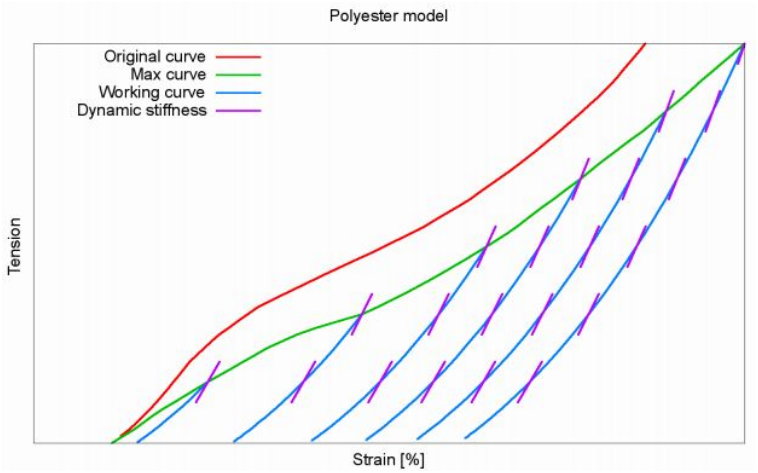

Figure 3.15: Typical polyester model [11]

During the installation of a fiber rope, a high tension is held for a long time to get visco-elastic strain and polymer strain in the rope. This is called the installation tension. The pre-tension is, as for a catenary chain mooring system, the tension when the mooring lines are at static equilibrium without being exposed to environmental forces. It is important to take the strain into consideration during installation. If the rope is installed with a pre-tension T_1 and a strain ϵ_1, and then increased to a tension T_2 and decreased back to T_1 during installation, the working

curve will move from the red curve to the green curve in Figure 3.16. Hence, the strain will increase from ϵ_1 to ϵ_2. In a similar way, if the tension was increased to T_3, the strain would be ϵ_3.

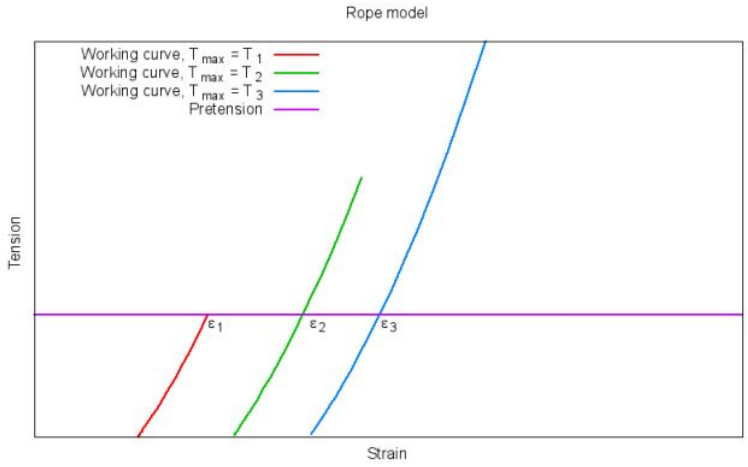

Figure 3.16: Consequences of increasing the tension during an installation [11]

3.8 The dynamic equation of motion

The dynamic equation of motion in six degrees of freedom is given by Equation 3.49 [23].

$$(M + A(\omega))\,\ddot{r} + D(\omega)\,\dot{r} + B_1\dot{r} + B_2\dot{r}|\dot{r}| + C(r)\,r = Q(t, r, \dot{r}) \tag{3.49}$$

where

- M is the mass matrix
- A(ω) is the added mass matrix
- D(ω) is the potential damping matrix
- B_1 is the linear damping matrix
- B_2 is the quadratic damping matrix
- C(r) is the stiffness matrix
- r, $\dot{r}$ and $\ddot{r}$ are the position vector, the velocity vector and the acceleration vector respectively

- Q(t,r,$\dot{r}$) is the excitation force vector, consisting of the terms below:
  - q^1_{wa}: First order wave forces
  - q^2_{wa}: Second order wave forces
  - q_{wi}: Wind forces
  - q_{cu}: Current forces

The first term of Equation 3.49 is representing the inertia forces term provided by the mass of the structure, and the hydrodynamic mass. The second term is the damping forces term, provided by mainly drag forces on the hull of the floating structure. The drag forces on the mooring lines also give some damping of the motions. The third term is representing the stiffness and restoring forces, which are provided by the mooring lines. The term on the right hand side represents the excitation forces from waves, wind, and current [23].

The stiffness term is determined by the mooring lines. The stiffness limits the mean offset and the LF motions. The total stiffness, k_T can be divided into two parts: Geometric stiffness, k_G, and elastic stiffness, k_E, as illustrated in Figure 3.17. The geometric stiffness comes from the weight of the line, the pretension of the line, the length of the line and buoy weights. The geometric stiffness is dominating when the mooring system is a catenary chain or steel wire system. The elastic stiffness comes from the line axial elongation/stretch. It is dominating for polyester ropes where the stiffness is provided by stretching of the line.

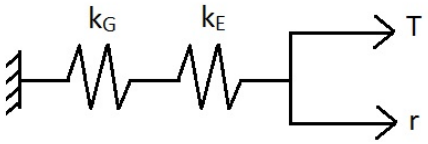

Figure 3.17: Geometric and elastic stiffness

The relationship between the total stiffness, and the elastic and geometrical stiffness can then be written as in Equation 3.50

$$\frac{1}{k_T} = \frac{1}{k_G} + \frac{1}{k_E} \tag{3.50}$$

3.8.1 Equivalent linearization

In the thesis, the natural periods and the linear and quadratic damping of the FWT are to be found by a decay test. The dynamic equation of motion given in Equation 3.49 is simplified to the one-degree of freedom system with non-linear damping given in Equation 3.51 [35]. Since the structure is oscillating freely in the decay test after being let go, there is no external load term on the right hand side of the equation.

$$M_{tot}\ddot{r} + B_1\dot{r} + B_2\dot{r}|\dot{r}| + Cr = 0 \tag{3.51}$$

Where

- M_{tot} is the mass of the system, including added mass.
- B_1 is the linear damping term of the system
- B_2 is the quadratic damping term of the system
- C is the restoring stiffness term of the system
- $\ddot{r}$ $\dot{r}$ and r are the displacement, velocity and acceleration of the system respectively

For an undamped system, the equation of motion can be written as in Equation 3.52

$$M_{tot}\ddot{r} + Cr = 0 \tag{3.52}$$

Assuming harmonic motion, the displacement, velocity and acceleration can be found as in Equation 3.53

$$r(t) = r_0\sin(\omega t), \quad \dot{r} = \omega r_0\cos(\omega t) \quad \text{and} \quad \ddot{r} = -\omega^2 r_0\sin(\omega t) \tag{3.53}$$

By inserting the expressions in Equation 3.53 into the equation of free undamped motion in Equation 3.52, the undamped natural frequency, ω_0, can be found as given in Equation 3.54

$$\omega_0 = \sqrt{\frac{C}{M_{tot}}} \tag{3.54}$$

If the natural period and the stiffness is known, the total mass, M_{tot} can be found. Then the added mass can be found by subtracting the known mass of the structure. The linear and non-linear damping is now to be found. Dividing Equation 3.51 by M_{tot}, Equation 3.55 can be found

$$\ddot{r} + p_1\dot{r} + p_2\dot{r}|\dot{r}| + p_3 r = 0 \tag{3.55}$$

Now, the method of equivalent linearization is applied. In this method, the non-linear damping term is replaced by a linear term, shown as p_{EQ} in Equation 3.56

$$\ddot{r} + p_{EQ}\dot{r} + p_3 r = 0 \tag{3.56}$$

The linear term, p_{Eq} is found from requiring equal damping per energy cycle, given in Equation 3.57

$$p_{EQ} = p_1 + \frac{8}{3\pi}\omega r_0 p_2 \tag{3.57}$$

where ω is the oscillation frequency, and r_0 is the amplitude of a motion cycle. Satisfying Equation 3.57, p_{EQ} is given as in Equation 3.58

$$p_{EQ} = 2M\omega_0\zeta = \frac{2C\zeta}{\omega_0} \tag{3.58}$$

where the damping ratio, ζ, is the ratio between the actual damping, p, and the critical damping, $p_{cr} = 2M\omega_0$ as in Equation 3.59

$$\zeta = \frac{p}{2M\omega_0} \tag{3.59}$$

where:

- $0 < \zeta < 1$: The system is underdamped
- $\zeta = 1$: The system is critically damped
- $\zeta > 1$: The system is overdamped

Figure 3.18 shows the response for different values of the damping ratio.

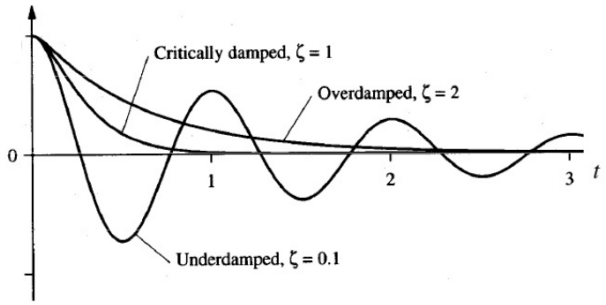

Figure 3.18: Damping of a system for different damping ratios, ζ

The logarithmic decrement, Λ is the natural logarithm of the ratio between two successive maxima r_1 and r_2, as given in Equation 3.60

$$\Lambda = ln\left(\frac{r_1}{r_2}\right) = \zeta\omega_0\frac{2\pi}{\omega_d} = 2\pi\frac{\zeta}{\sqrt{1-\zeta^2}} \tag{3.60}$$

Where ω_d is the damped natural frequency between two amplitudes, r_1 and r_2, which can be written as in Equation 3.61.

$$\omega_d = \omega_0\sqrt{1-\zeta^2} \tag{3.61}$$

Using this method, p_{EQ} and Λ can be found for each cycle of the measured logaritmic decrement. Then ζ can be plotted against the mean amplitude between two successive amplitudes, as in Figure 3.19. A linear least squares curve can then be fitted to the measured damping plot. The linear damping term, p_1, can now be found at the intersection with the abscissa. The nonlinear term, p_2, can be found as the slope of the fitted curve. As the figure illustrates, the first and last oscillations should be avoided due to transient effects and inaccuracy, respectively.

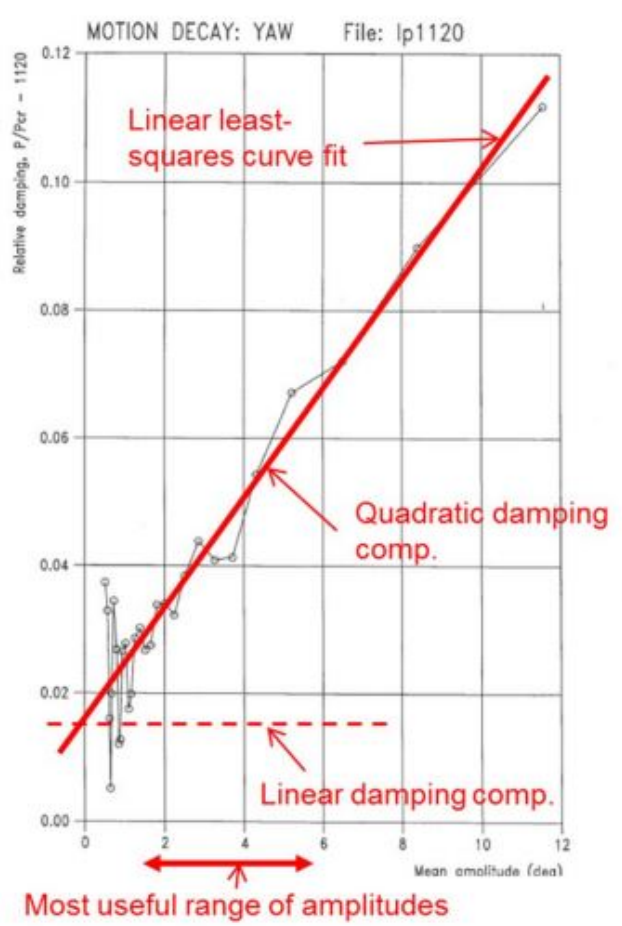

Figure 3.19: Example of equivalent linearization method for finding linear and quadratic damping terms [35]

Typical natural oscillation periods for semi submersibles are given in Table 3.1 [23].

Table 3.1: Typical natural periods for a semi-submersible [23]

Structure	Surge/sway period [s]	Heave period [s]	Roll/pitch period [s]	Yaw period [s]
Semi-submersible	>100	20-25	45-60	>100

3.9 Standards

In contrast to the oil- and shipping industry, there are currently few existing standards and procedures for offshore wind turbines.

The DNV (Det Norske Veritas) standard DNV-OS-J103 *Design of floating wind turbine structures* gives the requirements and guidelines for design of floating wind turbine structures. It also gives guidance about transportation, installation and in-service analyses. The parts covered are the substructure of the wind turbine, and the station keeping system. It does not give the standards for design of components in the drivetrain, like the nacelle, gearbox, generator and rotor. The rotor blade design can be found in the DNV-DS-J102. The DNV-OS-J101 *Design of Offshore Wind Turbine Structures*, gives the standards for fixed wind turbines. The IEC 61400-3 standard gives the additional structural design guidelines for components in offshore wind turbines that are not represented by DNV standards. The DNV-OS-E301 *Position mooring*, gives the standard for position mooring, and can hence be used for mooring line design and construction. The DNV-OS-C101 *Design of Offshore Steel Structures, General*, is the general certification for steel structures.

There are also other standards existing. The *Guideline for the Certification of Offshore Wind Turbines* by Lloyds Register (LR) contains guidelines and requirements for design of offshore wind turbines and wind farms. The *Guide for Building and Classifying Offshore Wind Turbine Installations* by ABS (American Bureau of Shipping) gives guidelines for construction, design, installation and survey of floating offshore structures. The *Guide for Building and Classing Bottom-Founded Offshore Wind Turbine Installations* by ABS gives the same criteria for bottom-fixed offshore wind turbines.

The following list presents some common standards for offshore wind turbines:

- Fixed offshore wind turbines
  - DNV-OS-J101 *Design of Offshore Wind Turbine Structures*, Det Norske Veritas AS, May 2014
  - *Guideline for the Certification of Offshore Wind Turbines*, Germanischer Lloyd, 2012
  - *Guide for Building and Classing Bottom-Founded Offshore Wind Turbine Installations*, American Bureau of Shipping, July 2014
  - IEC 61400-3,*Wind turbines-Part 3: Design requirements for offshore wind turbines*, International Electrotechnical Commission, 2009

- Floating offshore wind turbines
  - DNV-OS-J103 *Design of Floating Wind Turbine Structures*, Det Norske Veritas AS, June 2013
  - *Guide for Building and Classing Floating Offshore Wind Turbine Installations*, American Bureau of Shipping, July 2014
  - *Guideline for the Certification of Offshore Wind Turbines*, Germanischer Lloyd, 2012
- Steel structures and mooring
  - DNV-OS-C101 *Design of Offshore Steel structures, General*, Det Norske Veritas AS, April 2011
  - DNV-OS-E301 *Position mooring*, Det Norske Veritas AS, October 2010

3.10 Mooring line design criterias, mooring failure modes

When designing an offshore wind turbine, the ultimate (ULS), accidental (ALS), and fatigue (FLS) limit states should be considered. To find the limit states, the DNV standards DNV-OS-J103 *Design og Floating Wind Turbine Structures* [3] and DNV-OS-E301 *Position Mooring* [2] have been used.

3.10.1 Safety class

There are three safety classes for structures [3].

- Low safety class: Low risk of human injuries, environmental damages, economic losses, and no risk of human life.
- Normal safety class: Some risk of human injuries, environmental pollution and high economic loss
- High safety class: Significant risk of human injuries, environmental pollution and economic loss

Floating wind turbines are normally set to a normal or low safety class because they are unmanned during extreme conditions [3]. In addition, pollution is minor if a FWT fails. In this thesis, the safety class will be set to low.

3.10.2 Ultimate Limit State (ULS)

The Ultimate Limit State (ULS) is designing against failure due to extreme weather having a return period of e.g 50 years. Normal failures are yielding, buckling, capsizing and overturning. The limit state is the maximum resistance to the extreme loads [3].The ULS design requirement for both catenary mooring lines and taut mooring lines are given by Equation 3.62 [3].

$$S_C > T_d \tag{3.62}$$

where S_C is the characteristic capacity of the mooring line, and T_d is the design tension of a mooring line. T_d is given by Equation 3.63.

$$T_d = \gamma_{mean} T_{c,mean} + \gamma_{dyn} T_{c,dyn} \leq 0 \tag{3.63}$$

where γ_{mean} is a mean tension safety factor, and γ_{dyn} is a dynamic tension safety factor, which are found to be 1.3 and 1.75 respectively [3] for a normal safety class, which is the lowest safety class for ULS given in the standard. $T_{c,mean}$ is the characteristic mean line tension caused by pretension and environmental loads (static wind, wave drift and current), and $T_{c,dyn}$ is the characteristic dynamic line tension caused by wave-frequency (WF) and low-frequency (LF) motions. $T_{c,mean}$ and $T_{c,dyn}$ should be found for the combination of the significant wave height, H_s, the peak period, T_p, and wind velocity at 10 m above the SWL, U_{10} for a 50 year return period giving the highest line tension. It is also important to check for the rated wind speed, because this might give a higher line tension than at the extreme wind speed. The characteristic capacity, S_C, is given by Equation 3.64

$$S_C = \mu_S(1 - COV_S(3 - 6COV_S)), \quad COV_S < 10 \tag{3.64}$$

where μ_S is the mean breaking strength of the mooring line, and COV_S is the coefficient of variation for the breaking strength of the mooring line. If these parameters are unknown, Equation 3.65 can be used

$$S_C = 0.95 S_{mbs} \tag{3.65}$$

where S_{mbs} is the minimum breaking strength of the mooring line

3.10.3 Accidental Limit State (ALS)

Accidental Limit State (ALS) is designing against accidental events leading to collapse in extreme weather having a return period of e.g 50 years. The limit state will be a survival condition in damaged condition [3]. The mooring system should be able to survive when one mooring line has failed [10].

As for ULS, the ALS requirement is that the characteristic capacity, S_C should be greater than the design tension, T_d (Equation 3.62). However, T_d should be found for a FWT having one missing mooring line. S_C is calculated according to equation 3.64 or 3.65. T_d is calculated according to Equation 3.63, where the load factors are $\gamma_{mean} = 1.00$ and $\gamma_{max} = 1.10$ for a normal safety class [3].

A failure of a mooring line usually leads to a breakage of the power cable. It is important to design the fairleads to withstand the rotation/bending that happens to the connections when the wind turbine changes location due to a missing mooring line. The tension in the two remaining lines will be lower than the tension that was in the failed line before failure.

3.10.4 Permissible horizontal offset

It is important to have a sufficient horizontal distance between a moored structure and other structures. The distance should take into consideration horizontal offsets of the moored structure when exposed to environmental forces, and horizontal offsets after a line failure. For a catenary mooring system where anchors can not take any vertical forces, the length should be long enough to avoid uplifting of the mooring line at the anchor position in ULS condition. In ALS, the anchor may experience vertical forces if the characteristic capacity of the anchors is not highly reduced by the vertical forces [2].

3.10.5 Fatigue Limit State (FLS)

Fatigue Limit State (FLS) is designing against failure due to cyclic loads leading to crack growth. The limit state is the failure caused by the cyclic loads [3]. The fatigue life can be calculated by Palmgren Miner's sum as in Equation 3.66

$$D = \sum_{i=1}^{I} \frac{n_i}{N_i} \tag{3.66}$$

where D is the damage, I is the number of stress ranges, n_i is the number of cycles over a time period, and N_i is the number of stress cycles until failure at the given stress range.

The design criteria is that the fatigue damage, D, is smaller than 1: $D\gamma_F < 1$, where γ_F is a safety factor. The safety factor is in the range $3 < \gamma_F < 8$ for chain and wire depending on how often the wind turbine can be inspected, and $\gamma_F = 60$ for polyester rope [10].

FLS for chain and steel wire

Equation 3.67 can be used to calculate the component capacity against tension fatigue for chain and steel wire ropes.

$$n_c(s) = a_D s^{-m} \tag{3.67}$$

where $n_c(s)$ is the number of cycles, a_D is a parameter from the SN-curve given in Table 3.2, s is the stress range, and m is the slope of the SN-curve, given in Table 3.2. A typical SN-curve for the different mooring line materials is given in Figure 3.20. The linearized form of the equation is given as in Equation 3.68

$$\log(n_c(s)) = \log(a_D) - m\log(s) \tag{3.68}$$

Table 3.2: a_D and m for chain and steel wire [2]

Material type	a_D	m
Stud chain	1.2e11	3.0
Studless chain	6.0e10	3.0
Stranded rope	3.4e14	4.0
Spiral rope	1.7e17	4.8

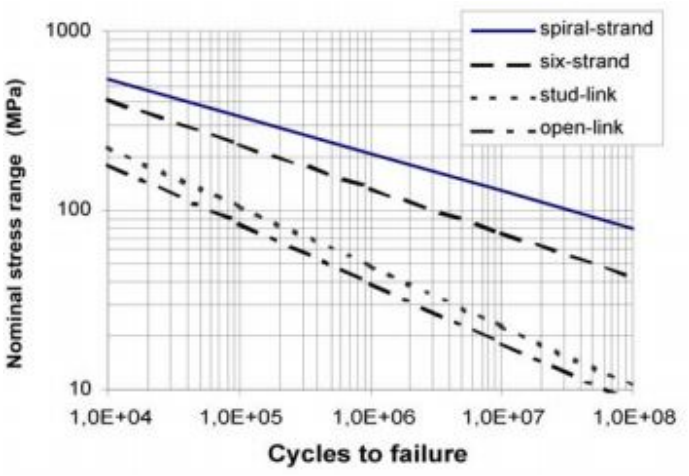

Figure 3.20: SN-curve for chain and steel wire [2]

FLS for fiber rope

To calculate the fatigue capacity for a fiber rope, the relative tension, R, should be used instead of the stress, s. The component capacity against tension fatigue can be calculated as given in Equation 3.69

$$\log(n_c(R)) = \log(a_D) - m\log(R) \tag{3.69}$$

where a_D and m are given in Table 3.3

Table 3.3: a_D and m for fiber rope [2]

Material type	a_D	m
Polyester rope	0.259	13.46

Since the relative tension, R, has to be used instead of the stress, s, an RN-curve has to be used instead of an-SN curve.

3.11 Extreme value statistics

Extreme value statistics will be used to find the distribution of the maximum values in an extreme condition. Figure 3.21 shows the distribution of the surface elevation, the individual maxima and the extreme values for a duration.

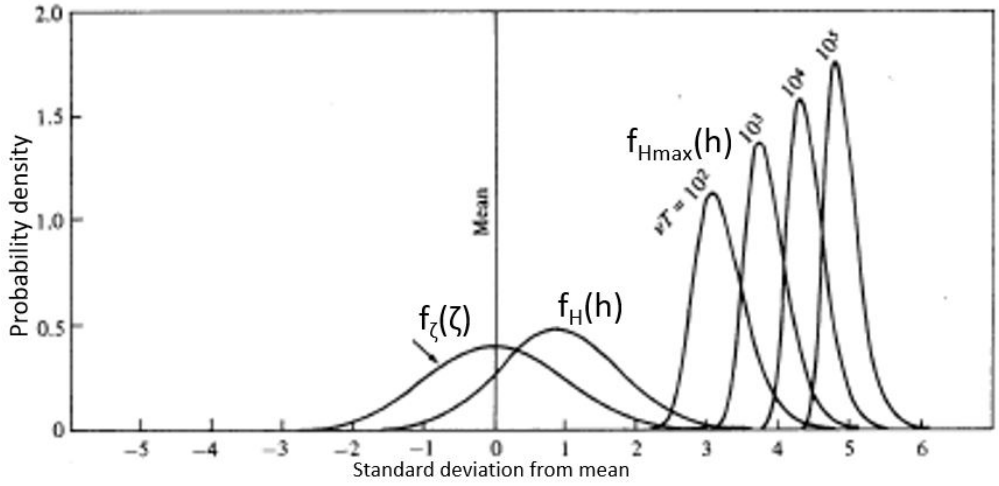

Figure 3.21: Extreme value distribution [21]

The different distributions in the figure are:

- $f_\zeta(\zeta)$ is the surface elevation distribution (Gauss distributed)
- $f_H(h)$ is the distribution of individual maxima (Rayleigh or Rice distributed)
- $f_{H_{max}}(h)$ is the distribution of the largest maximum among N maxima (extreme value distributed, e.g a Gumbel distribution).

For offshore structures, it is important to look at the extreme conditions. The extreme values will vary from one extreme condition to another. Therefore, a distribution can be made by taking the largest maxima from each extreme condition timeline in a large amount of extreme condition time lines, as shown in Figure 3.22.

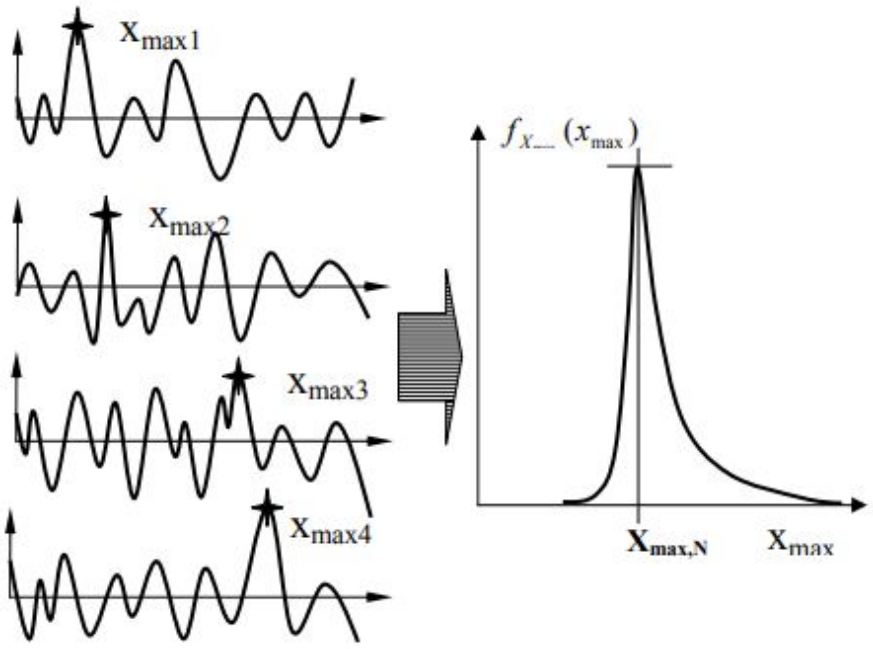

Figure 3.22: Extreme value distribution [21]

The extreme value distribution of the largest maxima, X_{max} can then be found to be given by 3.70 [21] where N is the number of maximas in a time period, σ_x is the standard deviation of the distribution and x_{max} is a given value of a maxima. It can be seen from the equation that the distribution depends on the duration of the seastate, unlike the Gauss distribution of the wave elevations, and the Rayleigh distribution of a single wave. If the duration increases, the extreme value distribution peaks will be narrower and move towards the right in the figure.

$$F_{x_{max}}(x_{max}) = P(X_{max} < x_{max}) = \left[1 - exp\left(\frac{-x_{max}^2}{2\sigma_x^2}\right)\right]^N \tag{3.70}$$

From equation 3.70, it can be found that the most probable maxima, X_{max_N} among N peaks, and the expected value of the maxima, $\overline{X}_{max_N}$ among N peaks are given by equation 3.71 and 3.72 [21].

$$X_{max_N} = \sigma_p \sqrt{2 \ln N} \tag{3.71}$$

$$\overline{X}_{max_N} = \sigma_p \left(\sqrt{2 \ln N} + \frac{0.5772}{\sqrt{2 \ln N}} \right) \tag{3.72}$$

where σ_p is the standard deviation of the Gauss distribution of the wave elevation. As seen in the two equatons, the expected value of the maxima, $\overline{X}_{max_N}$ will be larger than most probable value, X_{max_N}.

3.11.1 Gumbel distribution

The Gumbel distribution can be used to estimate the extreme value distribution. The Gumbel distribution, $F_y(y)$ and its probability density function, $f_y(y)$ is given by equation 3.73 and 3.74 respectively [25].

$$F_y(y) = e^{-\{e^{-\alpha(y-u)}\}} \quad -\infty \leq y \geq \infty \tag{3.73}$$

$$f_y(y) = \alpha e^{\{-\alpha(y-u) - e^{-\alpha(y-u)}\}} \tag{3.74}$$

where α, y, u can be found by the Gumbel estimators in equation 3.75 and 3.76

$$\hat{\alpha} = \frac{c_1}{\hat{s}_y} \tag{3.75}$$

$$\hat{u} = \hat{\mu}_y - \frac{c_2}{c_1} \hat{s}_y \tag{3.76}$$

where c_1 and c_2 are found from equation 3.77 and 3.78 respectively. N_y is the size of the extreme value sample.

$$c_1 = \sqrt{c_3 - c_2^2} \tag{3.77}$$

$$c_2 = \frac{1}{N_y} \sum_{i=1}^{N_y} -\ln \left[-\ln \left(\frac{i}{N_y + i} \right) \right] \tag{3.78}$$

$$c_3 = \frac{1}{N_y} \sum_{i=1}^{N_y} \left[\ln \left[-\ln \left(\frac{i}{N_y + i} \right) \right] \right]^2 \tag{3.79}$$

When using the Gumbel parameters $c_1 = 1.28255$ and $c_2 = 0.57722$ [25] in the calculations, it leads to Gumbel estimators $\hat{\alpha} = \frac{1.28255}{\hat{s}_y}$ and $\hat{u} = \hat{\mu_y} - 0.45\hat{s}_y$. $\hat{s}_y$ is the standard deviation of the data and $\hat{\mu}_y$ is the expected value of the data. When plotting the Gumbel probability density function (pdf), $\hat{u}$ will be the peak-value of the pdf (the most probable value), and $\hat{\mu_y}$ will be the expected value, being slightly larger than the most probable value

Chapter 4

Initial Model

4.1 Coordinate system

The origin of the coordinate system is set to be at the mean sea-level. The x-axis is pointing in the direction opposite of the wind-direction, normal to the rotor disk. The z-axis is pointing vertically upwards trough the center of the tower and the center column. The coordinate system, and the direction of the incoming weather is illustrated in Figure 4.1a. This coordinate system is in compliance with the degrees of freedom presented in Section 3.1. A picture of the model from SIMA can be seen in Figure 4.1b

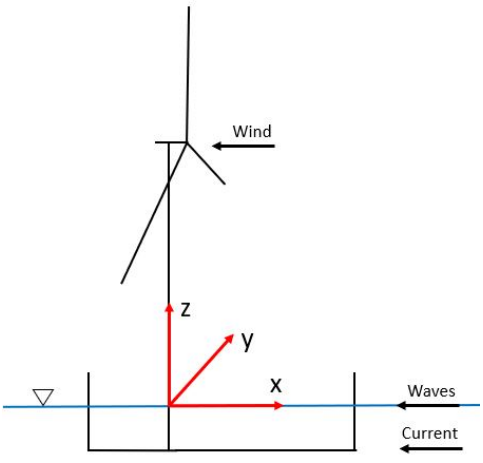

(a) Coordinate system of the floating wind turbine

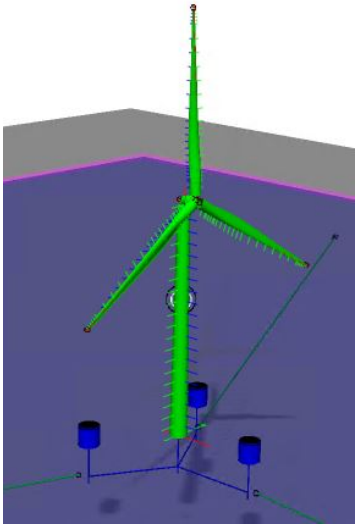

(b) The floating wind turbine in SIMA.

Figure 4.1

4.2 Wind turbine

The wind turbine chosen for the model is the DTU 10MW RWT, which is a reference wind turbine inspired by the NREL 5MW RWT [9]. The NREL 5MW RWT is a reference wind turbine made by the National Renewable Energy Laboratory [19]. Some important properties of the wind turbine are given in Table 4.1 [9].

Table 4.1: Properties of the wind turbine

Property	Value
Configuration	3 blades, upwind
Maximum thrust [kN]	1500
Cut-in wind speed [m/s]	4
Cut-out wind speed [m/s]	25
Rated wind speed [m/s]	11.5
Rated power [MW]	10
Rotor diameter [m]	178.3
Hub height [m]	119
Rotor mass [t]	231
Nacelle mass [t]	446
Tower mass [t]	628
Total wind turbine mass [t]	1304

4.2.1 Tower drag

Since the tower drag was not included in the model, the tower drag coefficients had to be found. This was done by using Figure 3.8 in Section 3.5.1. To use this figure, the Reynolds number for the tower had to be found by Equation 3.20. Since the diameter of the tower was varying, the tower was split up into 12 sections, as also done in the SIMA model. The cross sectional area of each section was found in the SIMA model, and the diameter, D, of each section was calculated from these. The kinematic viscosity, ν, was found from DNV-RP-C205 to be $\nu = 1.45e^{-5}$ for sea water of 15° [4]. The velocity, U at each cross section height was calculated by Equation 3.22. The tower is assumed to be smooth. The drag coefficients at some selected wind velocities are shown in Table 4.2. It was found that the drag coefficient was approximately constant for the whole tower for each of the wind velocities. Since the graph in Figure 3.8 does not show the drag coefficient for large Reynolds numbers, it is assumed that it will converge to $C_D = 0.7$ for large Reynolds numbers.

Table 4.2: Drag coefficients at tower for selected wind velocities

Wind velocity at hub height [m/s]	C_D
0.01	0
8	0.6
11	0.65
25	0.7
46.5	0.7

4.3 Mooring system

The reference 10MW floating wind turbine was originally designed for a 200 m water depth. In this Master thesis, the system will be adjusted to a 70 m water depth. The floating wind turbine has a catenary mooring system consisting of three lines made of chain. The three lines are equally spaced, giving an angle of 120 degrees between each line. The draft of the semi-submersible is 20 m. The fairleads are connected outside the columns of the semi-submersible, at a depth of 15 m below the water surface. Figure 4.2 and 4.3 illustrate the mooring system and the numbering of the mooring lines. The initial position of the three fairleads, and the corresponding initial anchor positions are given in Table 4.3.

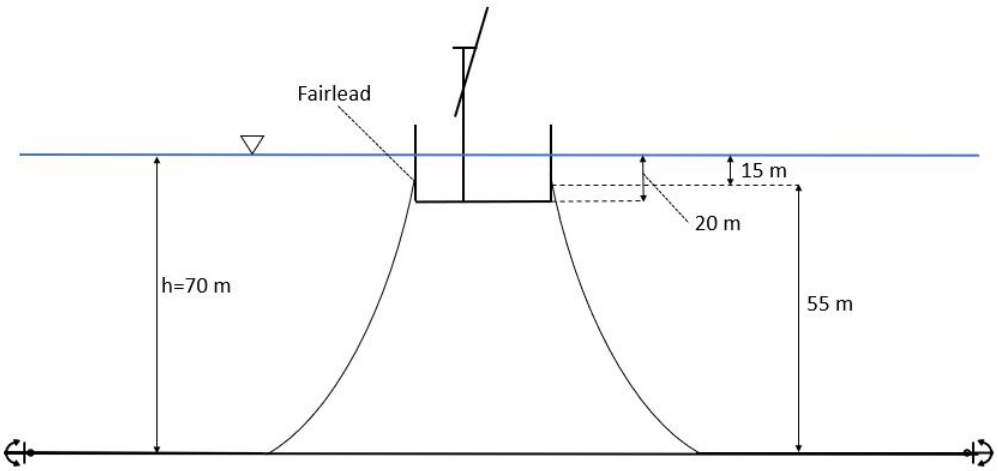

Figure 4.2: Illustration of mooring system and fairlead position

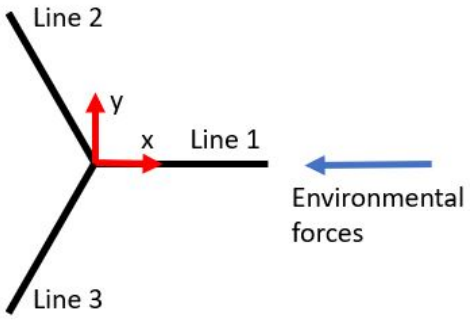

Figure 4.3: Line numbering and direction of incoming weather. The z-axis is pointing out of the paper

Table 4.3: Initial position of fairleads and anchors

	x [m]	y [m]	z [m]
Fairlead 1	50	0	-15
Fairlead 2	-25	43.301	-15
Fairlead 3	-25	-43.301	-15
Anchor 1	893.21	0	-70
Anchor 2	-446.60	773.54	-700
Anchor 3	-446.60	-73.54	-70

The weight and diameter of the mooring lines in the already existing SIMA model was changed to a chain type found in the given Ramnäs Bruk Product Catalogue [30]. The chain type, R4-studless, was chosen to be the same as for the existing model. The unit weight was chosen to be as close as possible to the existing unit weight of 465 kg/m. The chain is simplified into a cylinder form, giving it a circular cross-section. The force balance of the mooring line is given in Equation 4.1.

$$m_a g - F_{buoy} = m_w g \tag{4.1}$$

where m_a and m_w are the unit weight of chain in air and water, respectively, expressed in [kg/m]. g is the gravitational acceleration, and F_{buoy} is the buoyancy of the chain, found by $F_b = \rho_{water} A g$ where A is the external cross section area of the chain given by $A = \frac{\pi D^2}{4}$ where D is the diameter of the circular cross-section. When inserting the expression for the buoyancy, Equation 4.1 can be simplified into Equation 4.2

$$m_w = m_a - \rho_w A \tag{4.2}$$

Since the weight of chain in water, m_w, is not given in the Ramnäs Bruk Product Catalogue, the relationship between m_w and m_a, given in Equation 4.3 is used.

$$m_w = \left(\frac{\rho_{chain} - \rho_{water}}{\rho_{chain}} \right) m_a = 0.87 m_a \tag{4.3}$$

where $\rho_{chain} = 8759 kg/m^3$ is the density of the chain, $\rho_{water} = 1025 kg/m^3$ is the density of water. Using this relationship, the external area, A, in Equation 4.2, and the diameter, D, can be expressed as in Equation 4.4. The final parameters of the mooring system can be seen in Table 4.4.

$$A = \frac{0.13 m_a}{\rho_{water}}, \quad \text{and} \quad D = \sqrt{\frac{4A}{\pi}} \tag{4.4}$$

Table 4.4: Properties of the mooring system of the reference 10 MW wind turbine

Property	Value
Mooring system	Catenary
Material	Studless R4
Density steel chain [kg/m^3]	7850
Number of mooing lines	3
Angle between adjacent mooring lines [deg]	120
Length of each line [m]	845
Vertical length from fairlead to sea bottom [m]	55
Mass of each line in air [kg/m]	462
Mass of each line in water [kg/m]	401
Diameter of chain [m]	0.153
External area of each mooring line [m^2]	0.0590
External diameter of each line [m]	0.274
Elastic stiffness, EA [kN]	3.7789e6
MBS [kN]	20156

4.4 Semi-submersible

The semi-submersible is designed in Qiang Wang's Master Thesis [37]. The semi-submersible consists of a center column, and three side columns connected to the center column by pontoons. The center column has the same diameter as the bottom of the tower, which sits on this column. The three side columns reach 15 m above the still water line (SWL). The radius of 45 m of the side columns give the structure enough restoring stiffness [37]. The pontoons are connected to the columns 13 m below the SWL. They provide space for ballast, and connect the side columns. The total draft of the semi-submersible is 20 m. The fairleads are connected to the outer part of the columns 15 m below the SWL. Table 4.5 gives some of the main dimensions of the semi-submersible. A sketch of the main dimensions of the semi-submersible seen from the side and seen from above is given in Figure 4.4. The mass and buoyancy calculations of the semi-submersible are given in Section 4.5

Table 4.5: Properties of the floating wind turbine

Property	Value
Depth of fairleads [m]	15
Draft of substructure [m]	20
Freeboard [m]	15
Radius to fairleads from center of substructure [m]	50
Angle between pontoons [deg]	120
Thickness [m]	0.04

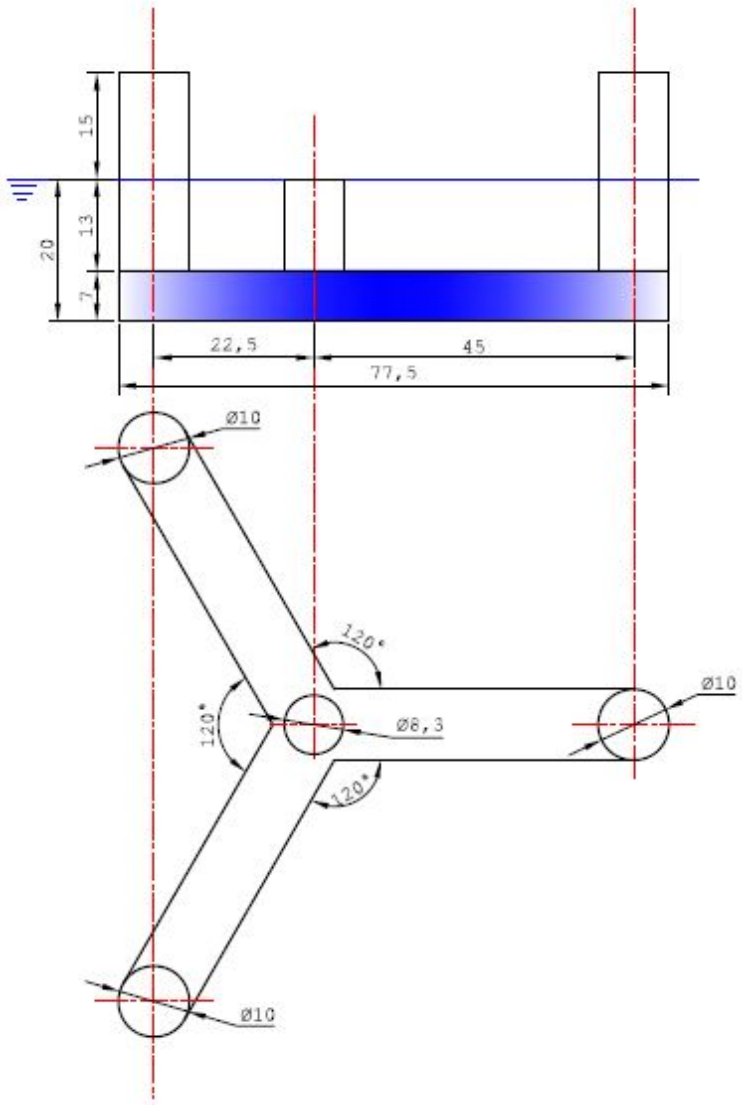

Figure 4.4: Dimensions of the semi-submersible [37]

4.5 Weight and hydrostatic stiffness calculations

SIMO assumes that the floating body is neutrally buoyant. This means that it sets the buoyancy of the SIMO body, F_{buoy} equal to the weight of the semi-submersible, $W_{semi} = m_{semi}g$, where m_{semi} is the mass of the semi-submersible. However, the buoyancy of the structure is in reality much larger than the weight of the semi-submersible due to the weight of the wind turbine and the mooring lines. To model this in SIMA, a specified force located in the origin is set to be equal to the missing buoyancy that is needed to obtain the wanted draft of the structure. The specified force is found by Equation 4.5, as seen in Figure 4.5.

$$F_{specified} = F_{buoy} - W_{semi} \tag{4.5}$$

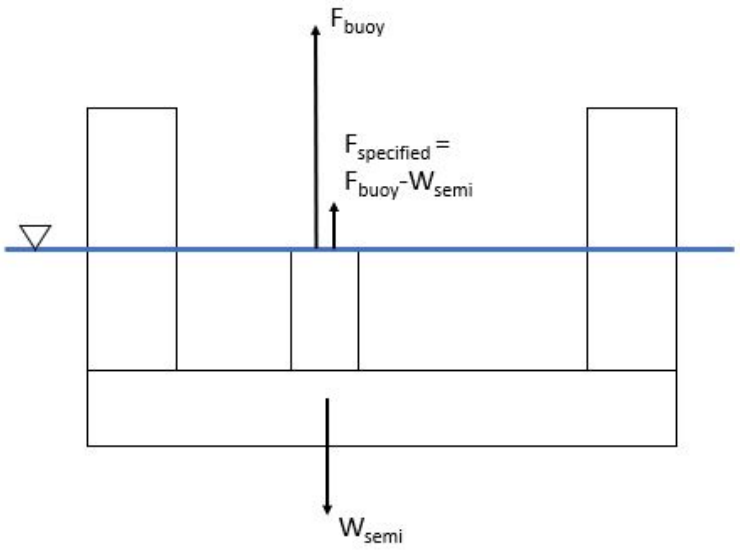

Figure 4.5: Forces on the semi submersible in SIMA

4.5.1 Buoyancy calculations

The buoyancy when having a draft of 15 m is found. The results of the buoyancy calculations are shown in Table 4.6.

Table 4.6: Semi calculations

Part	Immersed volume [m^3]	Weight displacement [t]	Buoyancy [kN]	CB [m]
Center column	703.38	720.96	7072.62	(0,0,-6.5)
Side columns	3063.05	3139.63	30799.77	(0,0,-6.5)
Pontoons	9971.56	10220.85	100266.54	(0,0,-16.5)
Total	13737.99	14081.44	138138.93	(0,0,-13.76)

4.5.2 Mass calculations

The mass and center of gravity of the semi-submersible without ballast are calculated from Figure 4.4. The semi-submersible is made of steel having a density of $\rho_{steel} = 7850 kg/m^3$. The walls of the different parts have a thickness of 40 mm. The mass calculations of the semi-submersible are given in Table 4.7.

Table 4.7: Mass calculations of the semi-submersible

Part	Outer volume [m^3]	Inner volume [m^3]	Steel volume [m^3]	Mass [kg]	CG [m]
Center column	703.38	689.89	13.49	105.90	(0,0,-6.5)
Side columns	6597.34	6482.93	114.41	898.12	(0,0,2.15)
Pontoons	9971.56	9769.22	202.34	1583.03	(0,0,-16.5)
Total	17272.28	16942.04	329.56	2587.05	(0,0,-9.62)

The mass and center of gravity of the different parts of the FWT are given in Table 4.8 [9]. The mooring lines are not taken into consideration when calculating the total center of gravity. It can be seen that the x-coordinate of the total center of gravity is 0.1 m. This is because of the weight of the turbine not being centered directly above the tower. The vertical center of gravity of 22.7 m is seen as too high above the SWL, and will give an unstable system. However, the ballast that is going to be added in the pontoons later will lower this center of gravity.

Table 4.8: Mass of the different parts of the FWT without ballast

Part	Mass [t]	CG [m]
Semi submersible (w/o ballast)	2587.1	(0,0,-9.6)
Mooring line	254.6	—
Nacelle	446.0	(-2.69,0,121.5)
Rotor	230.6	(7.1,0,119)
Tower	628.4	(0,0,47.6)
Total (w/o ballast)	4146.7	(0.1,0,22.7)

Since the total mass of 4146.7 t in Table 4.8 is smaller than the total buoyancy of 14081.4 t in Table 4.6, ballast corresponding to the difference of 9934.7 t is added. This corresponds to a seawater volume of $V_{ballast}$ = 9692.4 m^3. Table 4.7 shows that the ballast can be located in the pontoons since they have an inner volume of V_{inner} = 9769.2 m^3. Table 4.9 shows the new mass and the new center of gravity of the semi-submersible when adding the ballast. Now, the total weight of the FWT (Table 4.9) is equal to the total buoyancy (Table 4.6). Since the buoyancy and the weight of the semi-submersible with ballast is now known, the specified force is found to be 15300.6 kN by Equation 4.5.

Table 4.9: Mass of FWT when adding ballast

Part	Mass [t]	CG [m]
Ballast	9934.7	(0,0,-16.5)
Semi w/ballast	12521.8	(0,0,-15.1)
Total FWT	14081.4	(0.1,0,-5.5)

4.5.3 Hydrostatic stiffness

The hydrostatic stiffness terms C_{33}, C_{44} and C_{55} have to be calculated for the FWT. The hydrostatic stiffness term, C_{55}, found by Equation 3.8, can be written as in Equation 4.6 using Equation 3.1 for GM and Equation 3.2 for BM. Due to symmetry, C_{44} will have the same I_{wp} as C_{55}, hence $C_{44} = C_{55}$

$$C_{55} = \rho g \nabla KB + \rho g I_{wp} - \rho g \nabla KG \tag{4.6}$$

The hydrostatic stiffness term, C_{55}, in Equation 4.6 should be modified to account for the specified force in origin. Since the specified force is located in origin, the center of buoyancy, CB, and the center of gravity, CG, will be measured from origin (z_B and z_G), and not from the keel (KB and KG) as in the equation (calculating the distance between z_G and z_B). Furthermore, since the hydrostatic stiffness in SIMA is only calculated for the SIMO body, i.e the semi submersible, the mass, $m = \rho\nabla$, and the center of gravity, z_G will be calculated for only the semi submersible, and not for the whole structure. The rest of the equation is unchanged. Equation 4.7 shows the modified form of Equation 4.6.

$$C_{55} = \rho g \nabla z_B + \rho g I_{wp} - m_{semi} g z_{G\,semi} \tag{4.7}$$

The calculation of the second moment of inertia about the waterplane is given in Table 4.10. The second moment of inertia is calculated by using Steiner's theorem and the superposition principle. The second column in the table corresponds to the second moment of inertia for a circular cross section given by $I_y = \frac{\pi D}{64}$. The third column corresponds to the additional Steiner term given by $I_{steiner} = Ad^2$.

Table 4.10: Calculation of the second moment of inertia about the waterplane, I_{wp}

Part	I_y [m^4]	$I_{steiner}$ [m^4]	I_{wp} [m^4]
Center column	232.96	0	232.96
Side column 1	490.87	159043.13	159534.00
Side column 2	490.87	39760.78	40251.65
Side column 3	490.87	39760.78	40251.65
Total			240270.26

The three non-zero terms in the hydrostatic stiffness matrix are given in Table 4.11

Table 4.11: Non-zero terms in the hydrostatic cstiffness matrix

Term	Value
C_{33} [kN/m]	2913.18
C_{44} [kNm]	2.37e6
C_{55} [kNm]	2.37e6

4.6 Environmental conditions

The FWT in this thesis is located at Equinor's Scotland Hywind floating wind turbine park at Buchan Deep. The FWT should be able to survive extreme weather with all lines intact, and with one mooring line missing. In these cases, the wind turbine will be parked and feathered i.e in survival mode. Five extreme conditions are to be investigated:

- Only wind with 50 year return period
- Only waves with 50 years return period
- Only current with 10 year return period
- All the three conditions above combined with all mooring lines intact (ULS condition)
- The three upper conditions combined with one mooring line missing (ALS condition)

The environmental data is found from Equinor's Metocean Design Basis from Hywind Buchan Deep, 2013 [13]. The peak period, T_p is found as the maximum peak period on the contour line for the found 50 year H_s in the graph showing the relation between T_p and H_s for Buchan Deep [13].

The reference height for wind speed in SIMA is at hub height. Hence, the wind speed has to be scaled from the Metocean reference height of 10 m to hub height 119 m. This is done according to Equation 3.22, with a power coefficient of 0.12.

The wind will be set to constant uniform for the conditions with extreme waves and extreme current alone, so that only the effect of waves and current can be seen. For the conditions containing extreme wind, two different turbulent wind models will be used: NPD turbulent wind and TurbSim turbulent wind. For NPD wind, the reference height is set to 10 m above the SWL, since this is what NPD wind profile in SIMA uses as reference height [32], giving an extreme reference wind velocity of 34.5 m/s. In TurbSim, the Kaimal turbulence model (see Section 3.5.2) with turbulence characteristic B is used with Normal Turbulence type. The wind profile type is a power law profile having power law exponent 0.12, which is the coefficient used when scaling the wind according to Equation 3.22. The two first cases are run with no current. The combined conditions are run with 50 year return period for waves and wind, and 10 years return period for current. Table 4.12 gives the five extreme conditions. Table 4.13 specifies the 10 year extreme current, which is varying with depth.

Table 4.12: Environmental extreme conditions investigated

Weather type	Return period [yrs]	Wind speed at hub height [m/s]	H_s [m]	T_p [s]	Turbine status
Wind	50	46.4	0.01	10	Parked
Waves	50	0.01	10.5	14.3	Parked
Current	10	0.01	0.01	10	Parked
Combined ULS	all above	46.4	10.5	14.3	Parked
Combined ALS	all above	46.4	10.5	14.3	Parked

Table 4.13: 10 year extreme current at Buchan Deep

Depth [m]	Current velocity [m/s]
0	1.70
25	1.62
40	1.55
60	1.42
70	1.35

4.7 Static analysis

The static anchor positions were first calculated by the catenary equations for chain without elasticity found in Section 3.6. To do this, a MATLAB script was made. The script calculates the horizontal length of a mooring line from the anchor to the fairlead, X, the horizontal length of the line being in the vertical water span, x, and the length of the line being in the vertical water span, l_s, when the structure is in static equilibrium. It also calculates the initial and static position of the anchors. The already known parameters are the weight of the mooring line in water, w, the vertical distance from the fairleads to the sea bottom, d, and the length of the mooring line, l, which can all be found in Table 4.4.

The horizontal pre-tension was chosen to be the same as for the already existing SIMA model: 1494 kN. The static anchor positions, when the structure in water depth 70 m, and depth from fairleads to the bottom of 55 m is statically stable, are given in Table 4.14.

Table 4.14: Static position of anchors for the initial system when elasticity of the mooring line is not included

	x [m]	y [m]	z [m]
Anchor 1	885.33	0	-70
Anchor 2	-442.67	766.72	-70
Anchor 3	-442.67	-766.72	-70

To verify the positions of the anchors giving the correct pretension, a static analysis was run in SIMA. The static analysis gave an axial tension at the fairlead of 1528 kN with an angle of $\alpha = 60.6$ degrees between the substructure and mooring line (see Figure 4.6). The horizontal pretension at the fairlead was therefore found to be 1331 kN. A reason for the deviation from the pretension of 1494 kN could be that the MATLAB script does not take elasticity of the chain into account. Even though the effect of elasticity is low for catenary chain systems, a long line will lead to the elasticity being more important [22]. A new MATLAB script, taking elasticity into consideration, was made, using the catenary equations for chain with elasticity in Section 3.6.2. The resulting static anchor positions are given in Table 4.15.

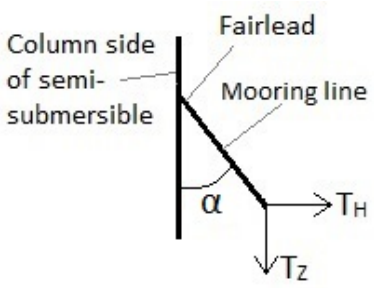

Figure 4.6: Sketch showing angles, and the horizontal and vertical tension

Table 4.15: Static position of anchors for the initial model when taking the elasticity into consideration

	x [m]	y [m]	z [m]
Anchor 1	885.67	0	-70
Anchor 2	-442.84	767.01	-70
Anchor 3	-442.84	-767.01	-70

The static axial pretension in SIMA when using the new anchor positions was found to be 1694 kN with an angle of 62.1 degrees giving a horizontal pretension of 1497 kN. This value is much closer to the chosen pretension of 1494 kN than the one not taking elasticity into consideration. Figure 4.7 shows the line characteristics of mooring line 1 of chain when and when not taking the elasticity into consideration. It can be seen that for an increasing offset, the elasticity of the chain is having a greater impact on the horizontal tension in the mooring line, making the system less stiff. Therefore, elasticity is taken into consideration for the rest of the chain systems.

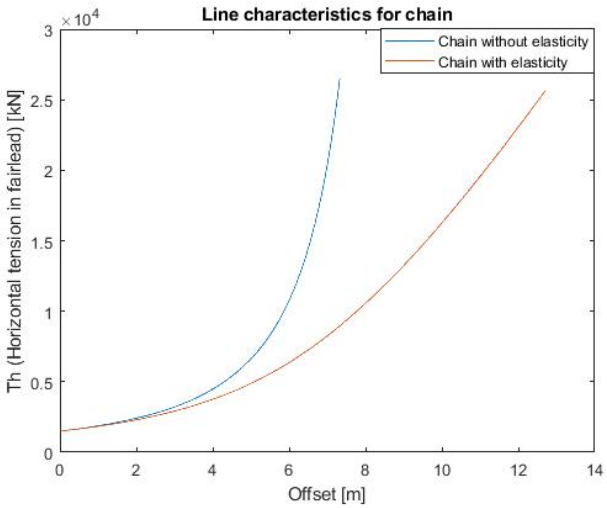

Figure 4.7: Line characteristics for chain with and without elasticity taken into consideration

Figure 4.8 shows the mooring line shape of the mooring line in SIMA. The figure shows that the line has a catenary shape, which is as expected. It can be seen that the anchor point is 835 m away from the fairlead in the horizontal direction. The mooring line hits the sea floor 202 m from the fairlead. This means that 633 m of the mooring line is resting on the sea floor when there is no offset. Table 4.16 gives the results of the static analysis conducted in SIMA for the initial model.

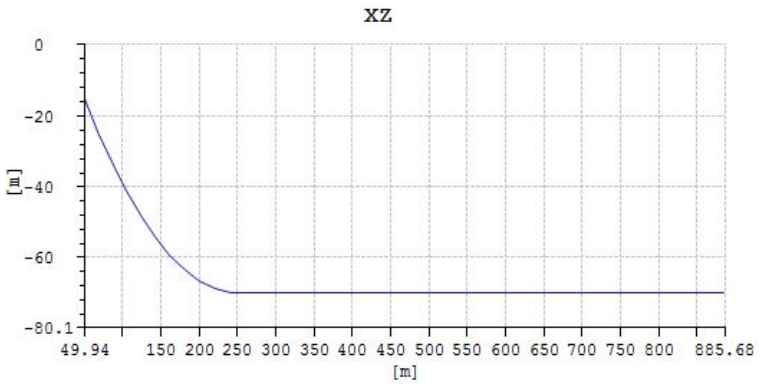

Figure 4.8: Shape of mooring line in static equilibrium

Table 4.16: Results from static analysis in SIMA

Water depth [m]	70
T in fairlead [kN]	1694
T_H in fairlead [kN]	1497
Angle between mooring line and z-axis [deg]	62.1
Total length of line [m]	845
Length of line in horizontal direction [m]	835
Length of line in vertical direction [m]	55
Horizontal length of line in the vertical water span [m]	202
Length of line in the vertical water span [m]	211

After finding the static anchor positions, the horizontal tension in the fairlead for different offsets can be investigated. Figure 4.9a shows the static analysis for different offsets conducted in MATLAB when using the catenary equations for chain with elasticity. The blue line shows the line tension for the most exposed line, which is line 1 (see Figure 4.3). The red line shows the total axial line tension for the two lee lines, which are line 2 and 3.

The intersection between the two lines corresponds to the axial pre-tension of the mooring lines at fairlead. As the figure shows, the tension in line 1 increase when the tension in line 2 and 3 decrease because the semi submersible is moving away from the anchor of line 1. This makes the

mooring line in the vertical water span longer for line 1, and shorter for line 2 and 3. Hence, more mooring line weight is pulling on fairlead 1, and less is pulling on fairlead 2 and 3. As explained in Section 3.6.2, the restoring force can be found as the difference between the tension in the two curves. The restoring force line characteristics for the initial model are illustrated in Figure 4.9b

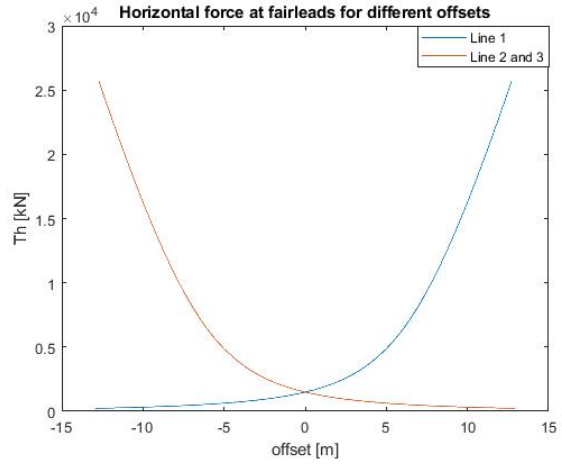

(a) Line characteristics showing horizontal line tension at fairleads for different offsets for leeward lines and windward line

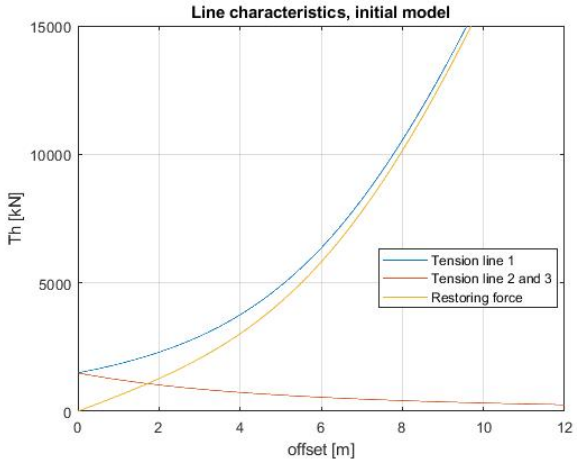

(b) Line characteristics showing horizontal line tension at fairleads for different offsets, and the restoring force

Figure 4.9

Chapter 5

Comparison Between Initial and Scotland Hywind Mooring System

Since the FWT is located at Equinor's Scotland Hywind floating wind turbine park at Buchan Deep, the initial mooring system presented in Chapter 4 is to be compared to the Hywind Scotland mooring system. Only the mooring system will be different for the two models.

5.1 Hywind Scotland model

The Hywind Scotland mooring system is used on the spar buoys in the pilot park. The mooring system is illustrated in Figure 5.1. The system consists of 50 m of bridles from each fairlead, and 609.4 m of mooring line between the bridles and the anchor. The diameter of the bridles and anchors are 132 mm and 147 mm respectively. The bridles are used to obtain stiffness in yaw for the spar floaters in the pilot park.

The mooring system described will be simplified to mooring lines of 659.4 m, meaning that the bridles will be modelled as mooring lines since the side columns in the semi-submersible will obtain the yaw stiffness. The chain diameter is chosen to be the same as for the Hywind mooring lines; 147 mm. The water depth and fairlead positions are the same as for the original system: 70 m water depth, and fairleads at depth 15 m, connected at a radius of 50 m from the center of the structure. The chain type chosen is the R4S-studless chain from the Ramnäs Bruk Product catalogue [30]. The axial pre-tension is chosen to be 1000 kN. The mooring system parameters are presented in Table 5.1. The initial mooring system is also presented in the table to make the comparison more clear.

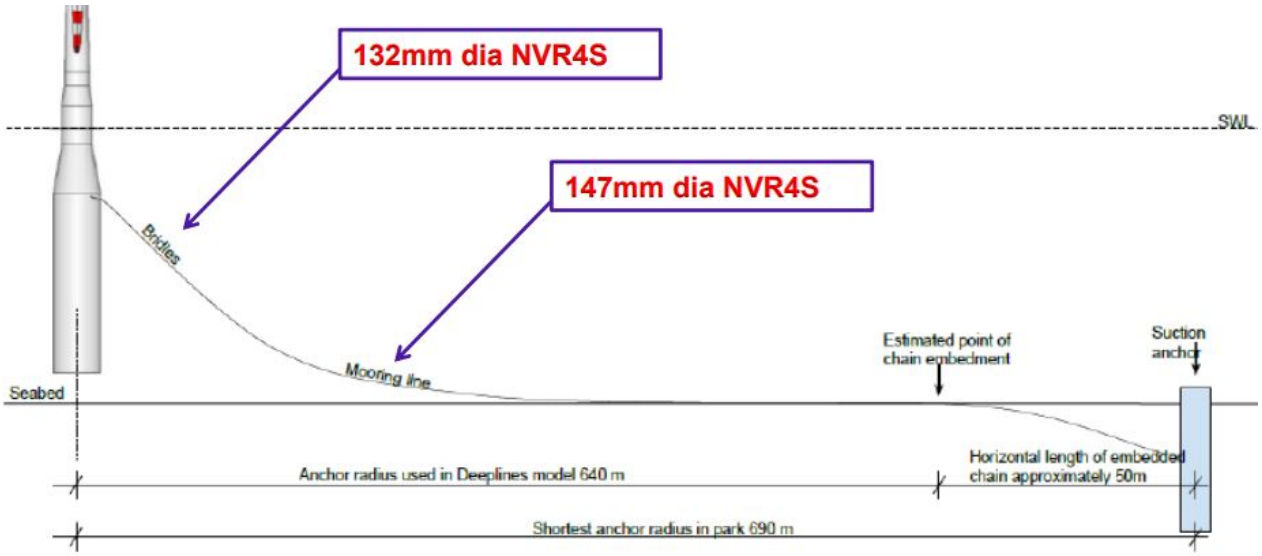

Figure 5.1: Hywind Scotland mooring lines [14]

Table 5.1: Properties of Hywind mooring system and the initial mooring system

Model	Hywind	Initial
Mooring system	Catenary	Catenary
Material	Studless R4S	Studless R4
Density steel chain [kg/m^3]	7850	7850
Number of mooing lines	3	3
Angle between adjacent mooring lines [deg]	120	120
Length of each line [m]	659.4	845
Vertical length from fairlead to sea bottom [m]	55	55
Mass of each line in air [kg/m]	432	462
Mass of each line in water [kg/m]	376	401
Diameter of chain [m]	0.147	0.153
External area of each mooring line [m^2]	0.0548	0.0590
External diameter of each mooring line [m]	0.264	0.274
Elastic stiffness, EA [kN]	3.5066e6	3.7789e6
MBS [kN]	21179	20156

The static anchor positions are found the same way as for the initial model, by use of the catenary equations with elasticity of the line taken into account. Table 5.2 shows the anchor position of the Hywind based mooring system. Figure 5.2 shows the shape of a Hywind based mooring line in static equilibrium.

Table 5.2: Static position of anchors and fairleads for Hywind Scotland based mooring system

Initial	x [m]	y [m]	z [m]
Anchor 1	707.10	0	-70
Anchor 2	-353.55	612.37	-70
Anchor 3	-353.55	-612.37	-70
Static	**x [m]**	**y [m]**	**z [m]**
Anchor 1	696.94	0	-70
Anchor 2	-348.47	603.57	-70
Anchor 3	-348.47	-603.57	-70

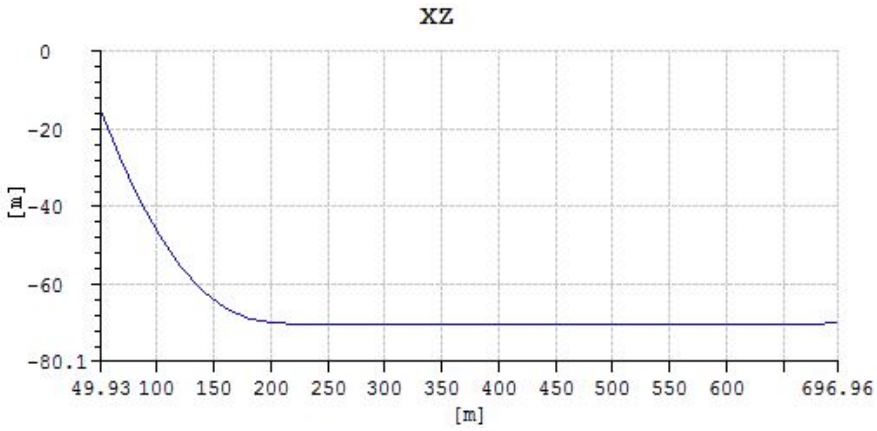

Figure 5.2: Shape of a mooring line with Hywind Scotland mooring system

Since the mooring lines are smaller and lighter than the ones in the initial system, the total weight of the FWT without ballast is smaller, leading to a need of more ballast than in the original system to obtain the same draft of 20 m. This leads to a center of gravity further down along the negative z-axix, and hence decreased hydrostatic stiffness terms C_{44} and C_{55}. C_{33} remains unchanged because it only depends on the water plane area, the density of water and the gravitational acceleration. Due to the increased weight of the semi-submersible, the specified force (found by Equation 4.5) has to be decreased. Table 5.3 shows the new parameters of the Hywind mooring system, and the corresponding parameters in the initial system.

Table 5.3: Properties of the Hywind and initial mooring system

Model	Hywind model	initial model
Mooring lines [t]	184.47	254.63
Ballast [t]	10004.9	9934.7
Semi w/ballast [t]	12591.9	12521.8
CG semi w/ballast [m]	(0,0,-15.09)	(0,0,-15.1)
Total weight FWT [t]	14081.4	14081.4
Specified force [kN]	14612.3	15300.6
C_{44} [kNm]	2.379e6	2.37e6
C_{55} [kNm]	2.379e6	2.37e6

The main differences between the two mooring line models are the pre-tension and mooring line diameter being larger, and the mooring lines being longer and heavier for the initial model than for the Hywind model. The line characteristics of the two models are illustrated in Figure 5.3. The line characteristics increase in a non-linear way for high tension, which is typical for catenary chain systems. The initial system reaches the transition from linear to non-linear faster than the Hywind system. The offset is larger for the Hywind system than for the initial system for a given axial tension. This is because the initial mooring system is stiffer than the Hywind mooring system. The initial system will reach the mean breaking strength of the line faster when increasing the horizontal offset.

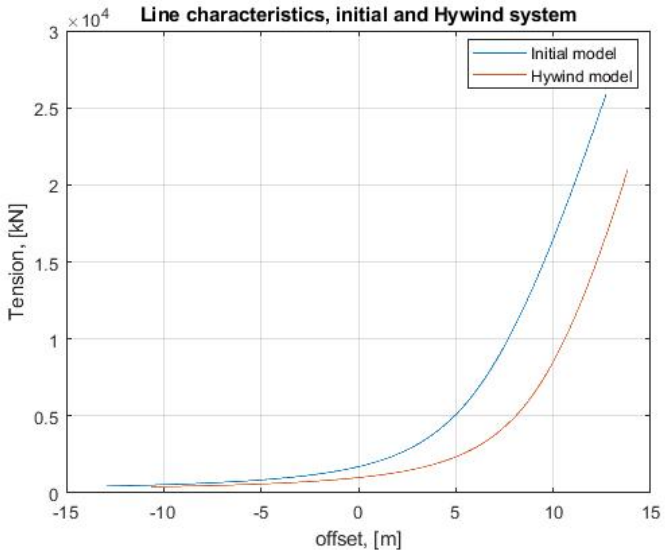

Figure 5.3: Line characteristics of the initial model and the Hywind model

5.2 Permissible horizontal offset

The maximum allowable horizontal offset is calculated to make sure that the anchor does not experience any vertical forces. This happens when the length of the line in the vertical water span, l_s is equal to the total line length, l. The maximum horizontal tension in the fairlead, T_H, and the maximum allowable offset for both models are given in Table 5.4. The parameters are calculated, using the catenary equations with elasticity taken into account in Section 3.6.2.

Table 5.4: Permissible line tension and horizontal offset

Model	T_{max} [kN]	MBS [kN]	Max horizontal offset [m]
Initial model	25860	20156	12.7
Hywind model	14736	21179	12.1

Note that the maximum tension of the initial model exceeds the MBS. This means that the permissible horizontal offset for the initial model will be lower than what written in the table.

5.3 Decay test

To find the natural frequencies in the six degrees of freedom (surge, sway, heave, roll, pitch and yaw) for the initial model and the Hywind model, a decay test was carried out. The decay test also determines the linear and quadratic damping. In the decay test, a force or moment is applied to the wind turbine in the wanted direction. When the force or moment is removed, the structure starts oscillating, and the motions damp out. To do this in SIMA, the turbine was first sat to parked condition with the blades feathered. The turbine was given a start up time (10 s) before the force or moment was applied in steps, called a ramp force, for a certain time until all the wanted force was applied. Then the force was held constant for a given time, and then let go. After doing the decay test in SIMA, MATLAB was used to pre-process the results.

The results of the decay test for the two models are given in Figure 5.4. The natural periods and damping coefficients found from the decay test for the two models are given in Table 5.5 and 5.6. There is not performed any decay test in sway and roll because they will give the same results as for surge and pitch, respectively.

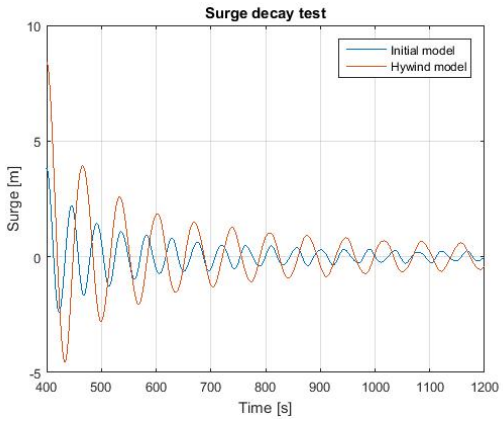

(a) Decay test in surge

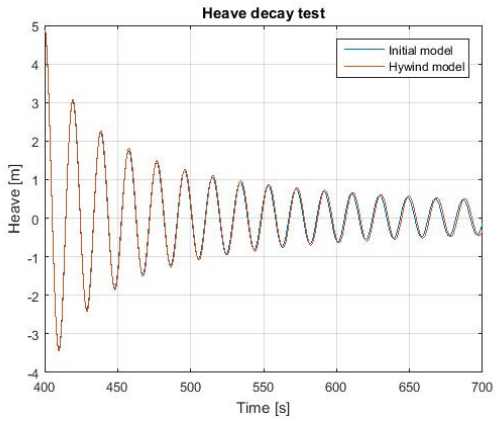

(b) Decay test in heave

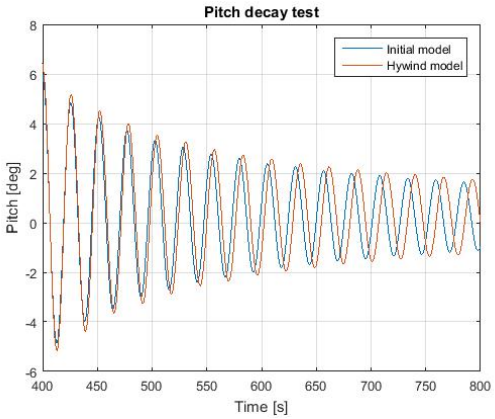

(c) Decay test in pitch

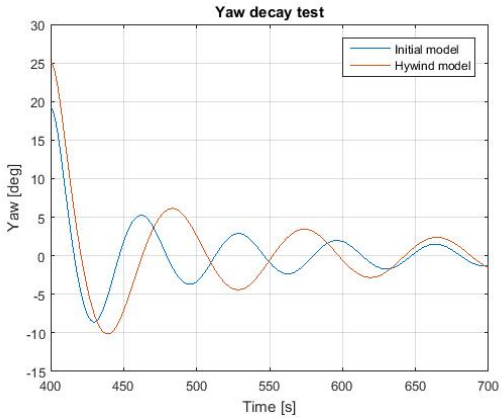

(d) Decay test in yaw

Figure 5.4: Decay test for initial model and Hywind model

Table 5.5: Natural periods for initial model and Hywind model

Degree of freedom	Natural Period for initial model [s]	Natural Period for Hywind model [s]
Surge/sway	45.4	68
Heave	19.1	19.2
Pitch/roll	25.7	26.1
Yaw	68	90

Table 5.6: Damping coefficients for initial and Hywind model

Initial model		
Degree of freedom	Linear damping	Quadratic damping
Surge/sway	0.0040	0.034
Heave	0.0060	0.026
Pitch/roll	0.00059	0.012
Yaw	0.0086	0.023
Hywind model		
Degree of freedom	Linear Damping	Quadratic damping
Surge/sway	0.0034	0.023
Heave	0.0057	0.026
Pitch/roll	0.00028	0.012
Yaw	0.0073	0.025

The results of the decay test show that the motions were coupled, meaning that a force applied in one direction will give small motions or disturbances in other directions. This is especially for surge-pitch and sway-roll motions. For example, for the initial model, a pitch moment gave a maximum amplitude of 0.8 m in surge, and a force in surge gave a maximum pitch angle of 1.3 degrees. However, since the coupled motions were small compared to the uncoupled motions, this is not seen as an important error source.

In surge/sway, illustrated in Figure 5.4a, the natural period for the initial model is much smaller than for the Hywind model. This is because the initial mooring system is stiffer than the Hywind mooring system. Increasing the length of the mooring lines leads to a less stiff system, but increasing the weight and the pre-tension of the mooring line lead to a stiffer system. Hence the combination of decreasing the weight, length and diameter of the mooring lines lead to a less stiff system. The surge period for the initial system, is considered too smalls since the surge period should be above 50-60 s. In addition, as the line characteristics in Figure 5.3 show, the Hywind model will get a larger horizontal offset than the initial model for a given axial tension. This can be seen by the larger red amplitudes in Figure 5.4a.

The natural period in heave, shown in Figure 5.4b, is similar for the two models. This shows that changing the parameters in the chain catenary mooring system does not affect the heave natural period. This can be explained by the mooring lines having very little effect on limiting the motion in the vertical direction. The heave natural period is within the range that is expected of a floating semi-submersible wind turbine.

The natural period in pitch/roll, seen in Figure 5.4c, is almost similar for the two models. It can be seen that the natural period and amplitude in pitch for the initial model is slightly smaller than for the Hywind model. This can be explained by the stiffer mooring system for the initial system. It should also be noted that the structure rotates around a pitch of 0.25 and 0.26 degrees for the initial model and Hywind model, respectively. This is because the center of gravity for the models has a z-coordinate of 0.1 m, due to the weight of the wind turbine, giving a small static pitching of the structure. The pitch natural period is smaller than what is expected for a semi-submersible (see Table 3.1). A too small pitch period will lead to resonance with the waves, containing most energy in the range of wave period 5-25 s.

The natural period in yaw is, like in surge, larger for the Hywind model than for the initial model. This might also be explained by the initial system being stiffer than the Hywind system, giving a smaller yaw period for the initial system. The yaw natural period is seen as acceptable for the Hywind system, but it might be too small for the initial model according to Table 3.1. For both models, it can be seen that the quadratic damping is the dominating damping form. The quadratic damping is due to drag forces on the mooring lines.

5.4 Wave-only response

In this wave-only response analysis, the RAOs (Response amplitude operators) in surge, heave and pitch are going to be found. The RAO is defined as the ratio between the motions of a structure and the wave amplitude causing the motions, over several time periods, as given in Equation 5.1.

$$RAO = \frac{\eta_a(\omega)}{\zeta_a} \tag{5.1}$$

It is important to study the RAOs of a floating structure to look at the impact of the motions of the structure coming from waves. Since most waves have periods of 5-25 s, the natural periods of the motions of the structure should be not be in this range because resonance may occur.

Figure 5.5 shows the results of the analysis when sending regular waves with amplitude ζ_a=1 m, and periods in the range $0 < T < 35$ s with a step of 1 s towards the structure in SIMA. The wind speed is set to constant uniform wind having wind speed 0.01 m/s. There is no current present.

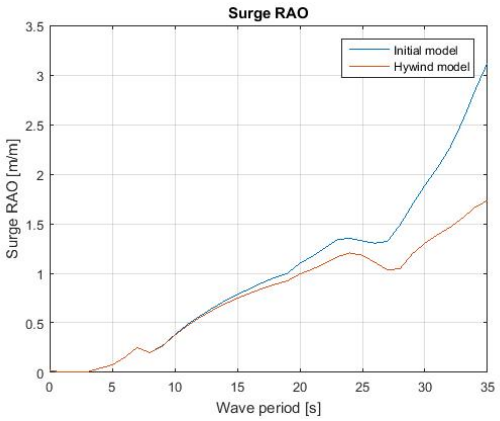

(a) RAO in surge

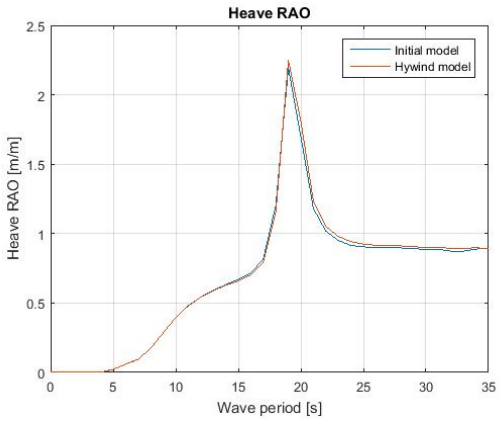

(b) RAO in heave

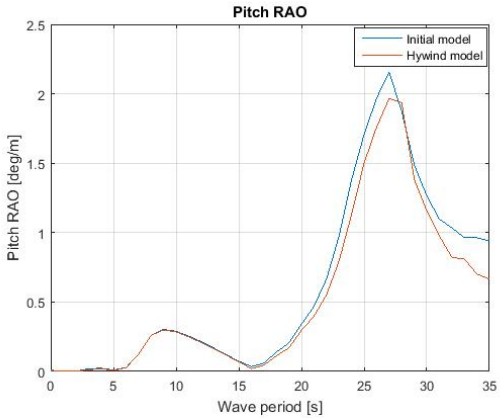

(c) RAO in pitch

Figure 5.5: RAOs in regular waves for the initial and the Hywind model

For surge motion, shown in Figure 5.5a, it can be seen that the response in the initial model is larger than in the Hywind model for high wave periods due to the low surge natural period of 45.4 s for the initial model. As the wave period is getting closer to the natural period, the offset is larger because it is approaching resonance. The small trough in the RAO at $T = 26$ s might be due to the pitch natural period of approximately 26 s for both models.

For heave, shown in Figure 5.5b, it can be seen that the two models have exactly the same RAO. This is explained by the response in heave not being affected by the changed mooring system. It can be seen that resonance occurs at a wave period of approximately 19 s, which is explained by the natural period in heave being around 19 s. Since the waves have most energy at periods 5-25 s, resonance in heave might be a problem when the FWT is exposed to waves.

For pitch motion, which is shown in Figure 5.5c, the same phenomena of resonance as for heave can be seen at a wave period around 26 s, which is the same as the natural period in pitch for the two models. The peaks show the slightly larger natural period in the Hywind model. The cancellation at $T = 16$ s corresponds to a wavelength of 400 m. The reason for this cancellation might be due to the length of the wave. Since the wave amplitude is only 1 cm, and the wave is 400 m long, the pitch will be very small when the FWT follows the motion of the wave.

5.5 Constant wind test

A constant uniform wind test was conducted to find the mean offsets in surge, heave and pitch, and the mean line tension. In the test, one below rated condition, the rated condition, one over rated condition and one 50 year extreme wind condition were run. The turbine was set to operational condition in all the cases, except for the extreme case, where the turbine was parked. The cut-out speed wind speed of 25 m/s was chosen to be run at operational condition, but it should be noted that the turbine should be parked when the wind speed passes the cut-out wind speed of 25 m/s. This is because the wind is so extreme that the wind turbine is not producing any energy. Instead, the purpose is just to survive the weather without any damage. The wind is set in the direction normal to the wind turbine disk, which that means no vertical or transverse velocity is present. H_s and T_p are set to the same as for the decay test: H_s being 0.01 m, and T_p being 10 s. The wind is constant uniform. The four cases can be seen in Table 5.7.

Table 5.7: Environmental conditions used in the constant wind test

Case	Wind speed at hub height [m/s]	H_s [m]	T_p [s]	Turbine status
Below rated	8	0.01	10	Operating
Rated	11	0.01	10	Operating
Over rated	25	0.01	10	Operating
Extreme	46.4	0.01	10	Parked

For the extreme wind condition, the pitch motion of the structure did not damp out after some time, like for the other conditions. This could also be seen in the roll motion. In addition, the thrust in this condition was varying with time. Furthermore, the rotor speed was varying between ± 8 degrees, even though the wind turbine was supposed to be parked. After looking at the rotor isolated from the rest of the structure, it could be seen that the problem was not located in the rotor. Therefore, the problem was assumed to be located in either the nacelle or the tower. Since this Master thesis is focusing on the mooring system and not on elastic effects in the turbine, the problem was not further investigated. To avoid the problems, the stiffness of

the blades, EI, were increased by 10 times, and the supernode closest to the turbine in the shaft and the supernode on the back end of the nacelle was set as slaves of the bottom of the tower instead of the top of the tower. In this way, the continuous change of pitch was avoided, and the rotor speed started to oscillate by ± 0.1 degrees and the thrust became constant instead of oscillating. The increase of EI and the change of supernode master from the top of the tower to the bottom of the tower will be used for the rest of the extreme condition simulations in this Master thesis.

The mean values of the chosen offsets and the line tension are given in Table 5.8. The time lines of the different conditions are given in Figure 5.6, 5.7, 5.8 and 5.9. It can be seen from the figures that the parameters become steady after approximately 300-400 s.

Table 5.8: Mean values from the constant wind test

Initial model				
Wind speed at hub height [m/s]	Mean offset in surge [m]	Mean offset in heave [m]	Mean offset in pitch [deg]	Mean line tension [kN]
8	-1.77	-0.050	-3.85	2332
11	-2.92	-0.13	-7.26	2943
25	-1.62	-0.019	-3.06	2274
46.4	-3.05	-0.087	-5.73	3031
Hywind model				
Wind speed at hub height [m/s]	Mean offset in surge [m]	Mean offset in heave [m]	Mean offset in pitch [deg]	Mean line tension [kN]
8	-3.21	-0.056	-3.91	1643
11	-4.97	-0.15	-7.39	2301
25	-2.95	-0.025	-3.05	1589
46.4	-5.18	-0.11	-5.78	2396

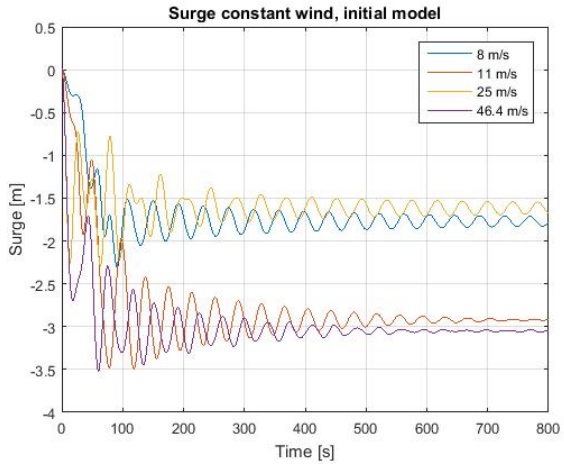

(a) Initial model

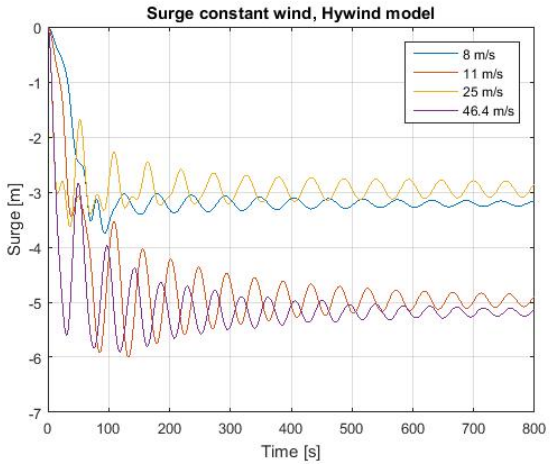

(b) Hywind model

Figure 5.6: Constant wind test in surge for the initial model and the Hywind model

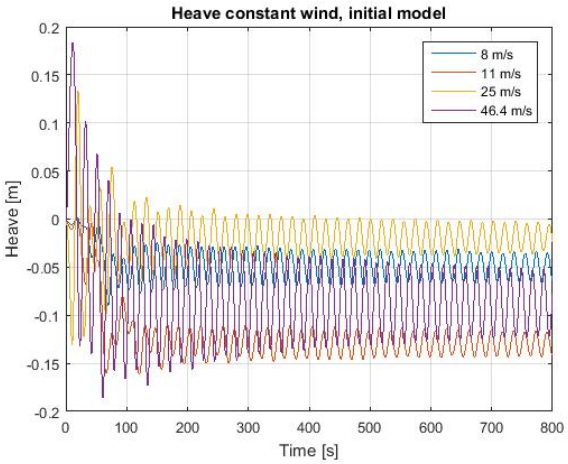

(a) Initial model

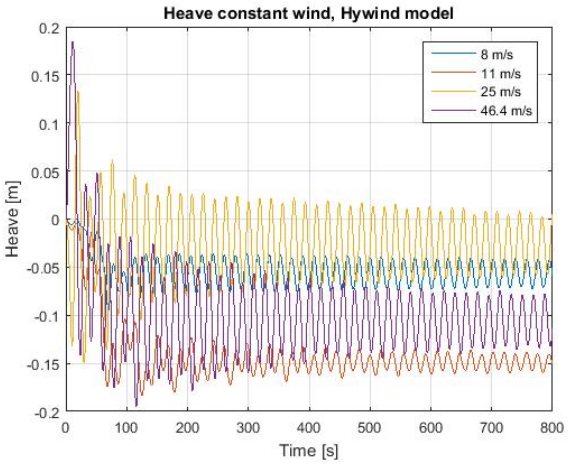

(b) Hywind model

Figure 5.7: Constant wind test in heave for the initial model and the Hywind model

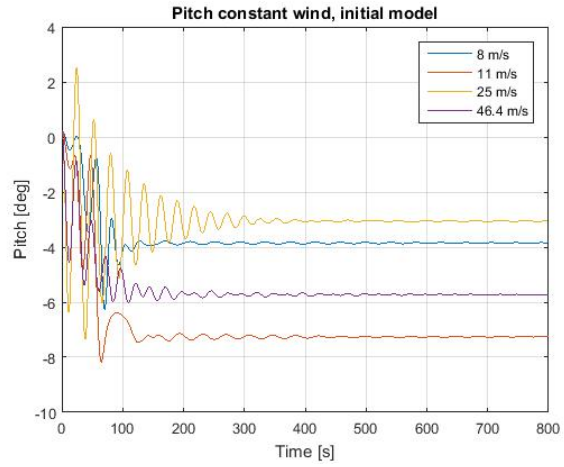

(a) Initial model

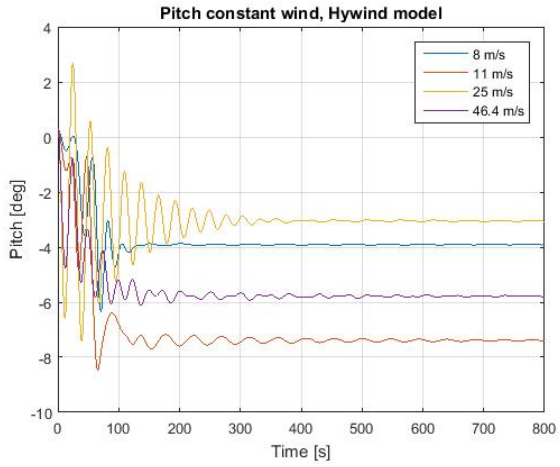

(b) Hywind model

Figure 5.8: Constant wind test in pitch for the initial model and the Hywind model

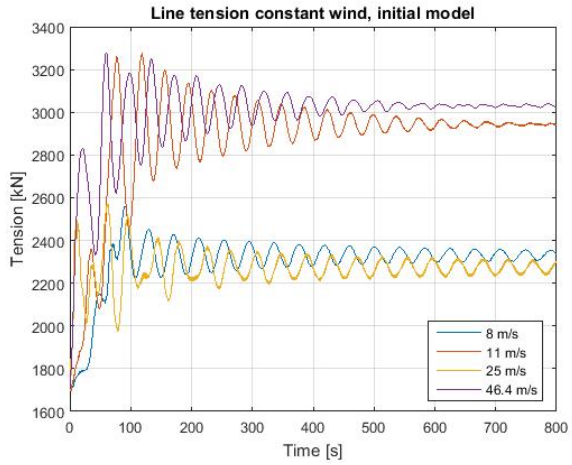

(a) Initial model

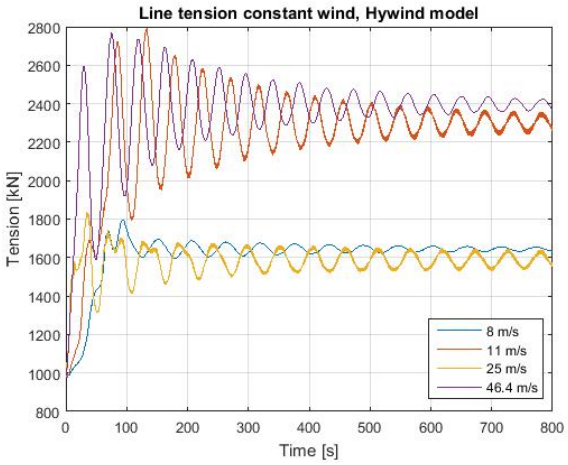

(b) Hywind model

Figure 5.9: Constant wind test of line tension in line 1 for the initial model and the Hywind model

In surge, the mean offset is almost twice as large for the Hywind model than for the initial model. This can be explained by the line characteristics in Figure 5.3, where the offset in surge is larger for the Hywind model at the given mean line tensions in Table 5.8. As expected, the offset is largest at rated condition and extreme condition. It can be seen that the extreme condition is giving a larger mean offset than the rated condition for both models.

In heave the offsets are very small, and the mean offsets are approximately the same for the two models since the change of mooring system is not affecting the offset in heave.

In pitch, the damping is approximately the same for the two models. In addition, as for heave, the mean pitch is approximately the same for the two models because changing the mooring chain system has a minor effect on the pitch motion. The largest mean pitch can be found at the rated condition. As Figure 5.8 shows, the pitch motion for the extreme condition is damped out, unlike the first model with too low stiffness of the blades, and the supernodes not being slaves of the tower bottom.

The mean line tension is larger for the initial model than for the Hywind model. This is expected since the initial model has a higher pre-tension. As expected, the mean line tension in the extreme condition and the rated conditions are the largest for the line tension and all the investigated offsets in Table 5.8. For mean line tension, the rated condition and the extreme condition give approximately the same results for both models.

5.6 Extreme conditions

Five extreme conditions were run. The extreme conditions are given in Table 4.12. The three first conditions show the effect of extreme wind, extreme waves and extreme current alone, and the last two conditions show the effect of the three first extreme conditions combined with all mooring lines intact, and one mooring line missing, respectively.

5.6.1 Extreme wind

In the extreme wind condition, both NPD turbulent wind and TurbSim turbulent wind were used. The results can be seen in Table 5.9. 5 runs with different wave and wind seeds were conducted.

Table 5.9: Results from extreme wind only condition for the initial model and the Hywind model

	NPD wind, initial model	TurbSim wind, initial model	NPD wind, Hywind model	TurbSim wind, Hywind model
V_{hub} [m/s]	44.49	45.67	44.46	45.65
$\sigma_{V_{hub}}$ [m/s]	5.28	4.93	5.27	4.92
Mean line tension [kN]	2795	2952	2137	2302
$\sigma_{line\,tension}$ [kN]	405.2	326.1	443.4	355.3
Mean surge [m]	-2.57	-2,88	-4.42	-4.88
σ_{surge} [m]	0.73	0.57	1.08	0.81
Mean heave [m]	-0.072	-0.088	0.085	-0.10
σ_{heave} [m]	0.068	0.088	0.071	0.088
Mean pitch [deg]	-4.94	-5.76	-4.99	-5.83
σ_{pitch} [deg]	2.09	1.71	2.16	1.76

In this condition, the wind speed at hub height is supposed to be 46.4 m/s. All the models have a wind velocity that is slightly lower than this. This means that the offsets and the line tension might be larger than what was calculated in SIMA.

Comparing NPD turbulent wind and TurbSim turbulent wind, it can be seen that the wind at hub height is larger and closer to the wanted wind velocity at hub height for the TurbSim model. This might be because NPD wind uses a scaling coefficient of 0.11, and not 0.12 as used in this thesis. In addition, the scaling of the NPD wind at high wind speeds is different than the scaling law used in this thesis (see Section 3.5.3). Due to the higher wind velocity at hub height when using the TurbSim model, the mean offsets and the mean line tension are larger for this turbulent model. It can also be seen that the NPD wind model gives a larger standard deviation for all the results in Table 5.9 (except for the heave motion, but the heave motions in this condition are very small).

Figure 5.10 and 5.11 show the time lines and the frequency contents of the incoming wind for the initial model. It can be seen that the NPD turbulent model has more low frequency content, and that the TurbSim model has more high frequency content. This can also be seen in the time lines, where the NPD time line has more low frequency motion. The figure also shows that the NPD time line has a larger standard deviation. The incoming wind at the Hywind model shows the same effect because the similar wind is simulated. The differences in the incoming wind are reflected in the resulting line tension and offsets in Table 5.9.

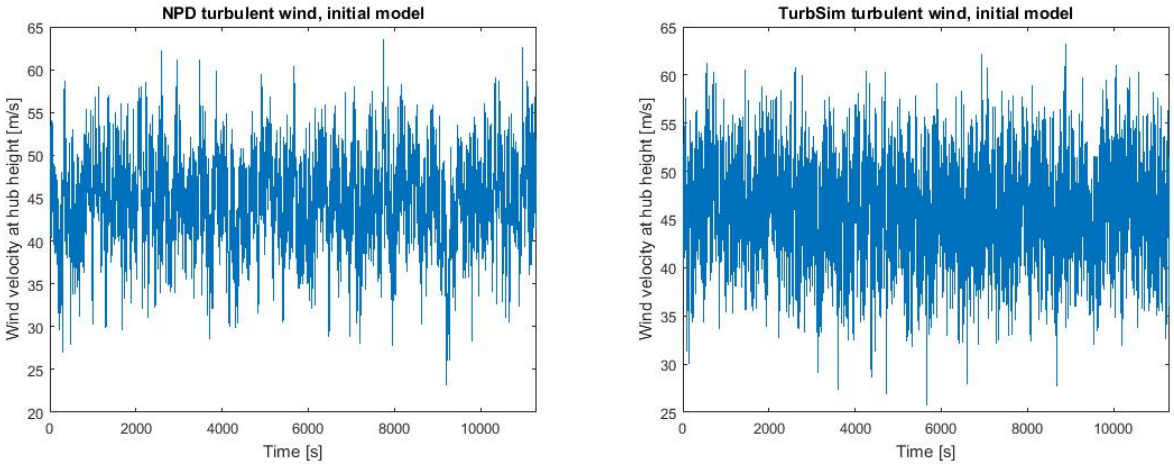

(a) NPD turbulent incoming wind

(b) TurbSim turbulent incoming wind

Figure 5.10: Wind velocity at hub height for extreme wind condition for the initial model

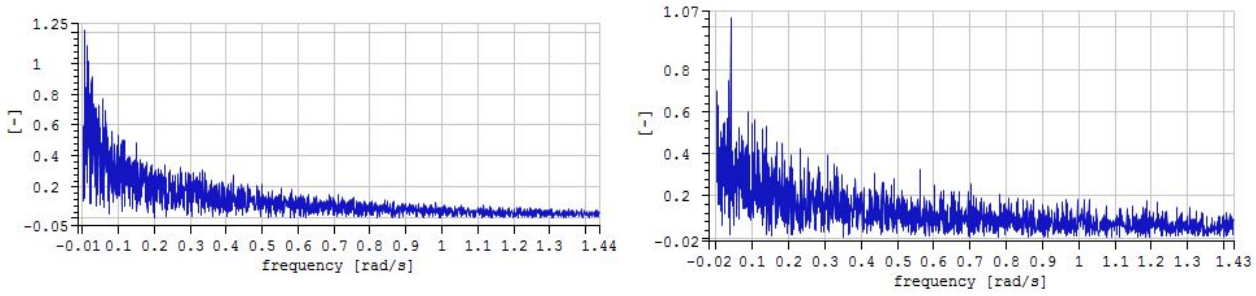

(a) NPD turbulent incoming wind

(b) TurbSim turbulent incoming wind

Figure 5.11: Frequency content of wind velocity at hub height for extreme wind condition for the initial model

Time lines of the line tension for the two models are shown in Figure 5.12 and 5.13. As for the incoming wind speed, the mean line tension is higher, and the standard deviation is lower when using the TurbSim turbulent wind model.

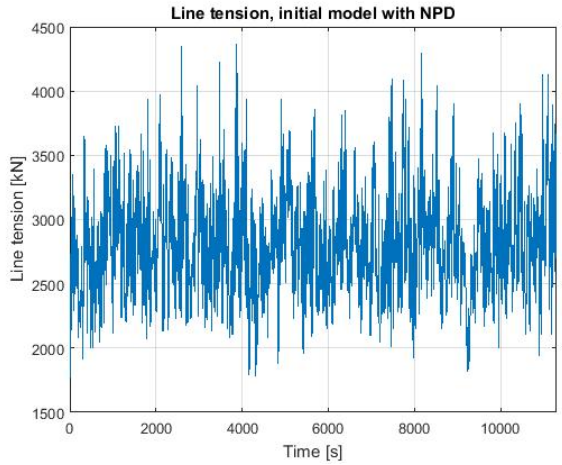

(a) NPD turbulent wind, initial model

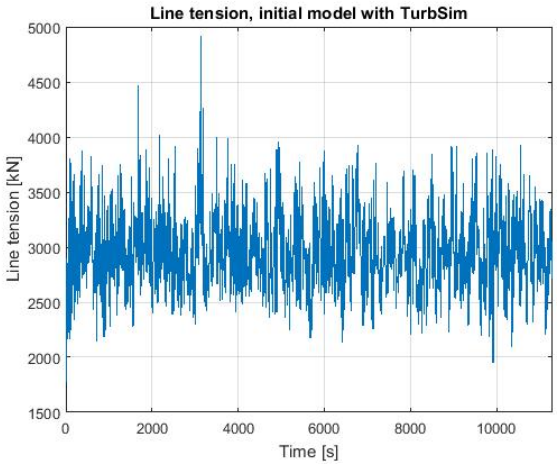

(b) TurbSim turbulent wind, initial model

Figure 5.12: Axial line tension in line 1 at fairlead for extreme wind condition for the initial model

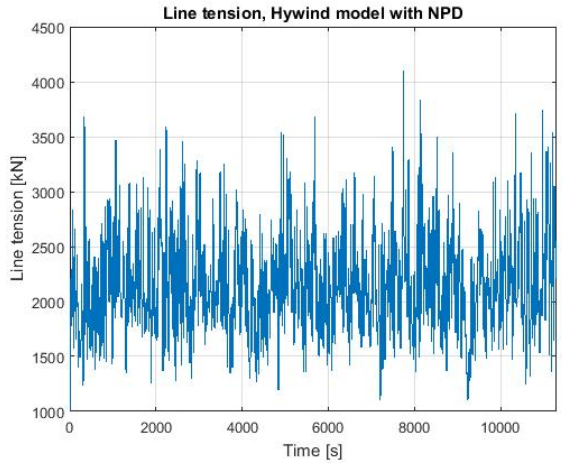

(a) NPD turbulent wind, initial model

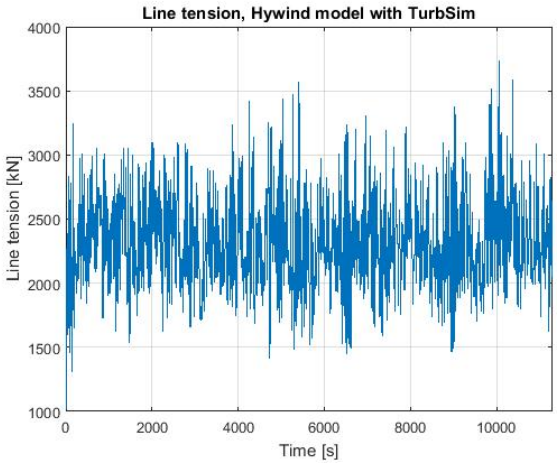

(b) TurbSim turbulent wind, Hywind model

Figure 5.13: Axial line tension in line 1 at fairlead for extreme wind condition for the Hywind model

The results in Table 5.9 reflect the results from the extreme condition in the constant wind test. The mean offsets are larger for the Hywind model than for the initial model. Furthermore, the mean line tension is larger for the initial model than for the Hywind model. The standard deviation of the different results is approximately the same for the two models. The results show that the extreme wind has most impact on the mean line tension, mean surge offset and mean pitch offset. This can also be seen in the time lines of the surge, heave and pitch offset in Appendix 8.2. Figure 5.14 shows the line tension in a lee line (line 2) when using the NPD turbulent wind model (the turbulent model giving the lowest line tension) for both the initial model and the

Hywind model. It shows that, as for line 1, line 2 will not go into slack. Slack happens when the line tension becomes negative.

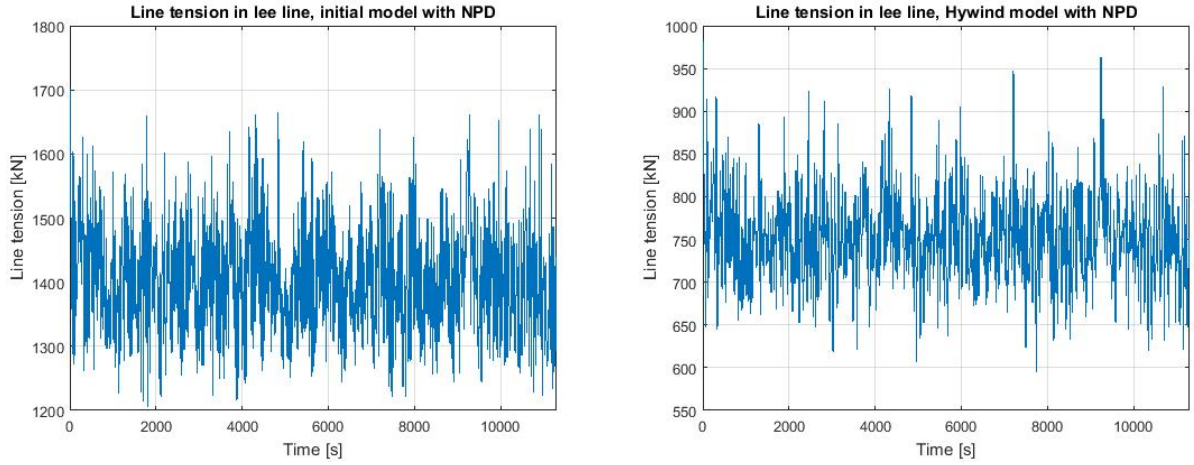

(a) NPD turbulent wind, initial model

(b) NPD turbulent wind, Hywind model

Figure 5.14: Axial line tension in lee line (line 2) at fairlead for extreme wind condition

5.6.2 Extreme waves

The results of the extreme 50 year return period waves condition in Table 4.12 are shown in Table 5.10 for both models. 5 runs with different wave and wind seeds were conducted.

Table 5.10: Results of the extreme waves only condition

	Initial model	Hywind model
Mean line tension [kN]	1766	1001
$\sigma_{linetension}$ [kN]	1022	465
Mean surge [m]	0.022	-0.082
σ_{surge} [m]	1.75	1.66
Mean heave [m]	0.12	0.12
σ_{heave} [m]	1.69	1.69
Mean pitch [deg]	0.23	0.23
σ_{pitch} [deg]	0.75	0.64

The results in Table 5.10 show that the extreme waves make the FWT oscillate approximately around the static equilibrium position. Therefore, the extreme waves do not affect the mean line tension and the mean offsets much. Figure 5.15 shows the line tension in line 1 for this condition for the first run of both models. It can be seen that the line will often go into slack

for both models. In addition, both models have some large maximum peaks that are higher than what is created by wind in Figure 5.12 and 5.13. Time lines and frequency content of surge, heave and pitch can be seen in Appendix 8.2. The same large maximum peaks can be seen in these figures as well.

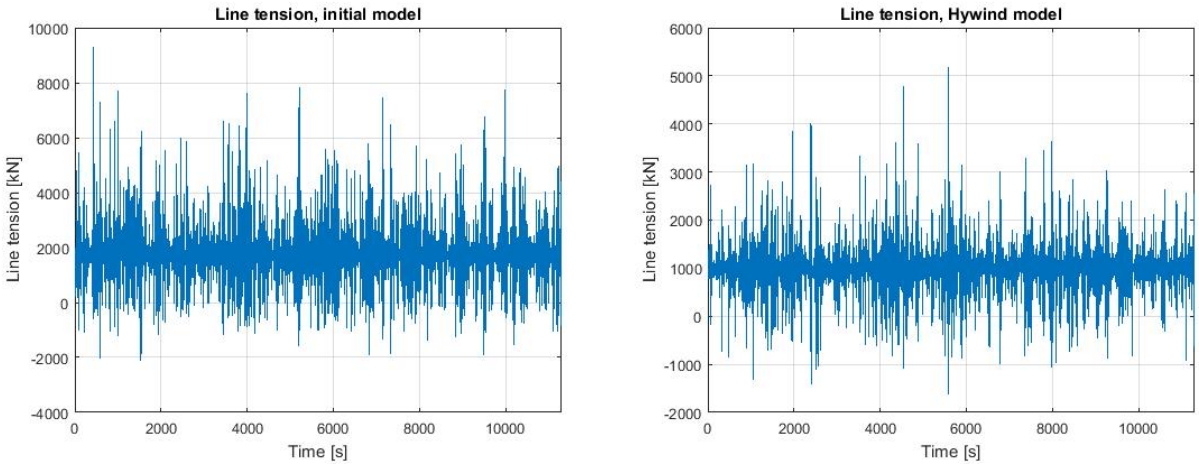

(a) Initial model

(b) Hywind model

Figure 5.15: Axial line tension in the most exposed line (line 1) at fairlead for extreme waves condition

The simulations of extreme waves alone show that the extreme waves affect the maximum peaks in surge, heave, pitch and line tension the most. The large peaks make the lines go into slack. However, the waves do not affect the mean line tension and the mean offsets much.

5.6.3 Extreme current

The results of the 10 year return period extreme current condition are given in Table 5.11. 5 runs with different wave and wind seeds were conducted.

Table 5.11: Results from extreme current only condition

	initial model	Hywind model
Mean line tension [kN]	1701	978
$\sigma_{linetension}$ [kN]	0.19	0.13
Mean surge [m]	0.0034	-0.005
σ_{surge} [m]	0.0011	0.0016
Mean heave [m]	-0.0026	0
σ_{heave} [m]	0.001	0.0023
Mean pitch [deg]	0.223	0.2354
σ_{pitch} [deg]	0	0

As Table 5.11 shows, the extreme current does not have much effect on the parameters. The maximum peaks are small, and the mean values are close to the static equilibrium potision with no offset.

5.7 Extreme weather, ULS condition

In the fourth condition, all the above extreme conditions will be run in the same condition (see Table 4.12). The offset in surge, heave and pitch, line tension in line 1, and slack of all the lines will be investigated. Both NPD turbulent wind and TurbSim turbulent wind will be used. ULS calculations will be executed to find out if the mooring lines can withstand the extreme weather conditions at Buchan Deep.

The weather is pointed in the direction giving the maximum tension in line 1. The environmental condition is a 3 h simulation, which has been run 50 times, varying the wave seed and wind seed every time. Since some wave and wind seed combinations will give large maximum tension peaks, and some will give smaller maximum tension, it is important to perform a convergence test. This is conducted in order to find the number of runs that are necessary to obtain a certain accuracy of the results. The convergence test is conducted for the mean of the maximum tension, and the standard deviation of the maximum tension peaks, after a certain number of runs. The convergence test is conducted for the environmental condition using NPD turbulent wind. This is because making TurbSim wind files is very time consuming, and because each TurbSim wind file needs a large storage space. Therefore, to avoid making 50 TurbSim turbulent wind files, it is assumed that the convergence when using NPD wind is approximately the same as when using TurbSim turbulent wind.

Figure 5.16 shows the mean of the maximum tension after a certain number of runs when using NPD turbulent wind for the initial model and the Hywind model. This means that the tension at a point along the x-axis corresponds to the mean of the maximum peak of each run after as many runs as shown by the x-axis. Figure 5.17 shows the standard deviation of the maximum tension after a certain amount of runs. It can be seen that for both models, the mean of the maximum tension starts to converge after 23 runs. The standard deviation of the maximum tension converges after 10 runs for both models.

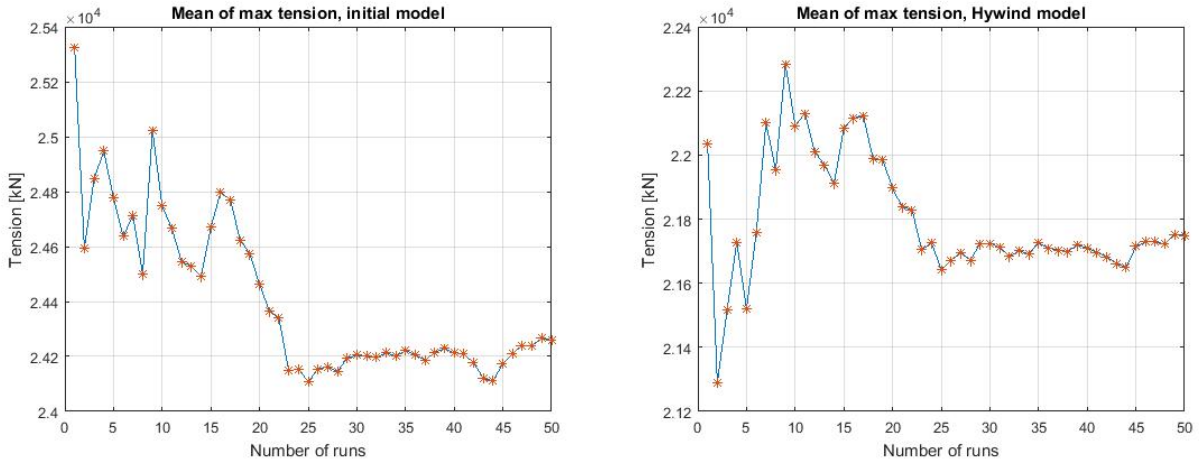

(a) Initial model (b) Hywind model

Figure 5.16: Convergence test of mean of the maximum tension after a certain number of runs

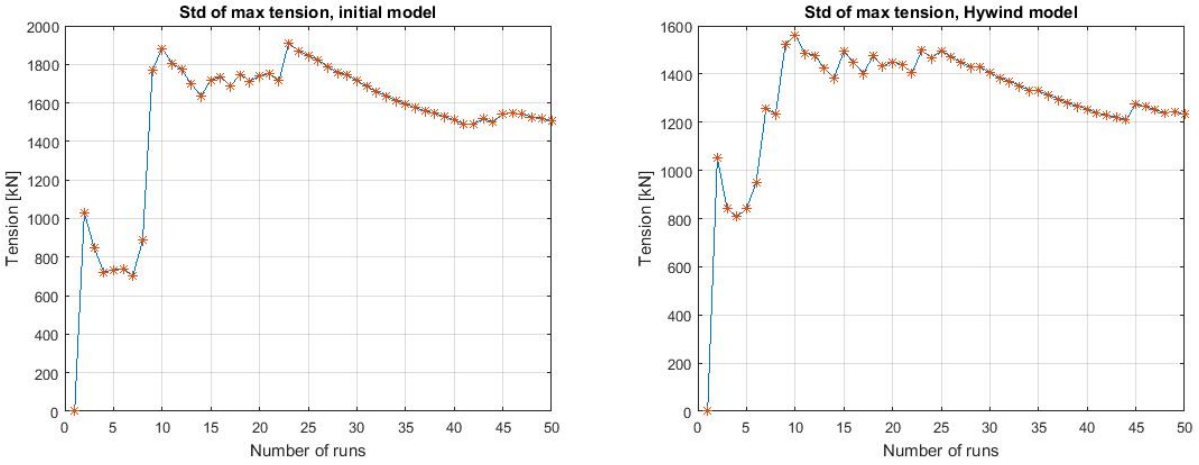

(a) Initial model (b) Hywind model

Figure 5.17: Convergence test of the standard deviation of the maximum tension after a certain number of runs

To get a better understanding of how many runs that are necessary, the percent change when increasing the number of runs should be investigated. Figure 5.18a shows the percent change of the mean of the maximum tension between a certain number of runs (shown at the x-axis) and the previous number of runs. Figure 5.18b shows percent change of the standard deviation of the maximum tension between a certain number of runs (shown at the x-axis) and the previous number of runs. As seen in Figure 5.18a, the percent change in mean of the maximum tension is small when increasing the number of runs. Hence, according to the graph, only one run is sufficient if a limit of maximum 10 % change is permitted. For Figure 5.18b, the standard deviation of the maximum tension converges after 10 runs for both models. The large peak just before 10 runs illustrates how the wave and wind seed combination can result in large (or small) maximum values. Based on this, it is concluded that 10 runs are sufficient to give reasonable results in the ULS calculations.

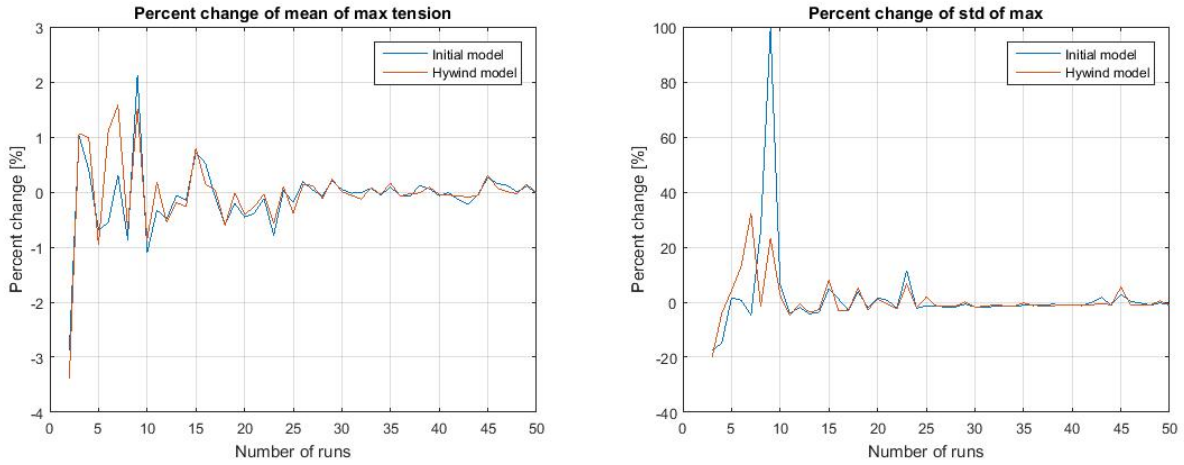

(a) Percent change of mean of maximum tension between a certain number of runs and the previous

(b) Percent change of the standard deviation of the maximum tension between a certain number of runs and the previous

Figure 5.18

Figure 5.19 shows the Gumbel distribution of the maximum tension for both models, as explained in Section 3.11.1. The most probable value of the maximum tension after a certain number of runs can be seen as the x-value of the peak of each corresponding curve. As the figure shows, the most probable maximum value does not vary much when increasing the number of runs. The black dotted lines illustrates limit of 5 % deviation from the most probable maximum tension when performing 10 runs. Since the most probable maximum value is within this limit when increasing the number of runs, 10 runs is a sufficient number of runs for both models. The yellow dots along the x-axis are illustrating the maximum value of each run. The Gumbel distributions are in compliance with the maximum values.

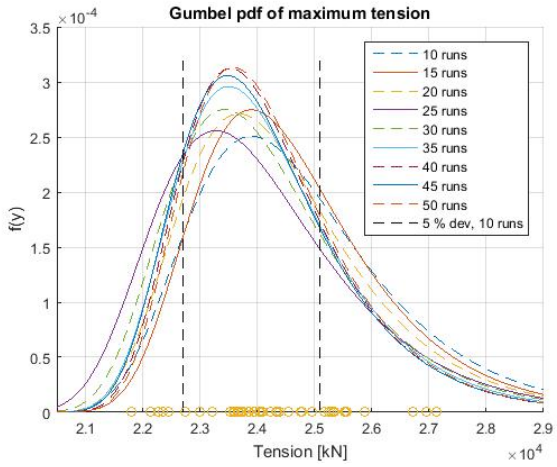

(a) Initial model

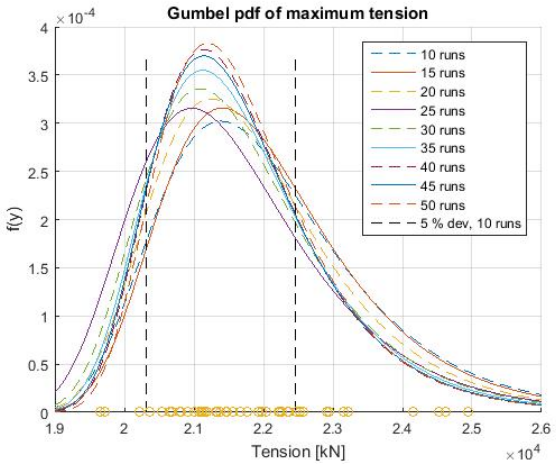

(b) Hywind model

Figure 5.19: Gumbel distribution of maximum tension after different number of runs. The yellow dots represent the maximum tension of each run

It is assumed that the convergence of mean and standard deviation of the maximum tension when using TurbSim turbulent wind is approximately the same as for when using NPD turbulent wind. The Gumbel distribution of maximum tension and when using 10 runs are shown in Figure 5.20. As discussed in Section 3.11.1, the expected maximum axial tension is larger than the most probable maximum tension. For both models, as already discussed, TurbSim turbulent wind gives a larger maximum and mean tension than NPD turbulent wind. Table 5.12 shows the results of the extreme condition after 10 runs.

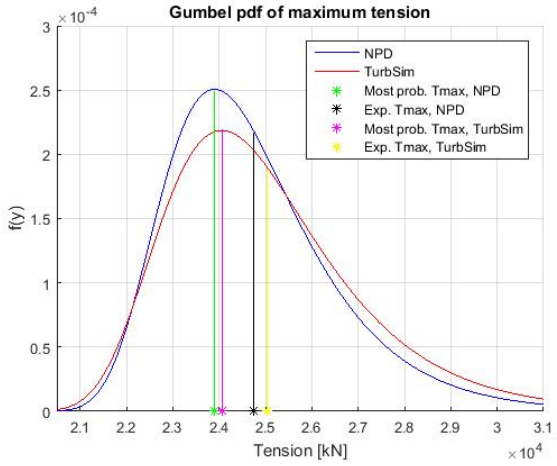

(a) Initial model

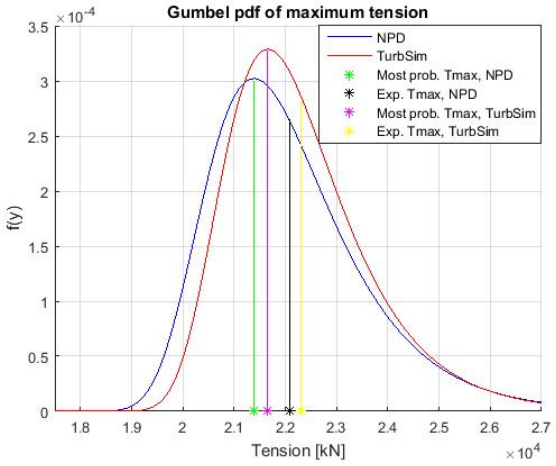

(b) Hywind model

Figure 5.20: Gumbel distribution of maximum mooring line tension at fairlead after 10 runs

Table 5.12: Results from ULS condition when conducting 10 runs

	NPD wind, initial model	TurbSim wind, initial model	NPD wind, Hywind model	TurbSim wind, Hywind model
V_{hub} [m/s]	44.71	45.94	44.70	45.93
$\sigma_{V_{hub}}$ [ms]	5.33	5.00	5.33	4.99
Mean line tension [kN]	6164	6344	5326	5511
$\sigma_{line\,tension}$ [kN]	3925	3985	3606	3682
Mean surge [m]	-5.84	-6.04	-8.30	-8.50
σ_{surge} [m]	1.83	1.82	1.77	1.75
Mean heave [m]	-0.16	-0.18	-0.19	-0.21
σ_{heave} [m]	1.8	1.80	1.82	1.83
Mean pitch [deg]	-3.58	-4.32	-3.62	-4.38
σ_{pitch} [deg]	2.02	1.82	2.03	1.80

The ultimate limit state calculations are calculated according to Section 3.10.2. The criterion is that the characteristic capacity of a mooring line, S_C should be larger than the design tension T_d. Table 5.13 shows the ULS results of the two models.

Table 5.13: ULS calculations after 10 runs for the initial model and the Hywind model

Model	Turbulent wind model	T_{max} [kN]	T_{mean} [kN]	T_d [kN]	S_C [kN]
Initial model	NPD	23900	6164	39051	19148
Initial model	TurbSim	24058	6344	39247	19148
Hywind model	NPD	21388	5326	35032	20120
Hywind model	TurbSim	21658	5511	35421	20120

The ULS analysis shows that none of the two models are within the ULS criteria. The design tension, T_d, needs to be decreased drastically, and the MBS of the mooring lines might need to be increased. Since the Scotland Hywind mooring system in reality is adapted to a different substructure than in this thesis, it is not the optimal mooring system for this FWT. The mooring lines are shorter, lighter and smaller than the initial system, and is therefore, as expected, too weak in an ULS analysis.

Possible solutions to make a chain system that is within the ULS criteria is to increase the mean breaking strength, MBS so that the characteristic tension, S_C increase. To do this, larger chain weight and diameter have to be used. However, this will also increase the costs. Another solution is to decrease the pre-tension at fairlead. Then the design tension, T_d will decrease.

Furthermore, the floating wind turbine can be moved to another location with less extreme wind, waves and current in a 50 year return period.

5.8 Accidental limit state (ALS)

The ALS analysis is calculated according to section 3.10.3. As for the ULS analysis, the criteria is that $T_d < S_C$. The combined extreme condition with 50 year wind and waves, and 10 year wind from the ULS-condition above is simulated in SIMA with line 1 missing. Since line 1 experience the greatest amount of the line tension in the ULS condition above, it is assumed that this line will fail first when the weather is pointed in this direction.

New Gumbel distributions are made for the maximum axial fairlead tension for both models. The Gumbel distribution of the the maximum tension the of ALS condition after a certain number of runs when using NPD turbulent wind for both models are shown in Figure 5.21. From Figure 5.21, it can be seen that the most probable maximum tension does not change with more than 5 % when conducting more than 10 runs. Hence, 10 runs will give a sufficient accuracy of the maximum tension.

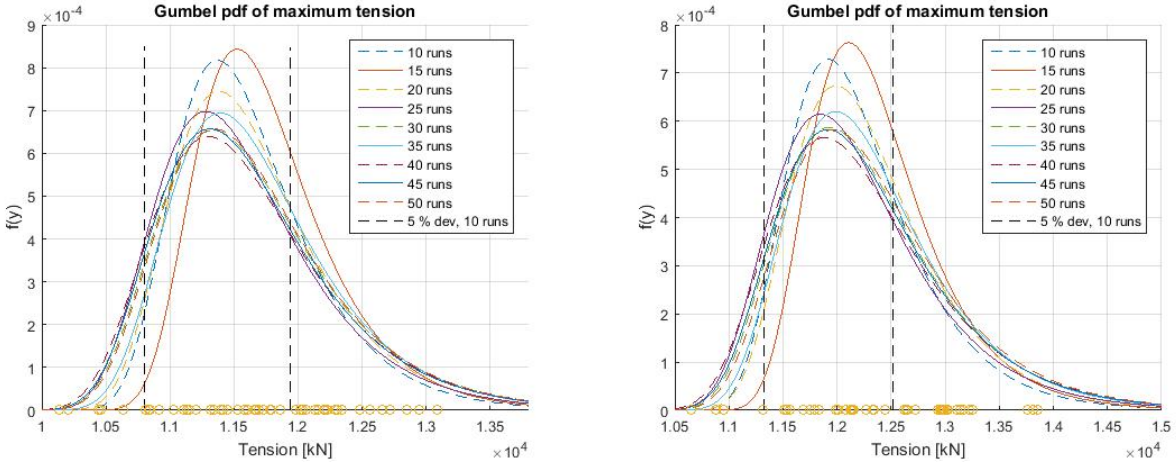

(a) Initial model

(b) Hywind model

Figure 5.21: Gumbel distributions of maximum mooring line tension at fairlead for ALS condition when using NPD turbulent wind

The Gumbel distributions when having 10 runs with NPD turbulent model and TurbSim turbulent model are shown in Figure 5.22. The results from the ALS calculation when using 10 runs are shown in Table 5.14. Both the initial model and the Hywind model are approved in the ALS calculations.

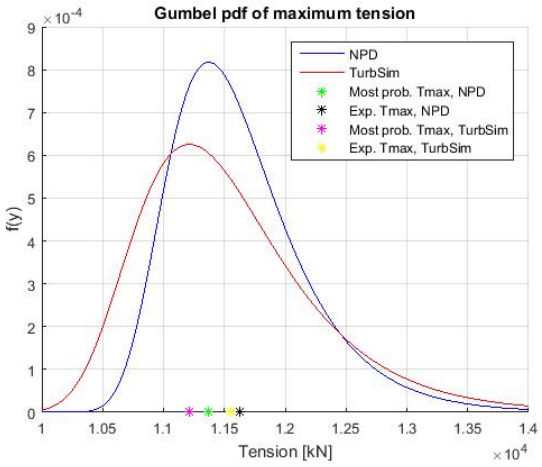

(a) Initial model

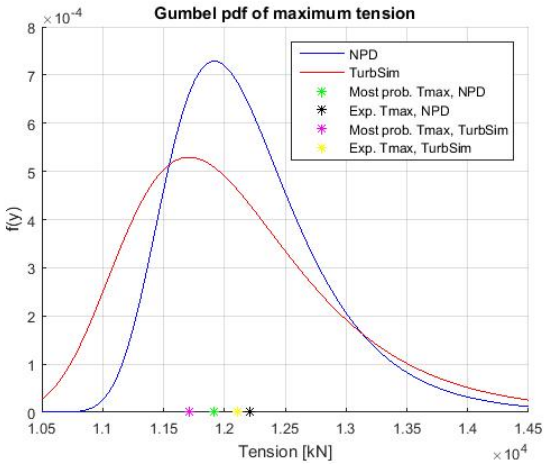

(b) Hywind model

Figure 5.22: Gumbel distributions of maximum mooring line tension at fairlead after 10 runs for ALS condition

Table 5.14: ALS calculations after 10 runs

Model	Turbulent wind model	T_{max} [kN]	T_{mean} [kN]	T_d [kN]	S_C [kN]
Initial model	NPD	11371	4350	12073	19148
Initial model	TurbSim	11212	4538	11879	19148
Hywind model	NPD	11918	4200	12690	20120
Hywind model	TurbSim	11709	4270	12452	20120

Chapter 6

Comparison Between Original and Simplified Hywind Model

The floating wind turbine model having the Hywind Mooring system presented in the previous chapter (Section 5.1) is to be compared to a simpler model of the same FWT developed by Master student Kjetil Blindheim Hole. The simplified model is presented in the section below.

6.1 Simplified model

The simplified model consists of the semi-submersible and the mooring system, where the tower and the wind turbine are not modelled. This shortens the calculation time because the model now consists of fewer RIFLEX elements, and because the complicated aerodynamics calculations in the top-structure are avoided. This is helpful when conducting e.g. extreme condition calculations and fatigue calculations. The weight of the missing parts of the FWT above the semi-submersible, (the tower and the wind turbine) is added to the substructure. In addition, the quadratic damping coefficients have to be calculated.

To account for the missing thrust force that is created when the wind meets the wind turbine and the tower [3], a total thrust coefficient, C is calculated based on a wanted wind speed, U. The wind is assumed to follow the power law given in Equation 3.22. The calculated thrust, T is a simplification of the complicated wind forces at the wind turbine and the tower. The thrust coefficient of the tower and wind turbine for a given wind speed is assumed to follow Equation 6.1. To find the coefficient, the thrust coefficients for the tower and the wind turbine are added together.

$$T = CU^2 \tag{6.1}$$

The calculation of the thrust coefficient of the wind turbine without the tower is based on the thrust curve found in Wang's Master thesis [37]. Following Equation 6.1, the thrust coefficient of the wind turbine for different wind velocities can be found by $C_{wind\,turbine} = \frac{T_{wind\,turbine}}{U^2}$. For the tower, the thrust is found as in Equation 6.2 [3], where the term $\frac{1}{2}\rho C_T A$ corresponds to C in Equation 6.1.

$$T = \frac{1}{2}\rho C_T A U^2 \tag{6.2}$$

where A is the projected area that meets the flow, and C_T is the thrust coefficient that is found as the geometrical coefficient for a cylinder in Figure 3.8. A total thrust coefficient for the tower is found by integration of each section of the tower.

Due to the control system of the turbine, the blade pitch is changed depending on the wind speed. Since this has to be taken into account for the model, it is designed with three different wind speed ranges: low wind speeds of 0-11 m/s at the hub, medium wind speeds of 11-25 m/s at the hub and extreme wind speeds above 25 m/s at the hub. The thrust coefficients are calculated for each of these three wind speed ranges.

Since the current natural period in pitch was found to be 20 s, this might cause resonance with incoming waves and the natural period in heave which is approximately 20 s for this model. To increase the pitch natural period, the ballast location was raised from the pontoons to the mass center of the submerged side columns. This is lifting the center of gravity, leading to a higher natural period. That is because the hydrostatic stiffness term in pitch, C_{55}, is decreasing due to an increased KG. For more information about this model, see Kjetil Blindheim Hole's Master thesis. The simplified model and the original model have similar mooring system, fairlead pre-tension and sub-structure, making them comparable.

6.2 Static analysis

Since the two models have the same mooring system and fairlead pre-tension, the static anchor positions and the shape of the lines are the same as for the previous chapter (Table 5.2 and Figure 5.2).

6.3 Decay test

The natural periods are found from the same decay test conducted in Chapter 5 (Section 5.3). The natural periods in the six degrees of freedom for the original Hywind model presented in Section 5.3, and the simplified Hywind model are given in Table 6.1. Table 6.1 shows that the two models have approximately the same natural periods. Hence, the results of the decay test are satisfying.

Table 6.1: Natural periods for the original model and the simplified model

Degree of freedom	Natural Period [s] of original model	Natural Period of simplified model [s]
Surge/sway	68	68.3
Heave	19.2	20.5
Pitch/roll	26	24.5
Yaw	85	81.9

6.4 Wave-only response

The RAOs in surge, heave and pitch for the two models have been plotted together in Figure 6.1. The RAOs have been made the same way as in the previous chapter (Section 5.4).

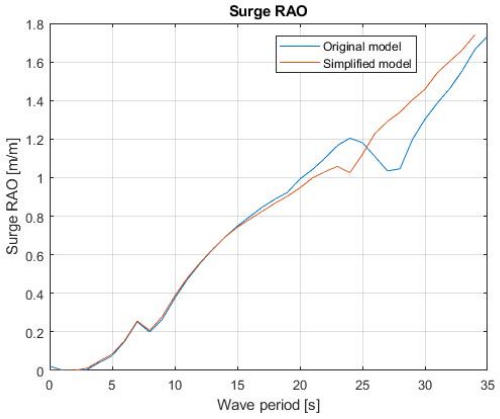

(a) RAO in surge

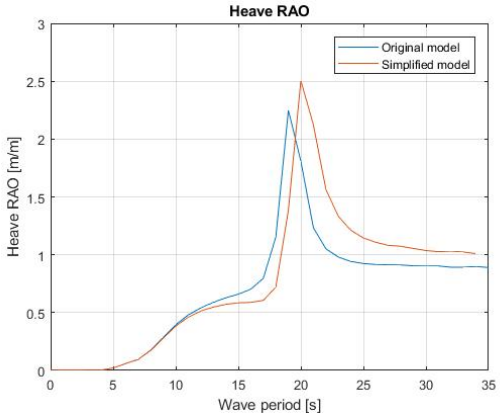

(b) RAO in heave

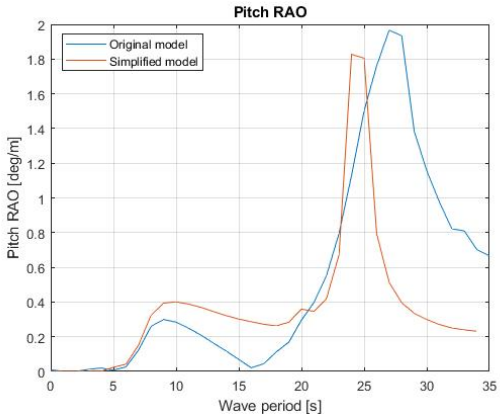

(c) RAO in pitch

Figure 6.1: RAOs in regular waves for original system

Some differences between the two models can be seen regarding the RAOs. For the surge RAO shown in Figure 6.1a, it can be seen that the two models are in compliance with each other. As explained in Section 5.4, the trough at $T = 25$ s for the simplified model and $T = 27$ s for the original model might be due to the natural periods in pitch, which corresponds to these periods. Since the surge period is $T = 68$ s for both models, resonance in surge due to waves do not occur.

For the heave RAO shown in Figure 6.1b, the two graphs are similar. The main difference is the small difference in natural period of the two models. The original model has a natural period of 19.2 s, and the simplified model has a natural period of 20.5 s, which are represented by the resonance peaks in the model. The response stabilizes at approximately 1 after the resonance peak, meaning that the waves are so long that the FWT starts following the waves here.

For the pitch RAO shown in Figure 6.1c, there are two main differences. The first difference is, like for the heave RAO, the difference in natural periods. The natural period in pitch for the original model and the simplified model are 26 s, and 24.5 s respectively, which can be seen as

resonance by the large peaks in the figure. The second difference between the two models in the pitch RAO is the response between 5 and 20 s. For both the models, a peak can be seen at approximately 8 s. However, for the original model, there is a cancellation at wave period 16 s. This can not be seen in the simplified model. The reason for the cancellation in pitch might be, as explained in the previous chapter, that the the waves are very long here, leading to a very small pitch angle when the FWT follows the long wave. Since the simplified model has a lower natural period in pitch than the original model, resonance starts to build up at a lower period than for the original model. This might be a reason for the missing cancellation in pitch at $T = 16$ s for the simplified model.

6.5 Constant wind

A constant uniform wind test was conducted to find the mean offsets in surge, heave and pitch, and the mean line tension. The same conditions as for the previous chapter (Table 5.7) were run. The time lines of the different conditions are given in Figure 6.2, 6.3, 6.4 and 6.5.

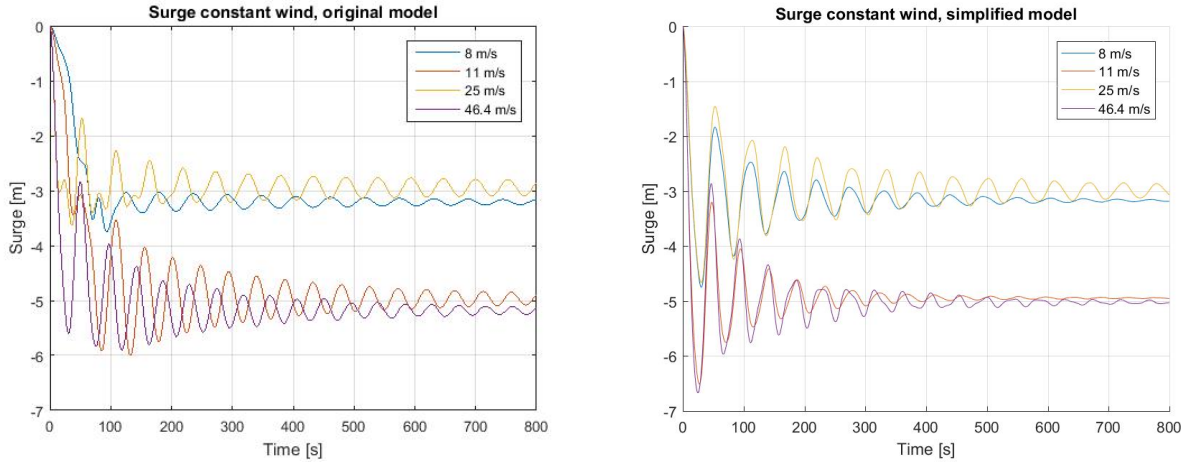

(a) Original Hywind model

(b) Simplified Hywind model

Figure 6.2: Constant wind test in surge for the original Hywind model and the simplified Hywind model. Wind velocities are at hub height

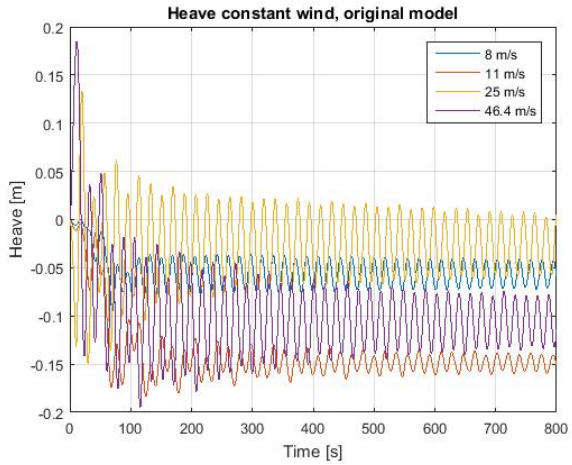

(a) Original Hywind model

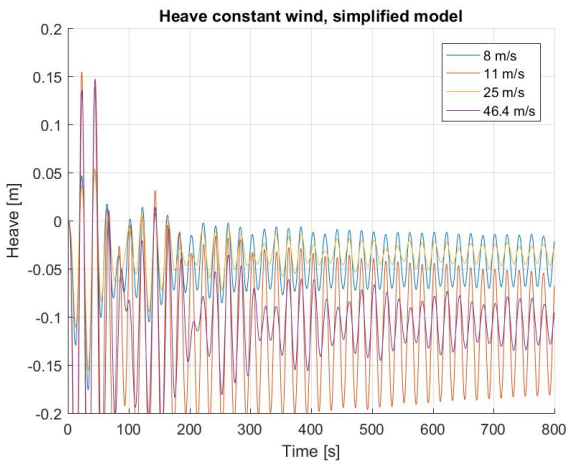

(b) Simplified Hywind model

Figure 6.3: Constant wind test in heave for the original Hywind model and the simplified Hywind model. Wind velocities are at hub height.

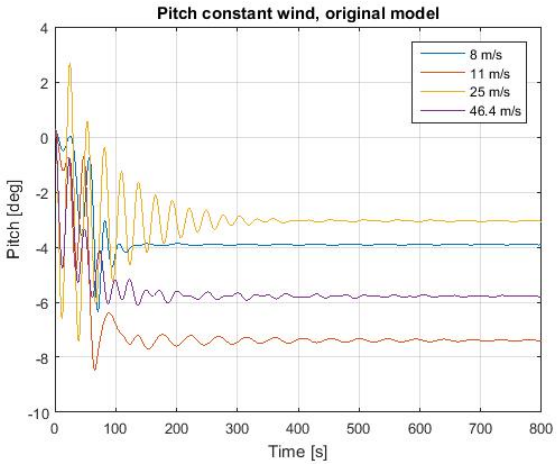

(a) Original Hywind model

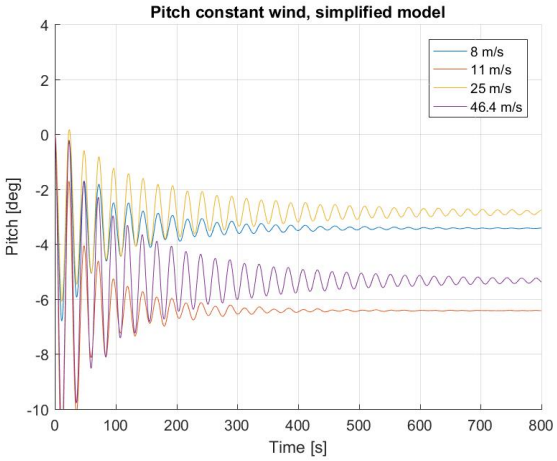

(b) Simplified Hywind model

Figure 6.4: Constant wind test in pitch for the original Hywind model and the simplified Hywind model. Wind velocities are at hub height.

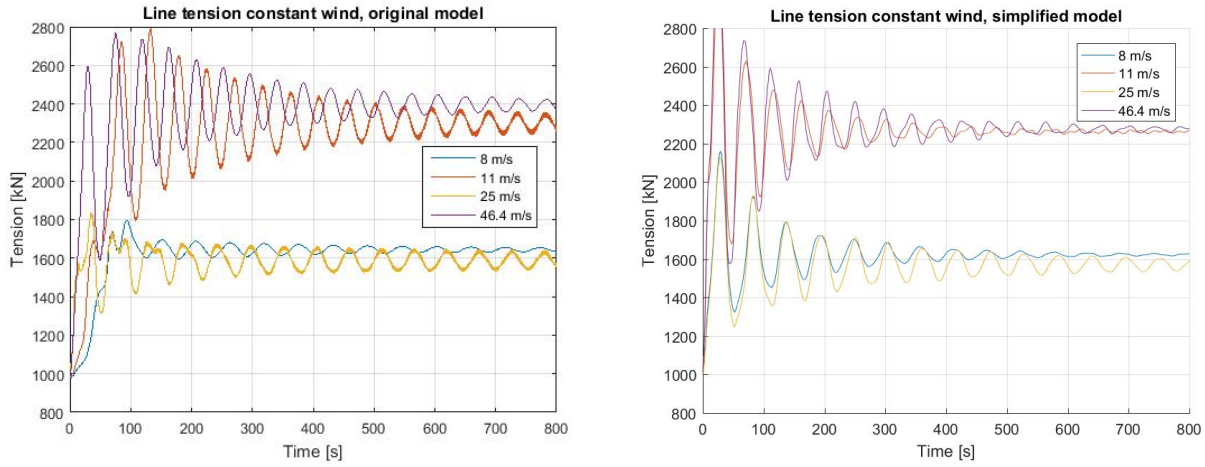

(a) Original Hywind model

(b) Simplified Hywind model

Figure 6.5: Constant wind test of line tension in line 1 for the original Hywind model and the simplified Hywind model. Wind velocities are at hub height.

It can be seen that it takes approximately 400 seconds before the results are steady. For surge, shown in Figure 6.2, the mean values are approximately the same for the two models for all the chosen wind velocities. As expected, the offset is greatest at rated condition and extreme condition. It can be seen that the extreme condition is giving a slightly larger mean offset than the rated condition for both models. For heave motion, which is shown in Figure 6.3, the offset is very small, and the mean offsets are approximately the same for the two models.

For pitch, shown in Figure 6.4 the offsets are larger for the original model than for the simplified model for all the wind velocities. The largest difference can be seen for the extreme wind velocity and the rated wind velocity, where the difference is approximately 1 degree. In addition, the damping of pitch motion is larger in the original model than in the simplified model. The mean line tension, shown in Figure 6.5, is approximately the same for the two models for all wind velocities except for the extreme wind velocity. At extreme wind velocity, the mean line tension is larger for the original model than for the simplified model, where the line tensions at rated and extreme wind velocity are approximately the same. As expected, the mean line tension in the extreme condition and the rated condition are the largest.

6.6 Extreme conditions

The extreme conditions simulated for the comparison between the two models are the two first extreme conditions in Table 4.12 (50 years return period extreme wind alone and 50 years return period extreme waves alone). In the original model, both the NPD turbulent model and the TurbSim turbulent model will be used in the extreme wind simulations. 5 runs of each condition are run for each model, with the same wave seeds, wind seeds, time steps and simulation time in both models. The results of the original model is the same as for the Hywind model in the previous chapter, but will be repeated below. Only the mean and standard deviation of the axial line tension, and the offsets in surge, heave and pitch are compared.

6.6.1 Extreme wind

The results from the simulations with 50 years return period extreme wind are given in Table 6.2. The mean values of the constant wind test are also given in the table to make the comparison easier. The standard deviations of the constant wind models are not included

Table 6.2: Results from extreme wind only simulations. The reference height is 119 m for the original model, and 10 m for the simplified model.

	Const. wind, orig. mod.	NPD wind, orig. mod.	TurbSim wind, orig. mod.	Const. wind, simpl. mod.	NPD wind, simpl. mod.
V_{ref} [m/s]	45.55	44.46	45.65	34.5	34.45
$\sigma_{V_{ref}}$ [m/s]	0	5.27	4.92	0	4.59
T_{mean} [kN]	2396	2137	2302	2275.4	2294.4
$\sigma_{linetension}$ [kN]	-	443.4	355.3	-	472.03
Mean surge [m]	-5.2	-4.42	-4.88	-5.03	-4.86
σ_{surge} [m]	-	1.08	0.81	-	1.096
Mean heave [m]	-0.11	-0.085	-0.10	-0.11	-0.12
σ_{heave} [m]	-	0.071	0.088	-	0.16
Mean pitch [deg]	-5.78	-4.99	-5.83	-5.51	-5.38
σ_{pitch} [deg]	-	2.16	1.76	-	2.91

One of the differences between the two models is the reference height for the output of the wind velocity in SIMA. The reference height is 119 m above the SWL for the original model, and 10 m above the SWL for the simplified model. That makes it hard to see if the incoming wind is the same for the two models, which it should be to make the comparison as correct as possible. The simplified model has only been run with NPD turbulent wind model. Since it was found

that the NPD turbulent wind model and the TurbSim turbulent wind gives different results of offsets and line tension, the comparison will be most correct when comparing the two models using the NPD turbulent wind model. However, the results when using TurbSim turbulent wind are also included in the table. It is assumed that the simulated wind will be similar for the two models using NPD turbulent wind since the input parameters for NPD turbulent wind model is for 10 m height for both models, making the scaling of the wind at different heights similar for both models.

It is also assumed that the mean values of this extreme turbulent wind test should be close to the values found in the constant wind extreme wind test in the previous section. Looking at the table, this is true for the simplified model. However, for the original model, the mean tension and mean offsets are larger in constant wind than in turbulent wind. Therefore, there might be something wrong with the results for the original model.

The table shows that all the mean results of the simplified model are larger than the results of the original model. This might be the reason for the slightly larger standard deviation for the simplified model. The results are seen as acceptable for the simplified model since there is not much difference between the results.

6.6.2 Extreme waves

The results of the simulations with 50 years return period extreme waves are given in Table 6.3.

Table 6.3: Results of the extreme waves only condition for the original Hywind model and the simplified Hywind model

	Original model	Simplified model
Mean line tension [kN]	1000	1001
$\sigma_{line\,tension}$ [kN]	456	370.3
Mean surge [m]	-0.070	0.032
σ_{surge} [m]	1.66	1.64
Mean heave [m]	0.12	0.017
σ_{heave} [m]	1.68	1.51
Mean pitch [deg]	0.25	-0.007
σ_{pitch} [deg]	0.59	0.93

The results in Table 6.3 show that the mean line tension is oscillating around the pre-tension, and that the offsets are oscillating around the static pre-positions. The pitch motion oscillates around the static pre-position, which is 0.25 degrees for the original model due to the weight of

the wind turbine, and 0 degrees for the simplified model because of the lack of a wind turbine. As for the extreme wind condition, the standard deviation is larger for the simplified Hywind model than the original Hywind model. The results of the simplified model when only exposed to extreme waves are acceptable when comparing to the original model.

6.7 Calculation time

The main reason for this comparison is to see if a simlified model will give sufficient results, and if it will save calculation time. The calculation time for the ULS condition in Table 4.12 was found by running one 3 h simulation of each of the two models using the same computer. It was found that one simulation took 580 s for the original model and 375 s for the simplified model, giving a decrease of 35 % when changing from the original model to the simplified model. Running e.g. 50 of these 3 h simulations, results in a computation time of approximately 8 hours for the original model and 5.2 hours for the simplified model. Hence, a lot of time is saved by using the simplified model. It should be noted that only one run was checked. Conducting more runs, or other environmental conditions might give other results of the calculation time in SIMA.

The original and the simplified model are in acceptable agreement with each other in the conducted tests. Before the comparison, the two systems were made as similar as possible, having the same mooring system and the same sub-structure. However, there might have been some differences that were overseen. In addition, the calculation of the thrust in the wind turbine and at the tower was simplified for the simplified model, and the quadratic damping coefficients had to be calculated. This might have been a reason for the differences between the models.

Even though the simplified model was seen as acceptable, this was only based on a few tests. Other tests that could have been conducted are combined extreme condition of extreme wind, waves and current to look at the ULS criterias, running the simulations with a missing line to look at the ALS calculations, and to look at fatigue in an FLS study.

Chapter 7

Comparison Between Chain and Polyester Mooring Systems

In this chapter, the chain catenary mooring systems will be replaced by a taut polyester fiber rope system. The fiber ropes will have the same minimum breaking strength (MBS) and axial pre-tension as the Hywind catenary chain system. The taut polyester system is compared to the initial catenary chain system. The polyester mooring system is presented below.

7.1 Polyester mooring system

The polyester mooring system has, like the chain mooring system, three mooring lines with 120 degrees spacing connected to the fairleads 15 m below the SWL. The length of each mooring line is chosen to be 800 m. The polyester rope material chosen is the Bridon Superline Polyester for permanent mooring, given in the Bridon Oil and Gas catalogue [8]. The mooring system and mooring line cross-section are given in Figure 7.1 and 7.2.

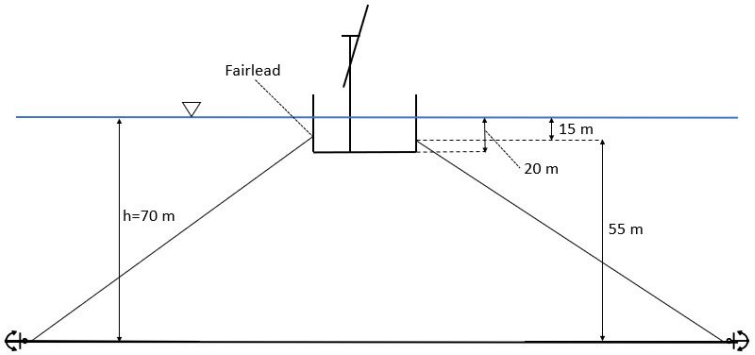

Figure 7.1: Polyester rope system

The external area and diameter have to be found because the polyester line is not completely dense, leading to water entering the rope. The weight of the mooring line in water and in air are given in the Bridon Oil and Gas catalouge. The external area in SIMA and its corresponding external diameter can be found by Equation 7.1

$$A = \frac{m_a - m_w}{\rho_{water}}, \quad \text{and} \quad D = 2\sqrt{\frac{m_a - m_w}{\pi \rho_{water}}} \tag{7.1}$$

The minimum breaking strength is chosen to be 21582 kN, which is the closest catalogue value to the reference value MBS=21179 kN for chain [8]. The elastic stiffness, EA, is calculated by Equation 7.2 [24]

$$\frac{EA}{MBS} = 20 + 25\left(\frac{T_{pre}}{MBS}\right) \tag{7.2}$$

where EA is the axial stiffness of the fiber rope, MBS is the minimum breaking strength of the rope, found in the Bridon polyester rope catalogue [8], and T_{pre} is the axial pre-tension of the rope. The taut polyester rope mooring system parameters are given in Table 7.1. As it can be seen from the table, the weight of the polyester rope is much lower than the chain weight given in Table 4.4.

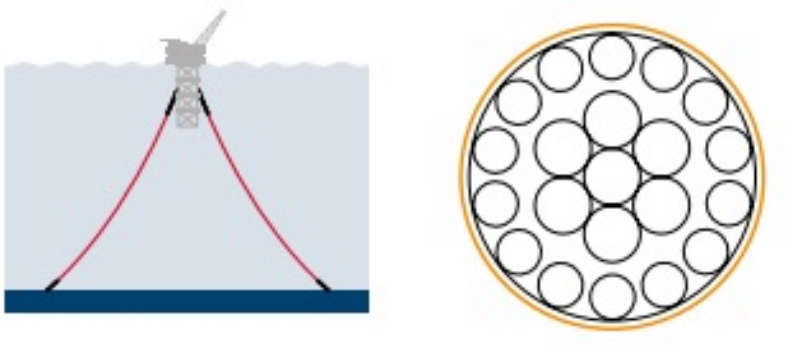

Figure 7.2: Bridon Superline Polyester [8]. Left: Illustration of mooring system. Right: Cross-section of the mooring line

Table 7.1: Properties of the polyester mooring system

Property	Value
Mooring system	Taut
Material	Superline Polyester (Permanent Mooring)
Number of mooing lines	3
Angle between adjacent mooring lines [deg]	120
Unstretched length of each line [m]	800
Vertical length from fairlead to sea bottom [m]	55
Mass of each line in air [kg/m]	50.7
Mass of each line in water [kg/m]	12.7
Cross-section area of each mooring line [m^2]	0.0620
Diameter of each line [mm]	281
External area of each line, SIMA input [m^2]	0.03707
External diameter of each line, SIMA input [mm]	217
Axial stiffness, EA [kN]	4.5664e5
MBS [kN]	21582

7.2 Static analysis

The anchor positions were found by MATLAB, using the static taut polyester theory discussed in Section 3.6.3. Since the theory does not take the weight of the polyester line in water into account, the static pre-tension found in SIMA with these anchor positions was too high. Therefore, the static anchor positions were changed until the correct axial pre-tension of 1000 kN was obtained in SIMA. The initial and final static anchor positions are given in Table 7.2. The mooring line shape is shown in Figure 7.3. The small curvature is due to the weight of the line.

Table 7.2: Initial and static positions of anchors for the taut polyester mooring system

Initial	x [m]	y [m]	z [m]
Anchor 1	848.11	0	-70
Anchor 2	-424.05	734.48	-70
Anchor 3	-424.05	-734.48	-70
Static	**x [m]**	**y [m]**	**z [m]**
Anchor 1	849.53	0	-70
Anchor 2	-424.76	735.71	-70
Anchor 3	-424.76	-735.71	-70

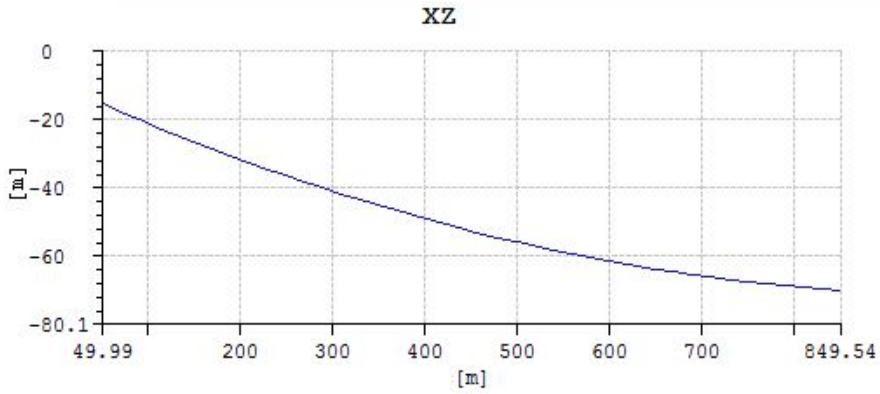

Figure 7.3: Mooring line shape of the taut polyester mooring system

The line characteristics of the initial, the Hywind and the polyester mooring system can be seen in Figure 7.4. The fiber mooring system has a linear line characteristic, and the chain systems have a non-linear line characteristic after the transition. This makes the polyester system optimal at high offsets because the axial line tension is significantly lower than for the chain systems.

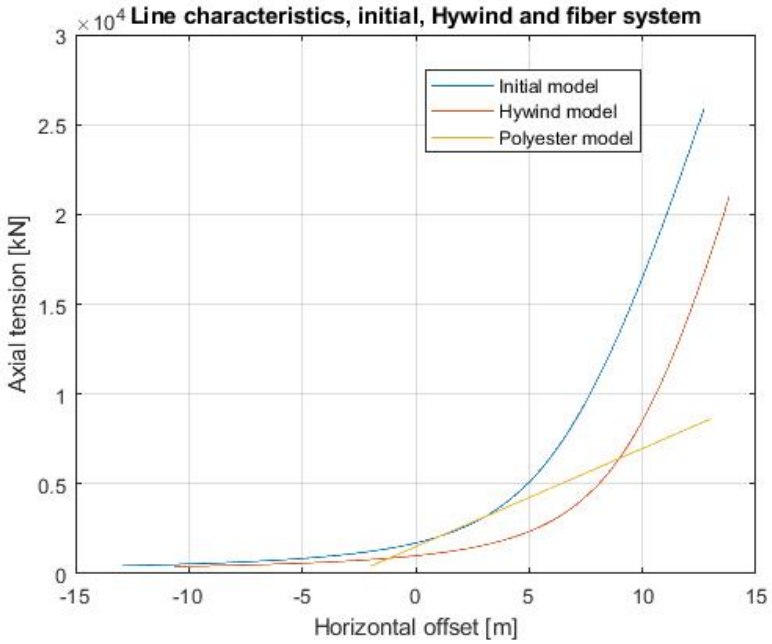

Figure 7.4: Line characteristics of the initial, Hywind and polyester mooring system

7.3 Decay test

The decay test of the taut polyester system was conducted the same ways as for the other systems (Section 5.3). The results can be seen in Figure 7.5 and in Table 7.3 and 7.4. The results of the initial system is included in the results.

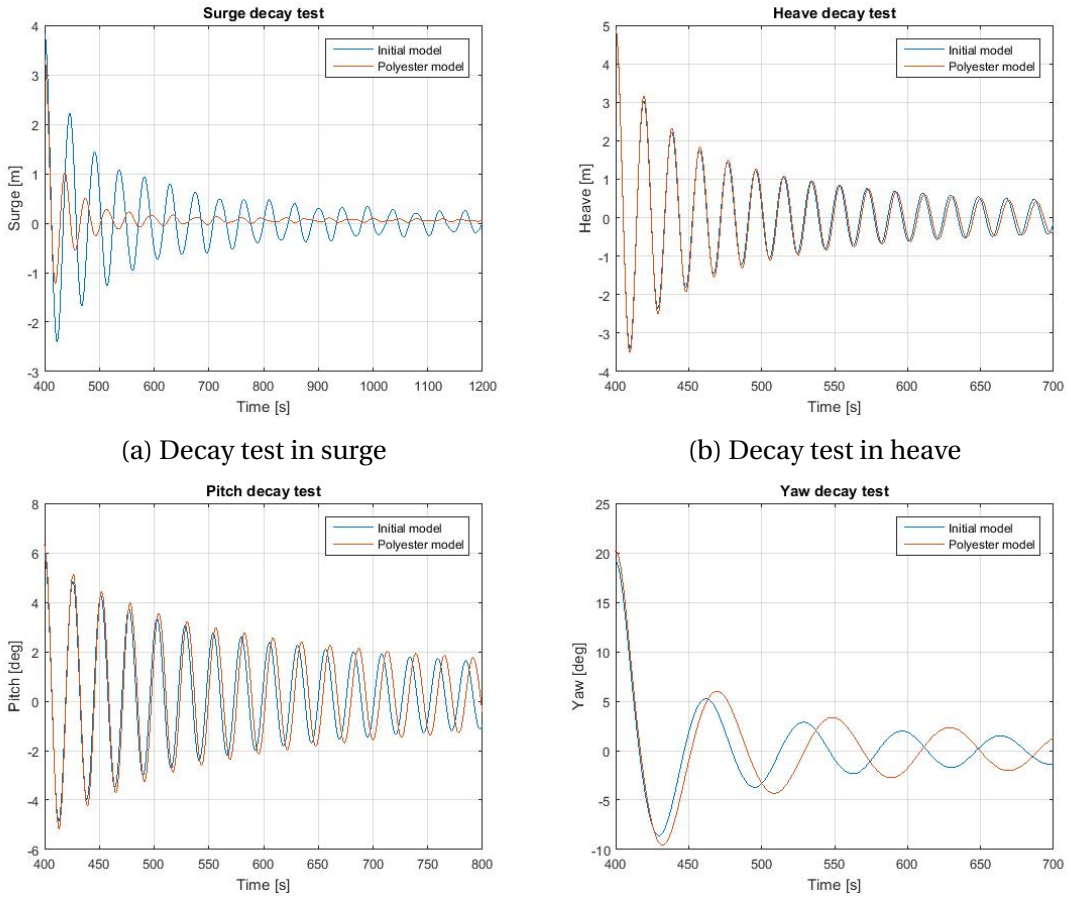

(a) Decay test in surge

(b) Decay test in heave

(c) Decay test in pitch

(d) Decay test in yaw

Figure 7.5: Decay test for the initial model and the polyester model

Table 7.3: Natural periods for initial model and polyester model

Degree of freedom	Natural Period [s] of initial model	Natural Period of polyester model [s]
Surge/sway	45.4	37
Heave	19.1	19.2
Pitch/roll	25.7	26
Yaw	68	80

Table 7.4: Damping coefficients of initial and polyester model

Initial model		
Degree of freedom	Linear damping	Quadratic damping
Surge/sway	0.0040	0.034
Heave	0.0060	0.026
Pitch/roll	0.00059	0.012
Yaw	0.0086	0.023
Polyester model		
Degree of freedom	Linear Damping	Quadratic damping
Surge/sway	0.051	0
Heave	0.0080	0.023
Pitch/roll	0.00053	0.0111
Yaw	0.0068	0.025

The natural period in surge/sway is smaller for the polyester model, as shown in Figure 7.5a and Table 7.3. The low natural period in surge might be a problem when it comes to resonance with waves, having the most energy in the range 5-25 s. The results show that changing the system into a polyester system reduces the natural period in surge. It can be seen from the figure that the initial model has significantly larger surge amplitudes than the polyester system.

The natural period in heave, which can be seen in Figure 7.5b, is similar for the two models. This shows that changing from the chain catenary mooring system to the taut polyester mooring system did not affect the heave natural period. The natural period in pitch/roll, which can be seen in Figure 7.5c, is almost similar for the two models. It can be seen that the natural period in pitch for the initial model is slightly smaller than for the polyester model. The natural period in yaw is larger for the polyester model than for the initial model. For both models, it can be seen that the quadratic damping is the dominating damping form, except for the surge motion in the polyester model, where it is zero.

7.4 Wave-only response

The RAOs in surge, heave and pitch for the initial model and the polyester model have been plotted together in Figure 7.6. The RAOs have been made the same way as in the previous chapters (Section 5.4).

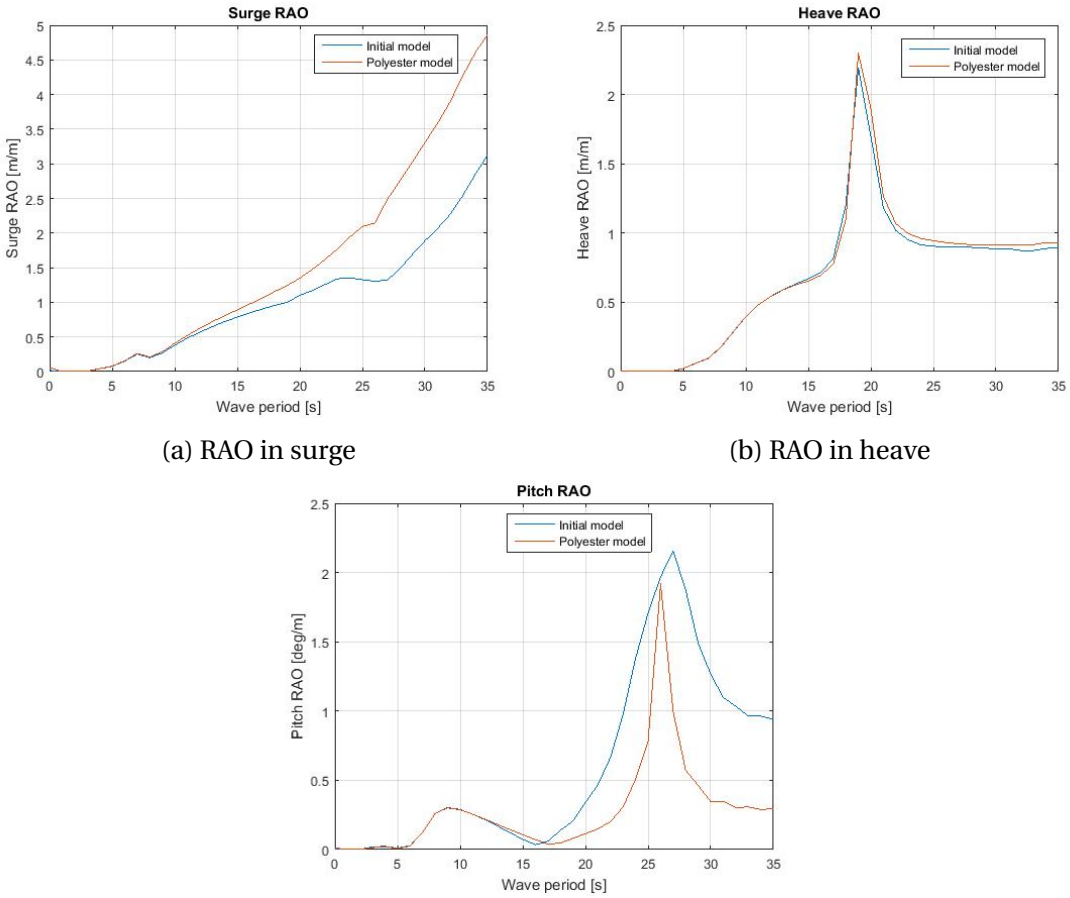

(a) RAO in surge

(b) RAO in heave

(c) RAO in pitch

Figure 7.6: RAOs in regular waves for initial and polyester models

For surge, shown in Figure 7.6a, it can be seen that the response in the polyester model is larger than in the initial model for high wave periods due to the low surge natural period of 37 s for the polyester model. As the wave period is getting closer to the natural period, the offset is larger because it is approaching resonance. The small trough in the RAO at $T = 26$ s might be due to the pitch natural period of approximately 26 s for both models.

For heave, shown in Figure 7.6b, the two models have exactly the same RAO. This is because, as already explained, that the response in heave is not being affected by the change of mooring system from chain to polyester. A resonance peak can be seen at the natural period in heave

of approximately 19 s for both models. Since the waves contain most energy at periods 5-25 s, resonance in heave might be a problem when the FWT is exposed to waves.

For pitch, which is shown in Figure 7.6c, a resonance peak can be seen at the natural period of around 26 s for both models. However, the increased response close to resonance starts earlier and ends later for the initial model. As for both the chain models, the polyester model has a cancellation at approximately 16 s.

7.5 Constant wind

A constant uniform wind test was conducted to find the mean offsets in surge, heave and pitch, and the mean line tension. The same conditions as for the previous chapters (Table 5.7) were run. The time lines of the different conditions for the polyester model and the initial model are given in Figure 7.7, 7.8, 7.9 and 7.10.

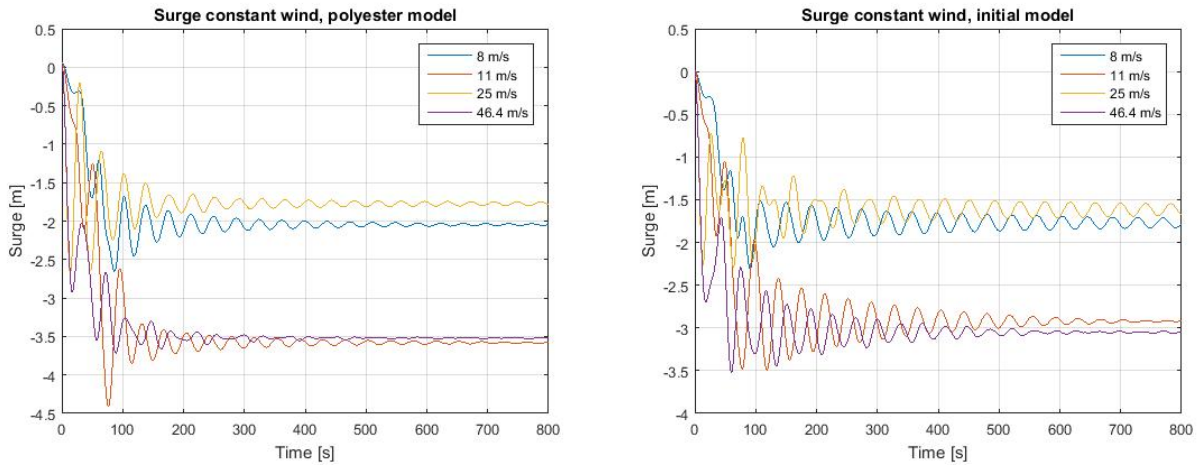

(a) Polyester model

(b) Initial model

Figure 7.7: Constant wind test in surge for the polyester model and the initial model

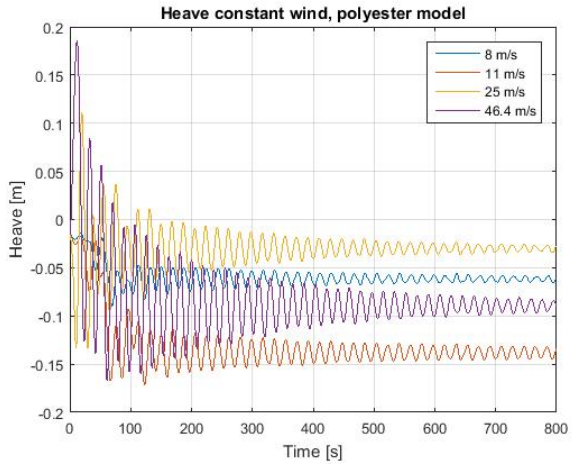

(a) Polyester model

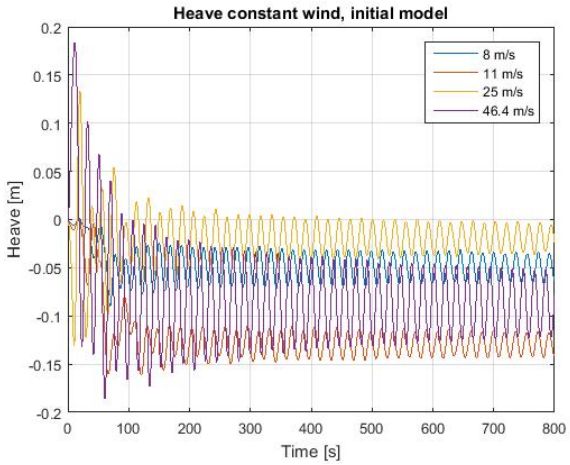

(b) Initial model

Figure 7.8: Constant wind test in heave for the polyester model and the initial model

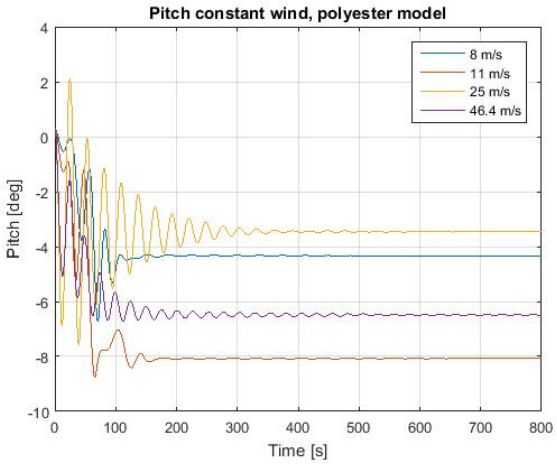

(a) Polyester model

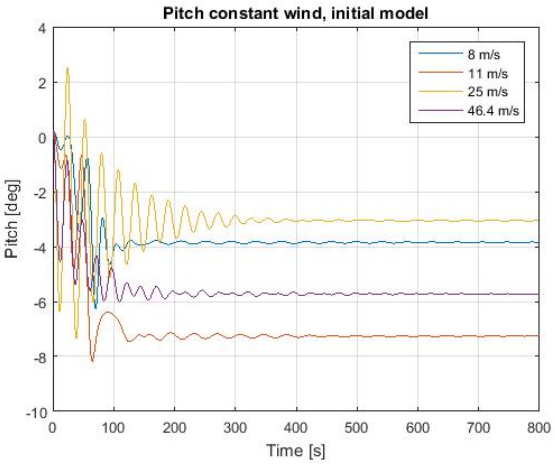

(b) Initial model

Figure 7.9: Constant wind test in pitch for the polyester model and the initial model

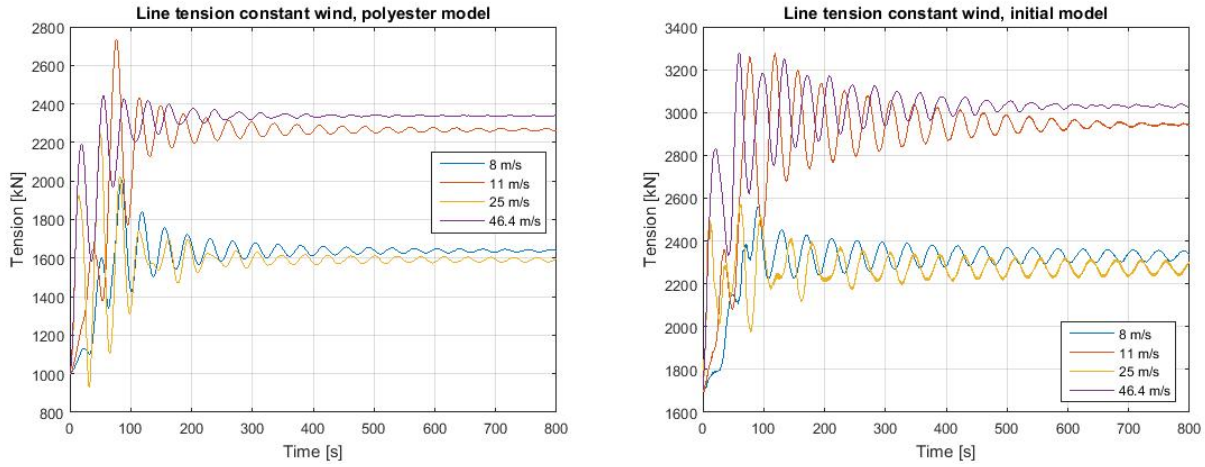

(a) Polyester model

(b) Initial model

Figure 7.10: Constant wind test of line tension in line 1 for the polyester model and the initial model

It takes approximately 400 seconds before the results are steady. In surge, which is shown in Figure 7.7, the mean values are slightly larger for the polyester model than for the initial model. As expected, the offset is greatest at rated condition and extreme condition. In heave, shown in Figure 7.8, the mean offsets are very small, and approximately the same for the two models.

In pitch, which is shown in Figure 7.9, the offsets are slightly larger for the polyester model than for the initial model for all the wind velocities. The mean line tension, shown in Figure 7.10, is larger for the initial model than for the polyester model. This can be explained by the line characteristics in Figure 7.4, where the tension in the polyester line is smaller than the tension in the chain mooring line for increasing tension. As expected, the mean line tension in the extreme condition and the rated conditions are the largest.

7.6 ULS calculations

The extreme ULS condition in Table 4.12 is investigated for the polyester model to see if the taut polyester model is doing better than the chain systems in the ULS analysis. The Gumbel distribution of the maximum line tension for the polyester rope model in ULS condition, with NPD wind is given in Figure 7.11. The figure to the left shows that 10 runs are sufficient to obtain accurate results of the maximum tension since all results of more runs than this is within the 5 % deviation limit. The right figure shows the Gumbel distribution after 10 runs when using NPD turbulent wind and TurbSim turbulent wind. The results of the ULS calculation is given in Table 7.5. The table shows that the fiber model is within the ULS criteria.

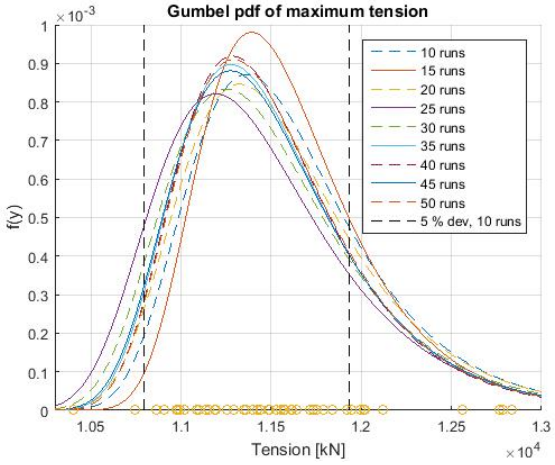

(a) Gumbel distribution of maximum tension when using NPD wind for different number of runs for the polyester model

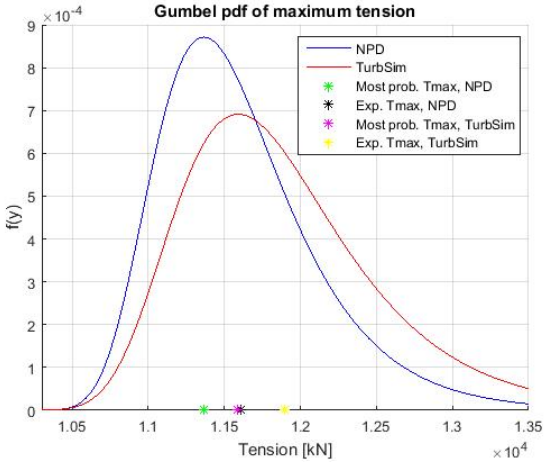

(b) Gumbel distribution of maximum line tension when using 10 runs for the polyester model

Figure 7.11

Table 7.5: ULS calculations after 10 runs for the polyester system

Model	Turbulent wind model	T_{max} [kN]	T_{mean} [kN]	T_d [kN]	S_C [kN]
Polyester model	NPD	11364	5806	17274	20503
Polyester model	TurbSim	11590	5976	17593	20503

7.6.1 Slack

For the polyester model, it is also important to look at slack. Figure 7.12 shows time lines of the axial tension in the most exposed line (line 1) and a lee line (line 2) when using NPD turbulent wind model. It can be seen that the lee lines will go into slack.

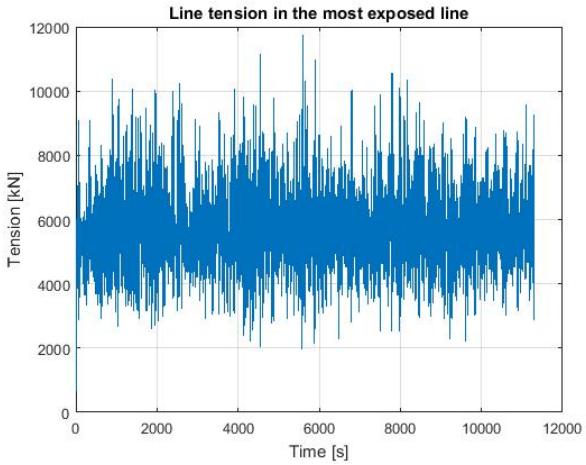

(a) Axial line tension in most exposed line (line 1) for the polyester model

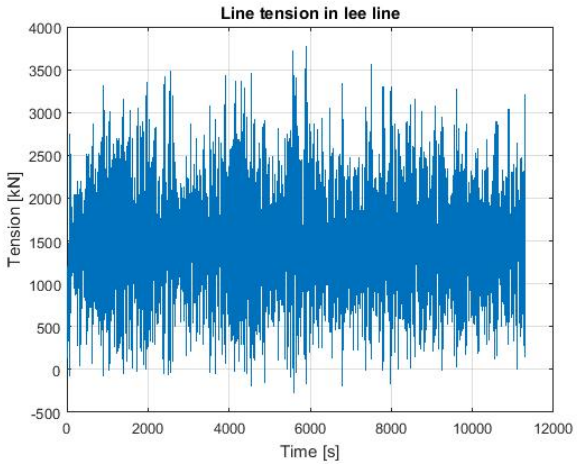

(b) Axial line tension in lee line (line 2) for the polyester model

Figure 7.12

The Gumbel distribution of the minimum tension in line 1 after 10 runs is shown in Figure 7.13. It can be seen that both the most probable minimum tension and the expected minimum tension are above zero. Hence, slack will occur in line 2 and 3, but not in line 1.

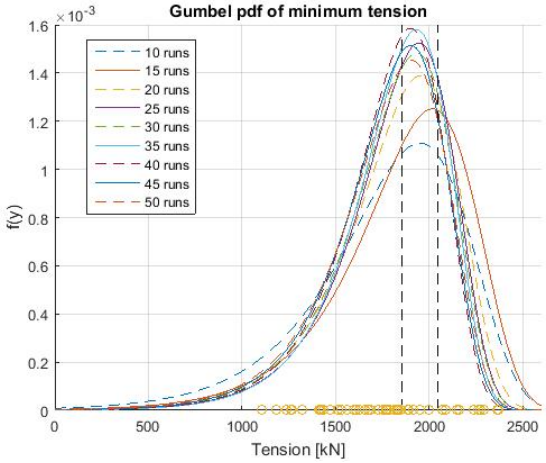

(a) Gumbel distribution of minimum tension in line 1 when using NPD wind for different number of runs for the polyester model

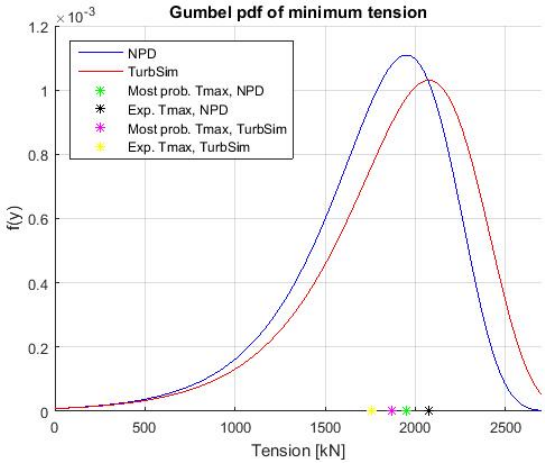

(b) Gumbel distribution of minimum tension when using 10 runs for the polyester model

Figure 7.13

Slack of a polyester line can lead to the fibers being broken. To avoid slack, the minimum peaks of the axial tension need to be above zero. To get this, the pre-tension in the line can be increased. Increasing the pre-tension might lead to too high design tension, T_d in the ULS calculations. A solution to this can be to raise the fairlead to the top of the columns. This leads to

a less stiff system, meaning that the axial tension is lower when increasing the offset. Furthermore, increasing the length of the polyester rope might give a less stiff system. However, since the vertical and horizontal length of the rope are 55 m and 800 m respectively, the angle at fairlead is already very small. This makes a large part of the mooring line being close to the SWL. This might be a problem for boats driving close to the FWT for maintenance, and that regular ships should have a large safety distance from the FWT. For chain, this is less of a problem due to the catenary shape of the line.

7.7 ALS calculations

The ALS calculations are conducted the same way as in the previous chapters (Section 5.8). It is assumed that 10 runs are sufficient to obtain accurate enough results. The results of the ALS calculations are given in Table 7.6. It can be seen that the polyester system is within the ALS criteria.

Table 7.6: ALS calculations after 10 runs for the polyester mooring system

Model	Turbulent wind model	T_{max} [kN]	T_{mean} [kN]	T_d [kN]	S_C [kN]
Polyester model	NPD	6568	4105	6814	20503
Polyester model	TurbSim	6488	4290	6708	20503

For the ULS and ALS calculations, the polyester system gives better results than the chain catenary systems. The polyester properties are especially good for large offsets because of the linear line characteristics giving a low axial tension. In addition, a polyester system will be cheaper and gives a smaller footprint on the sea bottom. However, since there is not yet that much knowledge about polyester mooring systems for semi-submersible wind turbines, and because the properties of polyester ropes are complex, the polyester system might not be the most optimal mooring system.

The consequences of slack should be investigated for all the systems. For the polyester system, a shorter line length having fairlead positions at the top of the side columns and an increased pre-tension should be investigated. For the chain system, a line with higher MBS, having fairlead positions at the top of the columns and a smaller pre-tension should be investigated. Also combined chain-polyester systems can be investigated.

Chapter 8

Conclusion and Recommendations of Further Work

8.1 Conclusion

In this Master thesis, the mooring system design of a large floating semi-submersible wind turbine in shallow water has been investigated. Three different mooring systems have been tested: The initial mooring system already being in the model, a catenary chain Hywind Scotland based mooring system and a taut polyester system. In addition, the Hywind Scotland model has been compared to a simplified Hywind Scotland model where the tower and the wind turbine are removed from the model.

The natural period of all the investigated systems are given in Table 8.1. It was found that the surge/sway natural periods for the initial model and the polyester model were too small. The heave and pitch/roll natural period was similar for all the models, meaning that the mooring system did not affect these natural periods much. For all the models, quadratic damping was the dominating damping form.

Table 8.1: Natural periods of initial model and Hywind model

Degree of freedom	T_n of initial model [s]	T_n for for original Hywind model [s]	T_n of simplified Hywind model [s]	T_n for polyester model [s]
Surge/sway	45.4	68	68.3	37
Heave	19.1	19.2	20.5	19.2
Pitch/roll	25.7	26.1	24.5	26
Yaw	68	90	81.9	80

The regular wave-only response showed that the RAOs in heave and in pitch were similar for all the models. Hence, the mooring system had a minor effect on the heave and pitch motion response. The largest differences were the response around resonance for the polyester system being smaller, and the non-cancellation at $T = 16$ s for the simplified model due to the slightly lower pitch natural period. All the systems experience resonance in heave and pitch within the wave period range of 5-26 s, seen by the resonance peaks in the RAOs. None of the systems have resonance in surge in the wave-period range, but due to the low surge period in the polyester system, the response for high wave periods for this model is the largest of all the systems.

Constant wind tests showed that the rated condition and the 50 years return period extreme wind condition gave the largest mooring line tensions and offsets. Comparing the three mooring line models, the Hywind model gave the largest mean offsets in surge, heave and pitch, while the initial model gave the largest mean line tension.It was found that only extreme wind alone affected the mean line tension and the mean offset in surge and pitch. Only extreme waves alone affected the maximum and minimum peaks of the line tension and the offset in surge, heave and pitch. Only extreme current alone did not affect the line tension and the offsets much.

When comparing the two turbulent wind models, NPD and TurbSim, it was found that the TurbSim turbulent wind gave a slightly higher wind speed and lower standard deviation of the wind speed at hub height than the NPD turbulent model. In addition, the spectral plots of the wind contained more high frequency motion for the TurbSim model, and more low frequency motion for the NPD model. This was reflected in the mean line tension and the mean offsets in surge, heave and pitch.

The results from the simplified model were acceptable when comparing to the original Hywind model. By changing from the original model to the simplified model, it was found that 35 % of the time used for SIMA calculations will be saved.

By Gumbel distributions of the maximum axial tension, it was found that 10 runs were sufficient to obtain an accurate result. Table 8.2 shows the results from the ULS and the ALS analysis. Only the polyester model was within the ULS criteria, and all the systems were within the ALS criteria. The polyester mooring lee lines will go into slack.

Table 8.2: ULS and ALS results after 10 runs for the initial model, the Hywind model and the polyester model model

Limit state			ULS		ALS	
Model	Turb. wind model	S_C [kN]	T_d [kN]	Acceptable?	T_d [kN]	Acceptable?
Initial model	NPD	19148	39051	No	12073	Yes
Initial model	TurbSim	19148	39247	No	11879	Yes
Hywind model	NPD	20120	35032	No	12690	Yes
Hywind model	TurbSim	20120	35421	No	12452	Yes
Polyester model	NPD	20503	17274	Yes	6814	Yes
Polyester model	TurbSim	20503	17593	Yes	6708	Yes

8.2 Recommendations of Further Work

The mooring line designs should be further investigated. A FLS condition should be carried out to look at the life time of the mooring lines. In addition, the simplified model should be compared to the original model regarding more tests than the ones conducted. Examples of tests are ULS calculations, ALS calculations and FLS calculations.

Several other chain and polyester systems should be investigated. As suggested, the catenary chain systems should be run with higher MBS, meaning a heavier and thicker mooring line, a lower fairlead tension and with the fairleads moved to the top of the side columns. The polyester system should be run with a shorter line length, fairlead positions at the top of the side columns and with an increased pre-tension to avoid slack. Other systems that can be investigated are combined polyester-chain systems, steel wire rope systems and combinations of all the above. In addition, mooring lines with buoys, clump weights and elastic components can be tested.

Furthermore, the costs of different mooring line designs, maintenance, and installation could be investigated, since costs are a large part of the choice of mooring line system. Moreover, a literature study regarding installation methods for different types of anchors and lines could be conducted since installation is an important part of mooring line design selection.

The main problems found in the mooring systems are when the structure is exposed to extreme weather. A way to find a mooring system design that is within the ULS and ALS criteria is to change location of the FWT. In this way, a location with less extreme environment might fit the mooring system better.

Bibliography

[1] (2005). IEC 61400-1. wind turbines, part 1: Design requirements.

[2] (2010). Offshore standard DNV-OS-E301, position mooring.

[3] (2013). Offshore standard DNV-OS-J103 design of floating wind turbine structures.

[4] (2014). Recommended practice DNV-RP-C205, environmental conditions and environmental loads.

[5] (2015). DNVGL-RP-E305, recommended practice: Design, testing and analysis of offshore fiber ropes.

[6] Bachynski, E. Basc aerodynamics for wind turbines. Lecture notes.

[7] Barthelemie, R. J. and Pryor, S. (2001). A review of the economics of the offshore wind farms. 25(4):203–213.

[8] Bridon (2013). Oil and gas, wire and fibre rope solutions for the world's most demanding applications. Information brochure.

[9] C. Bak; F. Zahle; R. Bitsche; T. Kim; A. Yde; L.C. Henriksen; P.B. Andersen; A. Natarajan, M. H. (2013). *Design and performance of a 10 MW wind turbine.* J. Wind Energy.

[10] Chakrabarti, S. K. (2005). *Handbook of Offshore Engineering.* Elsevier Ltd.

[11] DNV GL (2015). Syrope JIP, best practice for analysis of mooring systems with polyester ropes. Technical report.

[12] Equinor. How hywind was born. `https://www.statoil.com/en/magazine/how-hywind-was-born.html#floating-wind`. Accessed: 08.12.2017.

[13] Equinor (2013). Hywind buchan deep metocean design basis.

[14] Equinor (2014). Mooring: Detail design. Company presentation.

[15] et al., J. A. (2013). *TMR4105 - Marin Teknikk Grunnlag*. Center of Marine Technology, Trondheim, NTNU.

[16] Faltinsen, O. (1990). *Sea Loads on Ships and Offshore Structures*. Cambridge University Press.

[17] Hansen, M. O. (2008). *Aerodynamics of wind Turbines*. Earthscan, 2nd edition edition.

[18] Ishihara, T. and Taki, S. Fukushima floating offshore wind farm demonstration project (Fukushima FORWARD). `http://www.fukushima-forward.jp/english/pdf/pamphlet4.pdf`. Accessed: 08.12.2017.

[19] J. Jonkmann et al. (2009). Definition of a 5-mw reference wind turbine for offshore system development. Technical report, National Renewable Energy Laboratory (NREL).

[20] Jonkman, B. and Kilcher, L. (2012). Turbsim user's guide. Technical report, National Renewable Energy Laboratory (NREL).

[21] Larsen, C. M. (2015a). *Marine Dynamics*. Department of Marine Technology, NTNU.

[22] Larsen, K. (2015b). Static equilibrium of a mooring line.

[23] Larsen, K. (2017). TMR4225 marine operations. lecture notes 6b and 7 - station keeping and mooring systems. Lecture presentation.

[24] Larsen, K. (2018). Personal communication, March 2.

[25] Leira, B. J. (2010). *TMR4235 Stochastic Theory of Sealoads, Probabilistic Modelling and Estimation*. Center of Marine Technology, Trondheim, NTNU.

[26] NWTC Information Portal (2016). Turbsim. `https://nwtc.nrel.gov/TurbSim`. Accessed: 23.05.2018.

[27] Pelastar. Pelastar. `http://pelastar.com/`. Accessed: 15.12.2017.

[28] Pettersen, B. (2007). *TMR4247 Marin Teknikk 3 Hydrodynamikk*. Institute of Marine Technology, Trondheim NTNU.

[29] Power, P. Windfloat. `http://www.principlepowerinc.com/en/windfloat`. Accessed 08.12.2017.

[30] Ramnäs Bruk AB. Ramnäs bruk product catalogue, top quality mooring products for harsh offshore conditions. Information brochure.

[31] Schröder, T. (2016). Sustainable power genereation, wind without end. https://www.siemens.com/innovation/en/home/pictures-of-the-future/energy-and-efficiency/sustainable-power-generation-hywind.html. Accessed: 14.12.2017.

[32] SINTEF Ocean (2017a). *SIMO 4.10.1 Theory Manual*. Center of Marine Technology, Trondheim, Norway.

[33] SINTEF Ocean (2017b). *SIMO 4.10.1 User Guide*. Center of Marine Technology, Trondheim, Norway.

[34] SINTEF Ocean (2017). *RIFLEX 4.10.1 User Guide*. Center of Marine Technology, Trondheim, Norway.

[35] Steen, S. (2014). *Lecture notes. TMR7 Experimental Methods in Marine Hydrodynamics*. Marine Technology Centre, Department of of Marine Techonlogy, Trondheim Norway.

[36] The European Wind Energy Association (EWEA) (2013). Deep water, the next step for offshore wind energy. Technical report, EWEA.

[37] Wang, Q. (2014). Design and dynamic analysis of a steel pontoon-type semi-submersible floater supporting the dtu 10mw reference turbine. Master's thesis, Delft University of Technology and Norwegian University of Schience and Technology.

[38] WindEurope (2017a). The european offshore wind industry, key trends and statistics 2016.

[39] WindEurope (2017b). Wind in power 2016, european statistics.

Appendix A: Time Lines and Spectral Plots for the Initial Model, Hywind Model and Polyester Model

Extreme wind only

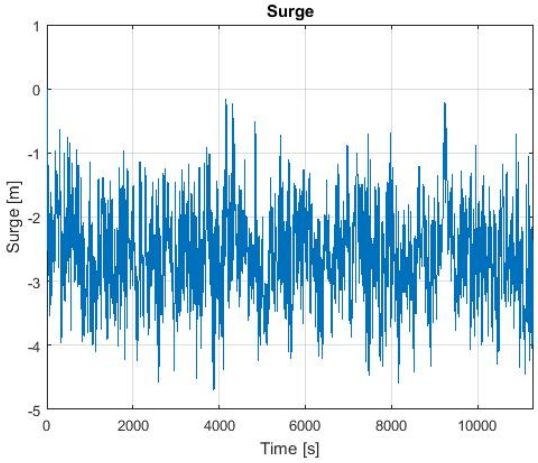

(a) Initial model, NPD turbulent wind

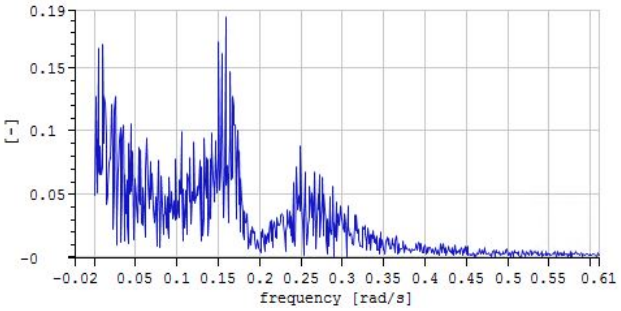

(b) Initial model, NPD wind

Figure 1: Surge motion for extreme wind condition

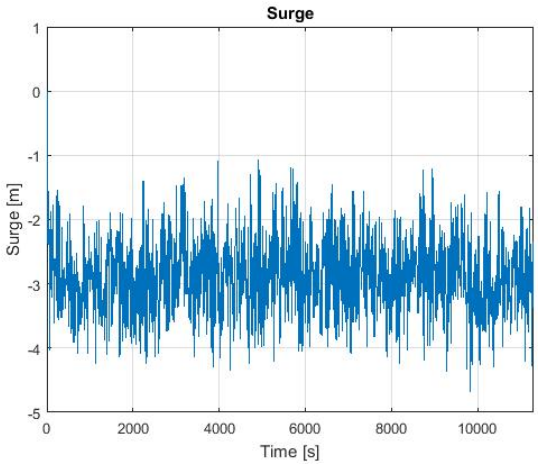

(a) Initial model, TurbSim turbulent wind

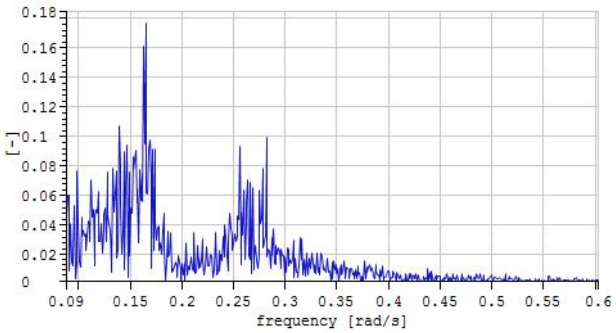

(b) Initial model, TurbSim wind

Figure 2: Surge motion for extreme wind condition

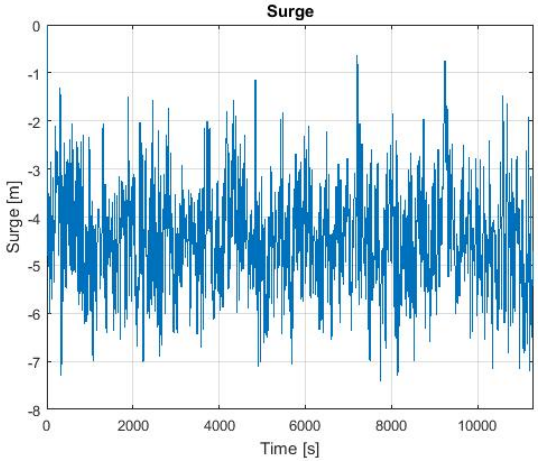

(a) Hywind model, NPD turbulent wind

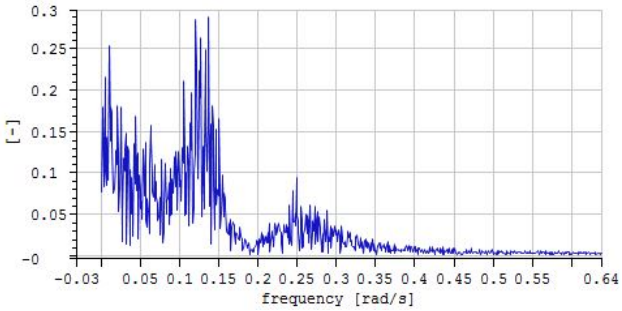

(b) Hywind model, NPD wind

Figure 3: Surge motion for extreme wind condition

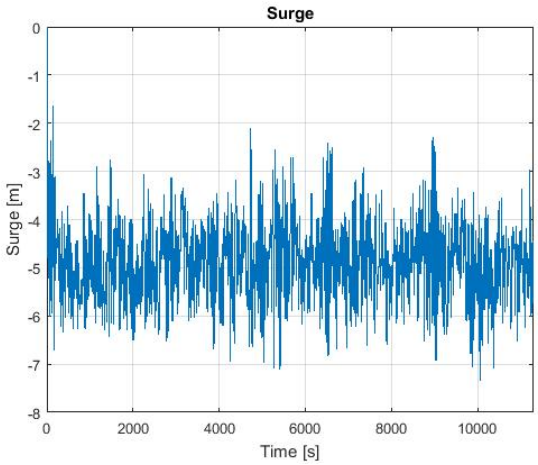

(a) Hywind model, TurbSim turbulent wind

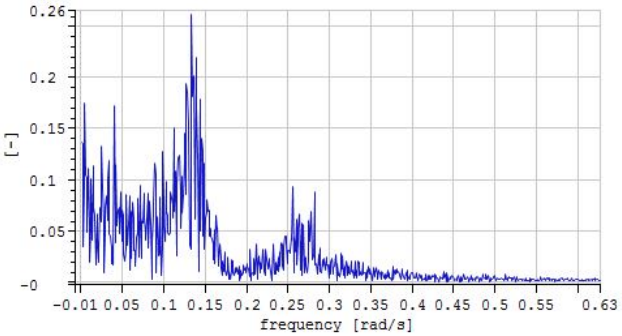

(b) Hywind model, TurbSim wind

Figure 4: Surge motion for extreme wind condition

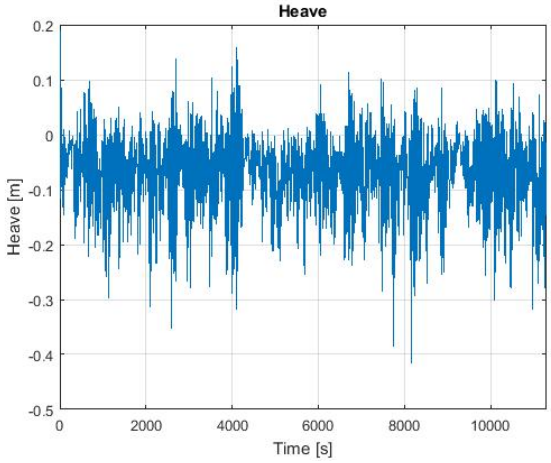

(a) Initial model, NPD turbulent wind

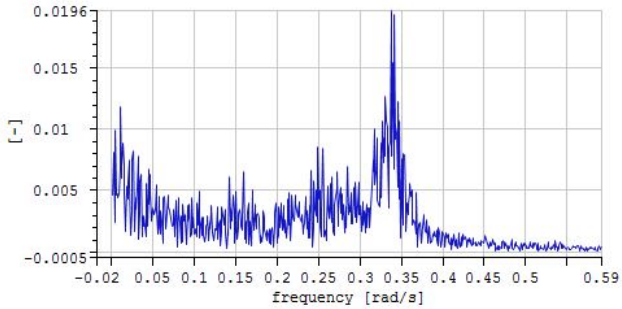

(b) Initial model, NPD wind

Figure 5: Heave motion for extreme wind condition

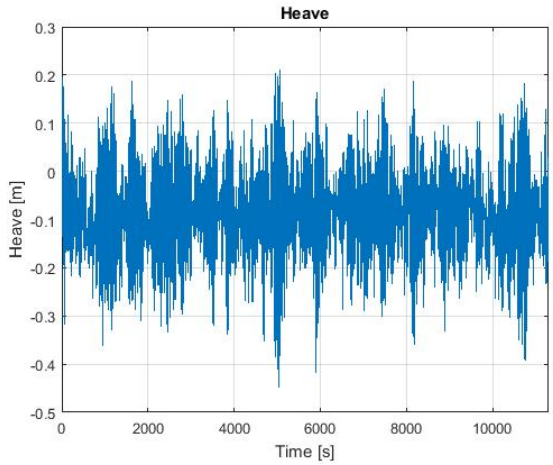

(a) Initial model, TurbSim turbulent wind

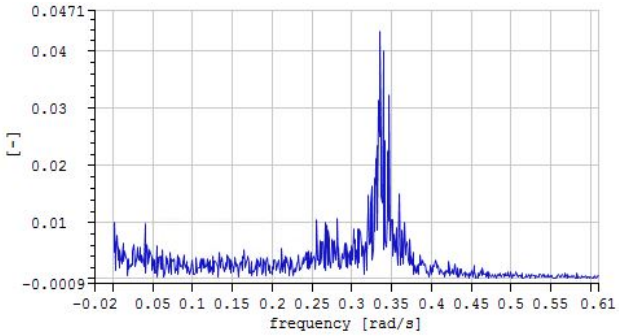

(b) Initial model, TurbSim wind

Figure 6: Heave motion for extreme wind condition

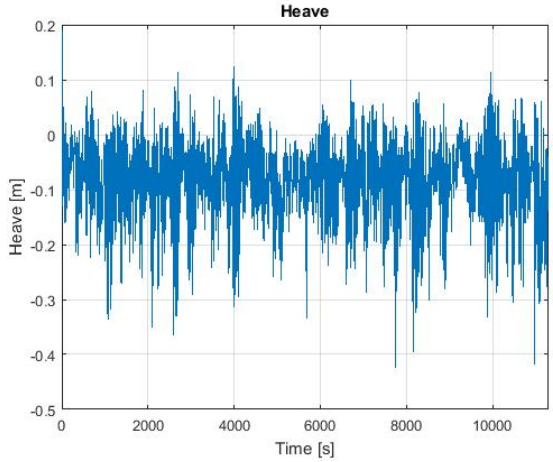

(a) Hywind model, NPD turbulent wind

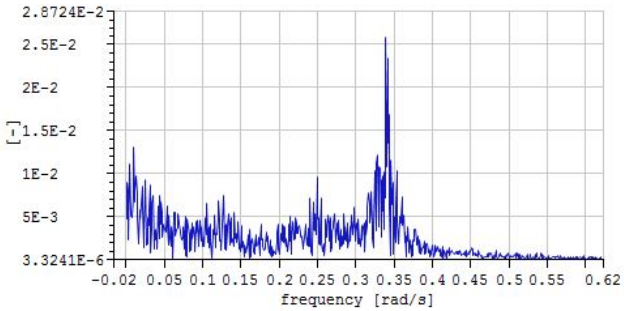

(b) Hywind model, NPD wind

Figure 7: Heave motion for extreme wind condition

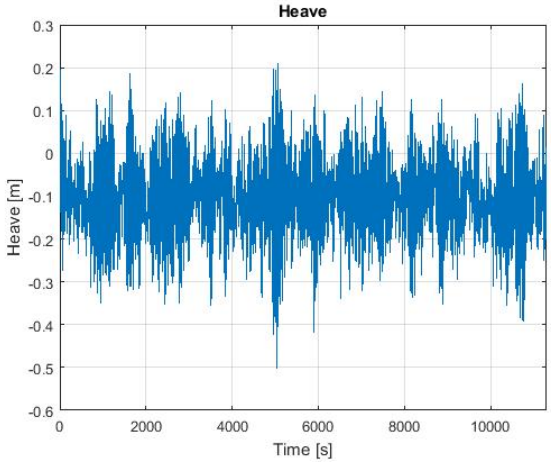

(a) Hywind model, TurbSim turbulent wind

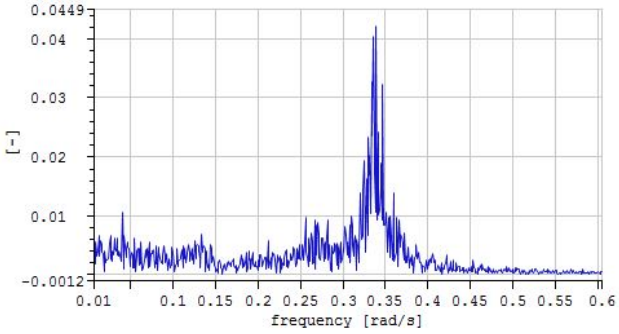

(b) Hywind model, TurbSim wind

Figure 8: Heave motion for extreme wind condition

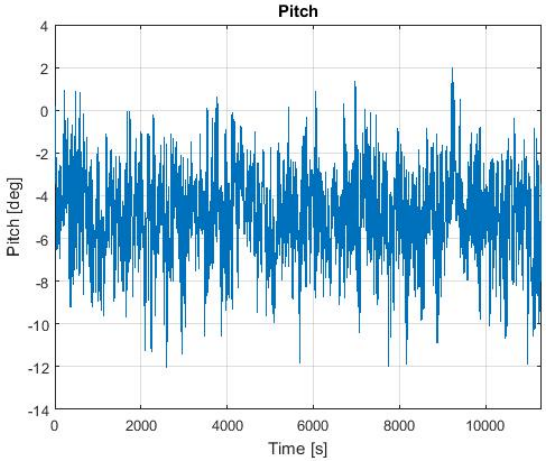

(a) Initial model, NPD turbulent wind

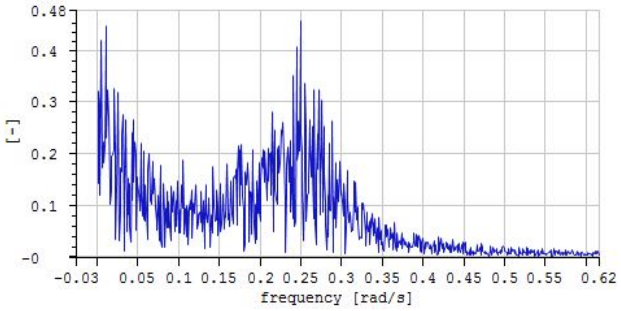

(b) Initial model, NPD wind

Figure 9: Pitch motion for extreme wind condition

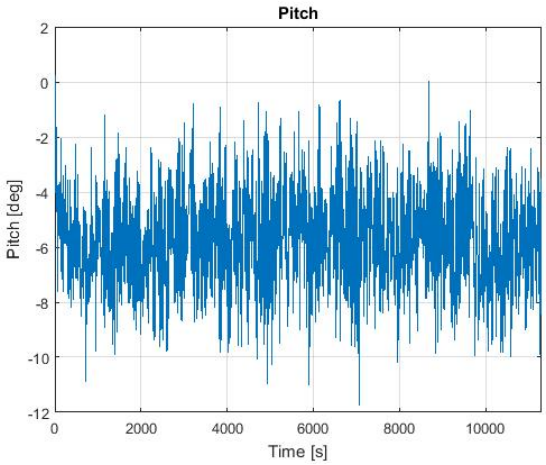

(a) Initial model, TurbSim turbulent wind

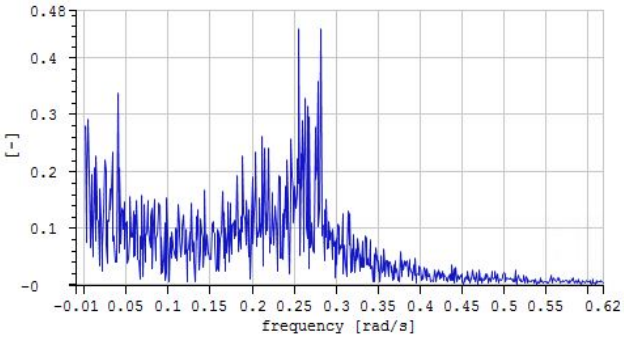

(b) Initial model, TurbSim wind

Figure 10: Pitch motion for extreme wind condition

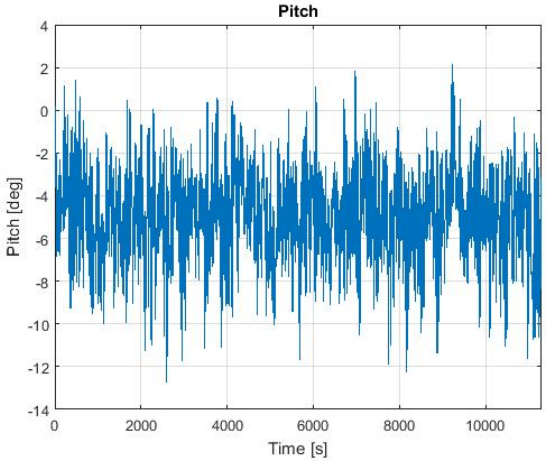

(a) Hywind model, NPD turbulent wind

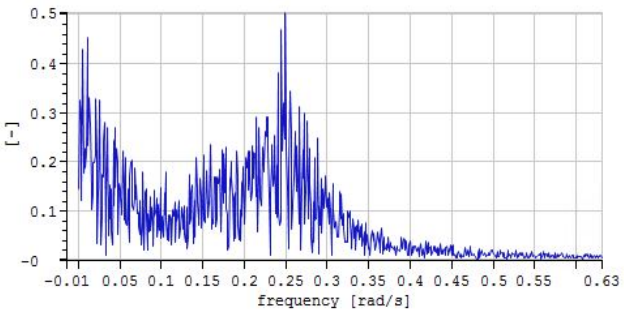

(b) Hywind model, NPD wind

Figure 11: Pitch motion for extreme wind condition

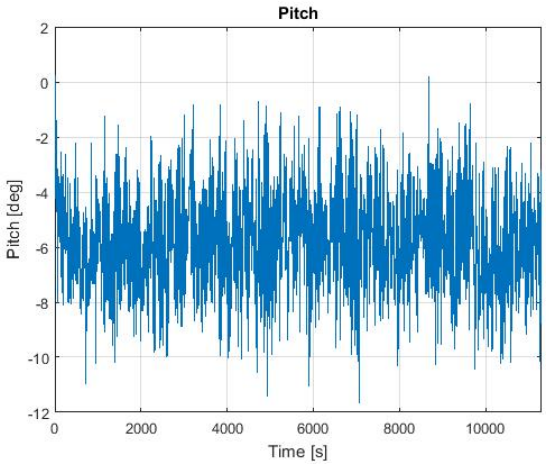

(a) Hywind model, TurbSim turbulent wind

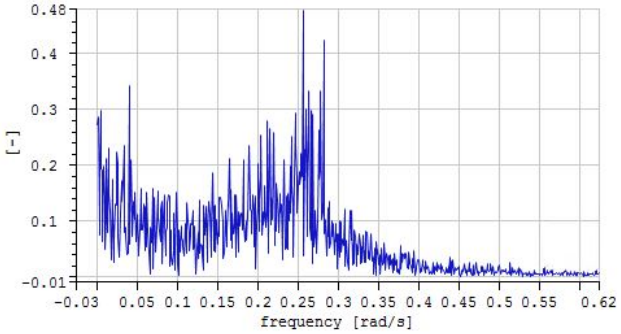

(b) Hywind model, TurbSim wind

Figure 12: Pitch motion for extreme wind condition

Extreme waves only

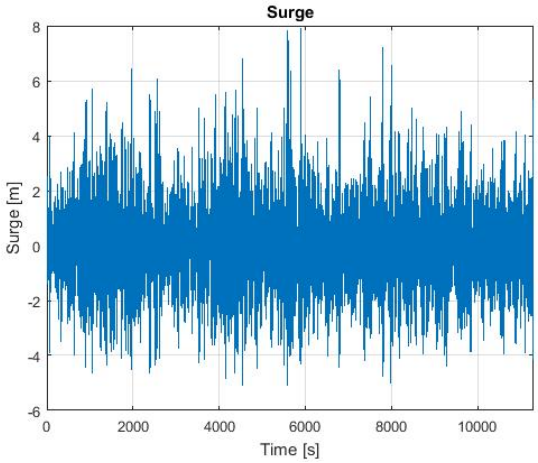

(a) Initial model

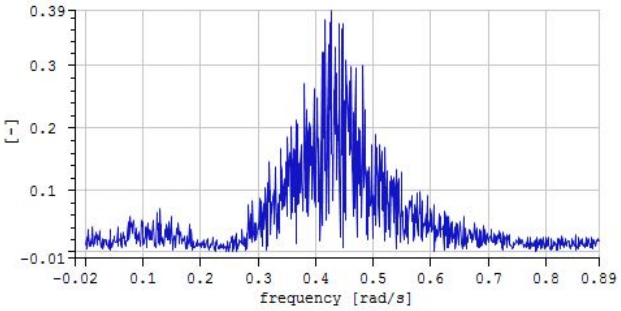

(b) Initial model

Figure 13: Surge motion for extreme waves condition

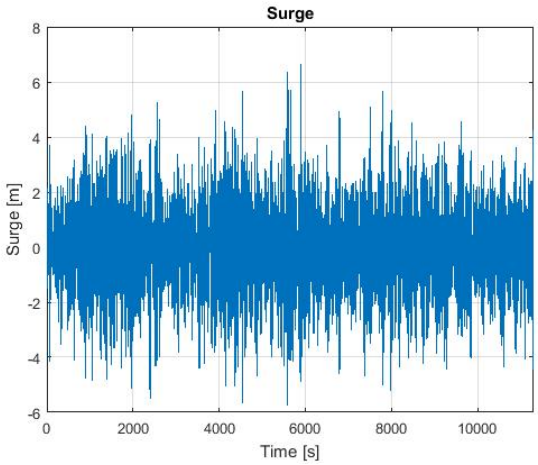

(a) Hywind model

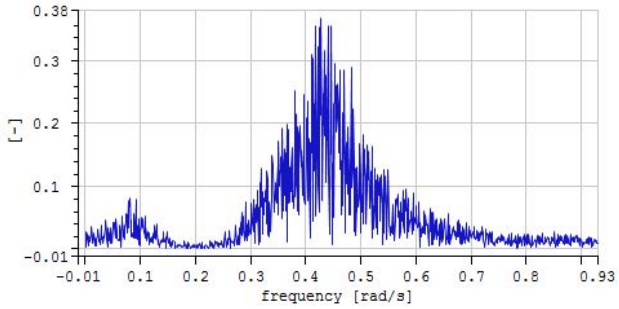

(b) Hywind model

Figure 14: Surge motion for extreme waves condition

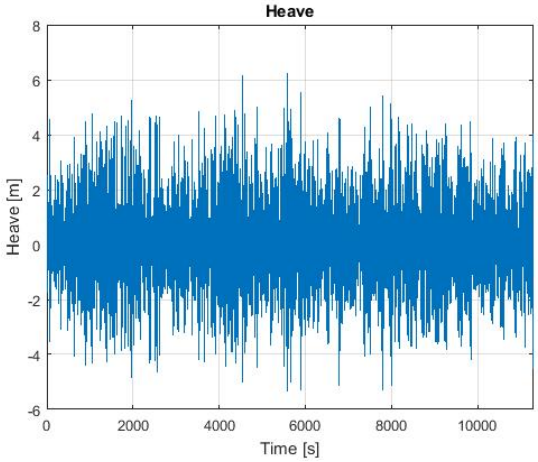

(a) Initial model

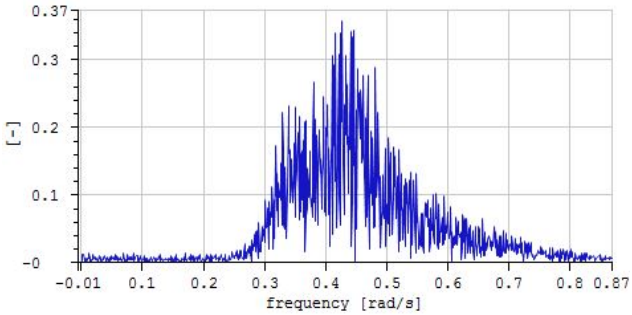

(b) Initial model

Figure 15: Heave motion for extreme waves condition

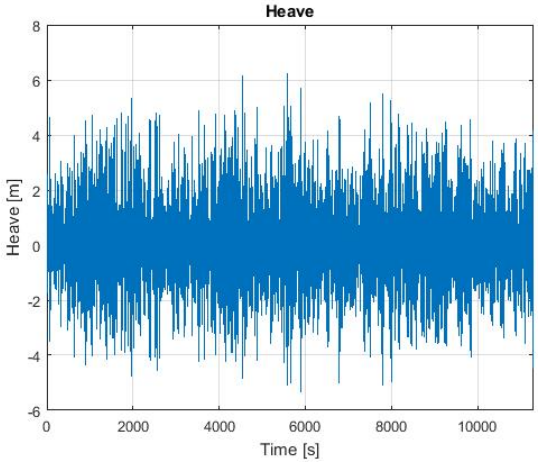

(a) Hywind model

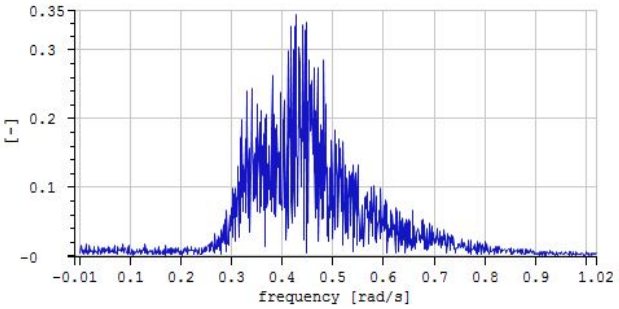

(b) Hywind model

Figure 16: Heave motion for extreme waves condition

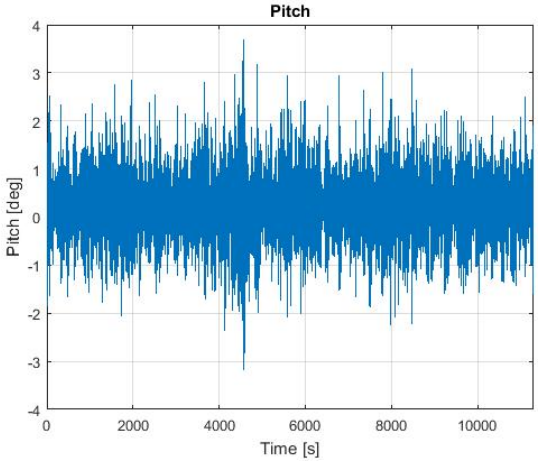

(a) Initial model

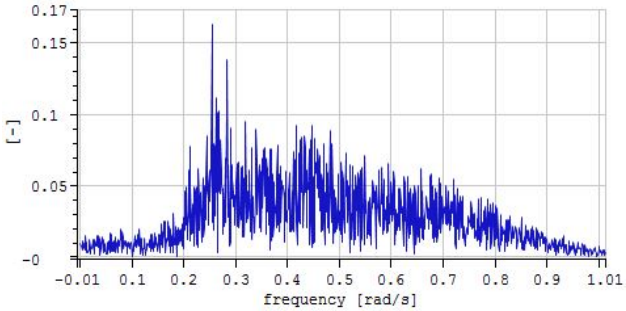

(b) Initial model

Figure 17: Pitch motion for extreme waves condition

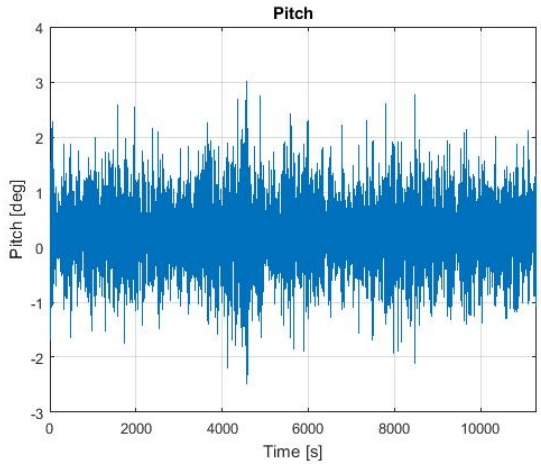

(a) Hywind model

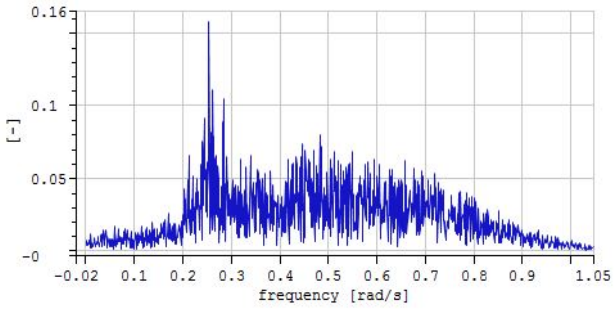

(b) Hywind model

Figure 18: Pitch motion for extreme waves condition

ULS condition

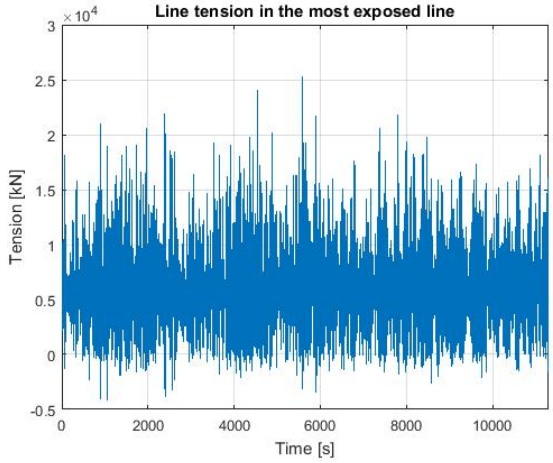

(a) Initial model

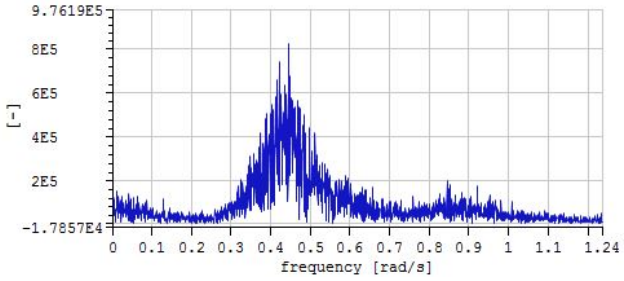

(b) Initial model

Figure 19: Axial line tension in line 1 for ULS condition and NPD turbulent wind

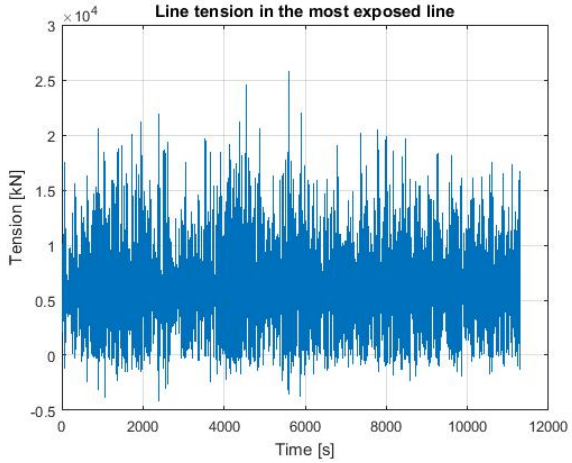

(a) Initial model

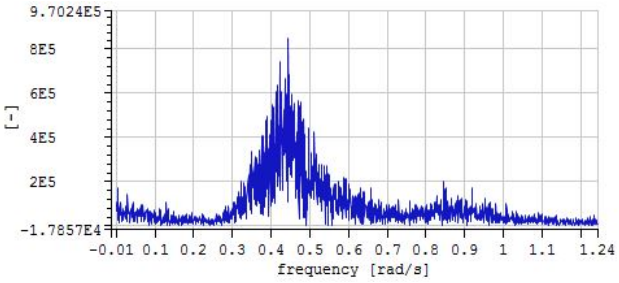

(b) Initial model

Figure 20: Axial line tension in line 1 for ULS condition and TurbSim turbulent wind

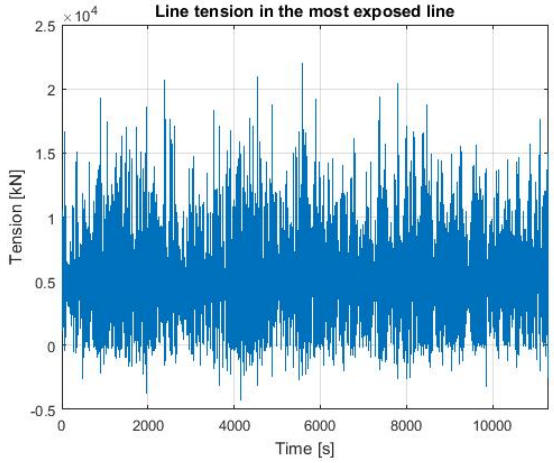

(a) Hywind model

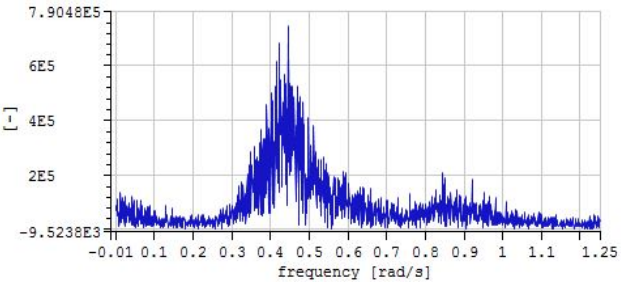

(b) Hywind model

Figure 21: Axial line tension in line 1 for ULS condition using NPD turbulent model

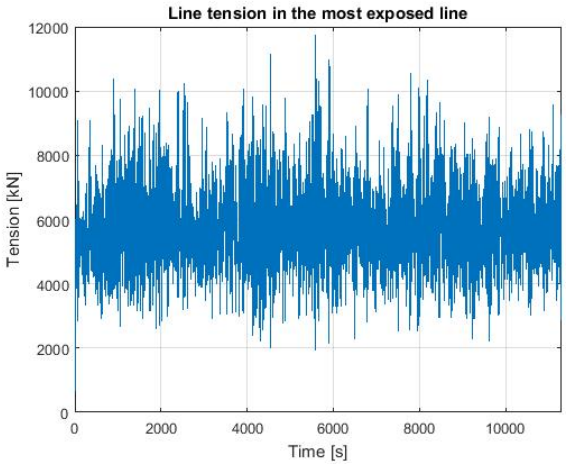

(a) Polyester model

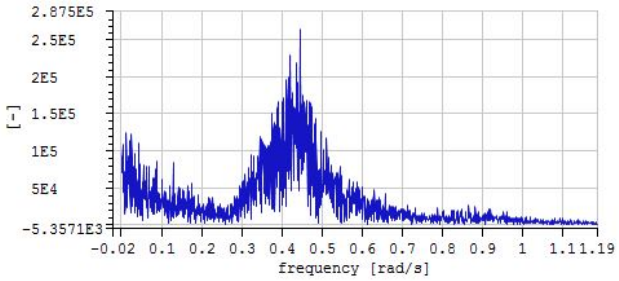

(b) Polyester model

Figure 22: Axial line tension in line 1 for ULS condition using NPD wind

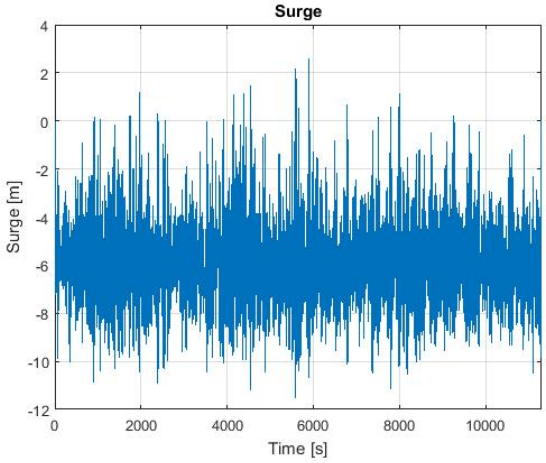

(a) Initial model

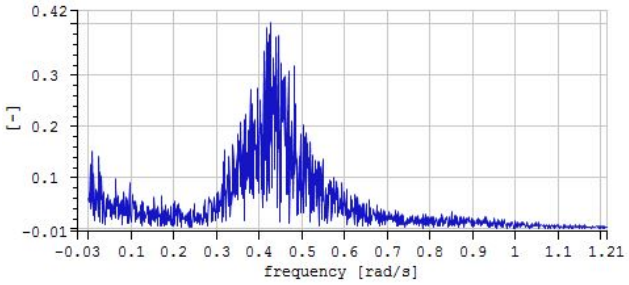

(b) Initial model

Figure 23: Surge motion for ULS condition and NPD turbulent wind

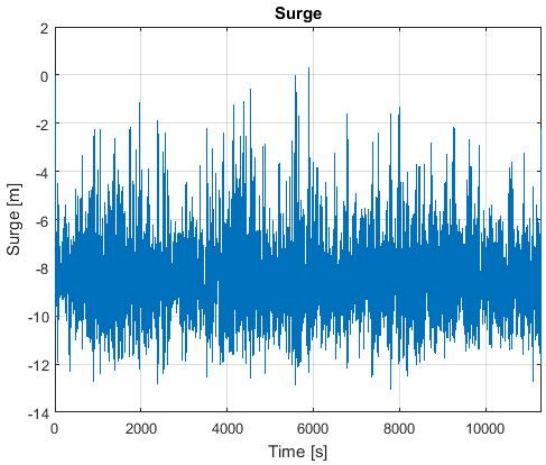

(a) Hywind model

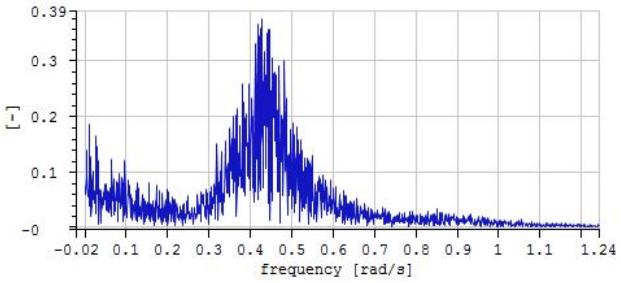

(b) Hywind model

Figure 24: Surge motion for ULS condition and NPD turbulent wind

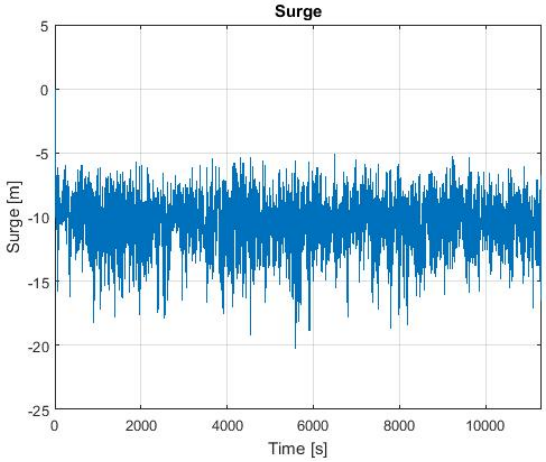

(a) Polyester model

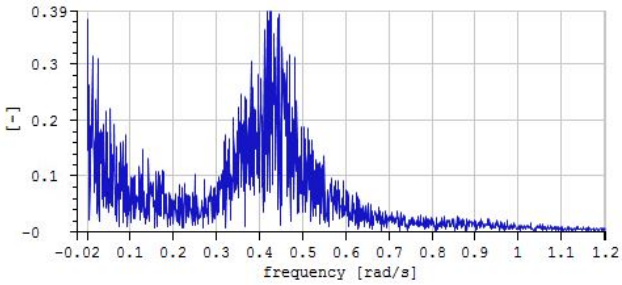

(b) Polyester model

Figure 25: Surge motion for ULS condition and NPD turbulent wind

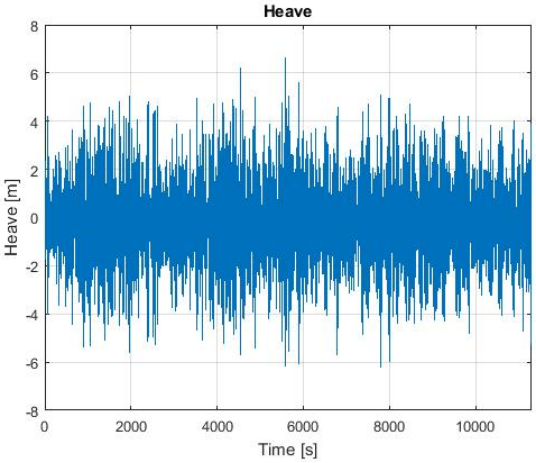

(a) Initial model

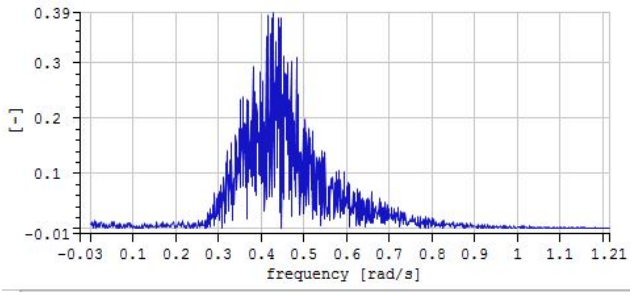

(b) Initial model

Figure 26: Heave motion for ULS condition and NPD turbulent wind

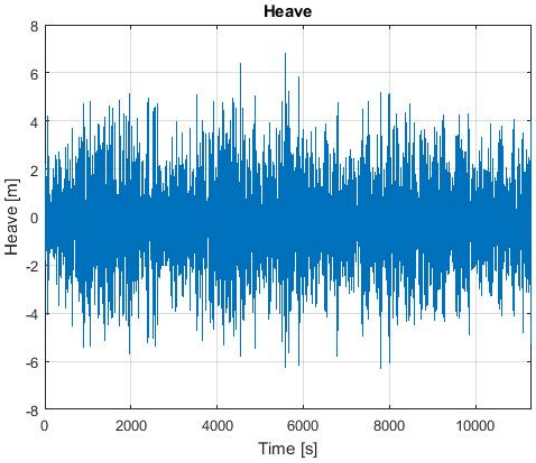

(a) Hywind model

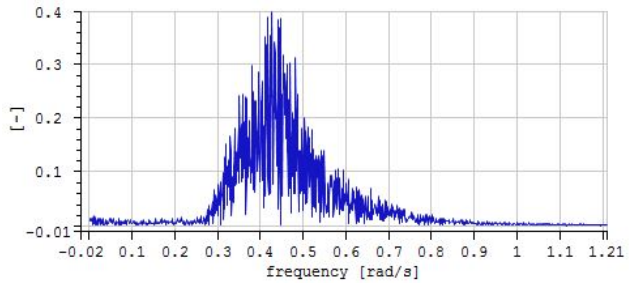

(b) Hywind model

Figure 27: Heave motion for ULS condition and NPD turbulent wind

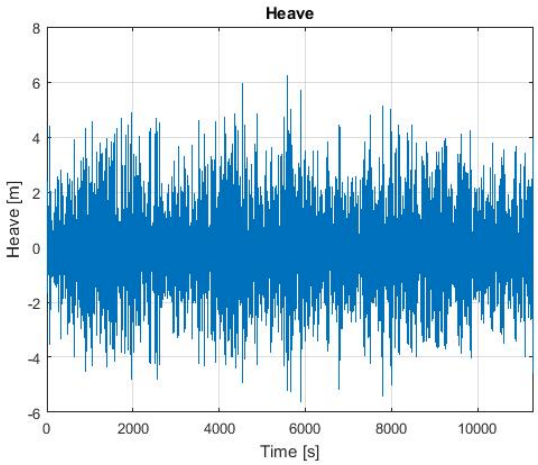

(a) Polyester model

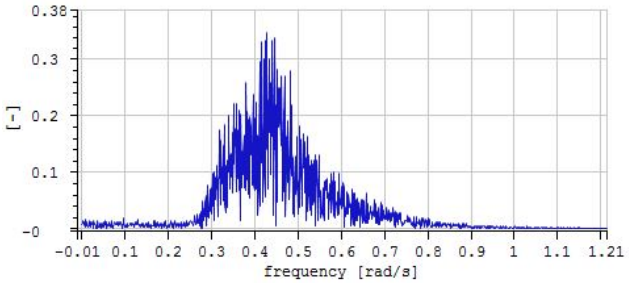

(b) Polyester model

Figure 28: Heave motion for ULS condition and NPD turbulent wind

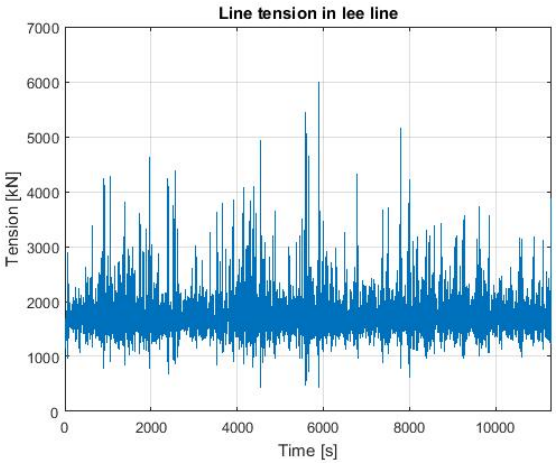

(a) Initial model

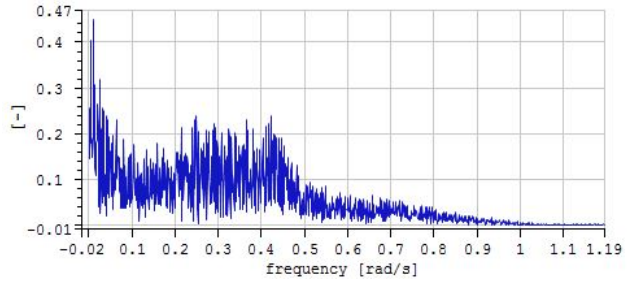

(b) Initial model

Figure 29: Pitch motion for ULS condition and NPD turbulent wind

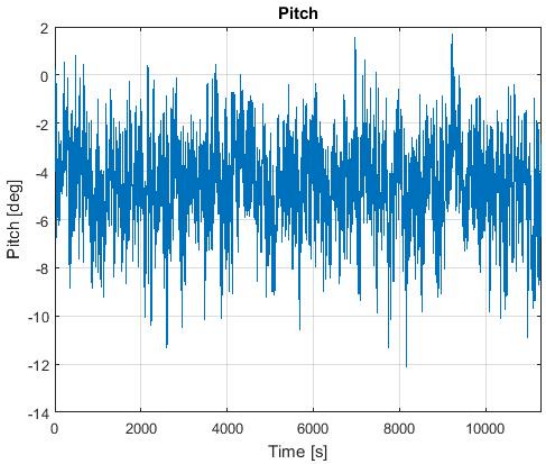

(a) Hywind model

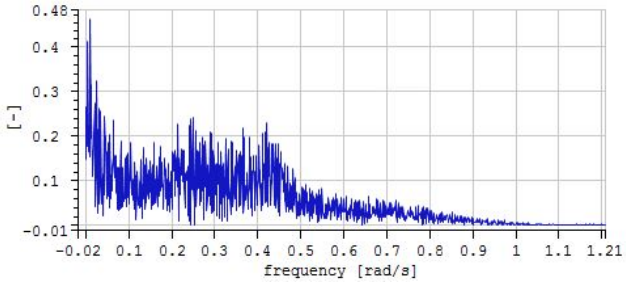

(b) Hywind model

Figure 30: Pitch motion for ULS condition and NPD turbulent wind

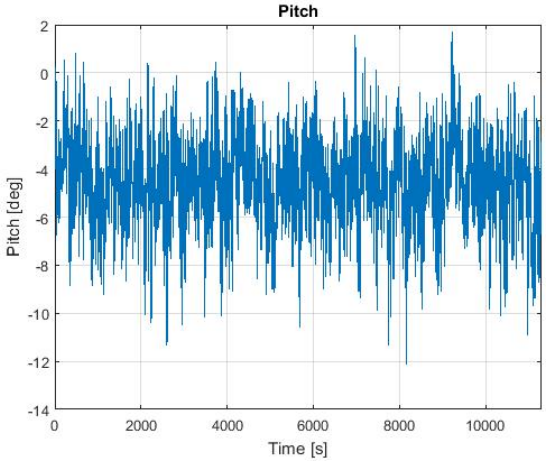

(a) Polyester model

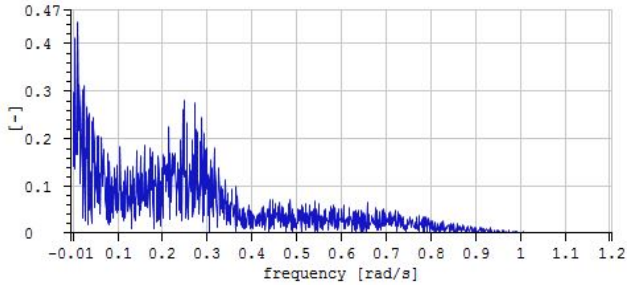

(b) Polyester model

Figure 31: Pitch motion for ULS condition and NPD turbulent wind